

DOE/ET-53088-588

IFSR #588

**Nonlinear Instability and Chaos in  
Plasma Wave-Wave Interactions**

CHRISTOPHER SHANE KUENY  
Institute for Fusion Studies  
The University of Texas at Austin  
Austin, Texas 78712

(THESIS)

**January 1993**

NONLINEAR INSTABILITY AND CHAOS IN  
PLASMA WAVE-WAVE INTERACTIONS

APPROVED BY

DISSERTATION COMMITTEE:

Philip A. Moun

Wendell Stator

R. D. Hazeltine

R. F. Williams

R. B. D'Azavedo

Copyright  
by  
C.S. Kueny  
1993

To my parents

**NONLINEAR INSTABILITY AND CHAOS IN  
PLASMA WAVE-WAVE INTERACTIONS**

by

**CHRISTOPHER SHANE KUENY, B.S.**

**DISSERTATION**

Presented to the Faculty of the Graduate School of

The University of Texas at Austin

in Partial Fulfillment

of the Requirements

for the Degree of

**DOCTOR OF PHILOSOPHY**

**THE UNIVERSITY OF TEXAS AT AUSTIN**

May, 1993

## Acknowledgments

Many people helped make it possible to complete this work.

First and foremost, I am grateful to Prof. Philip Morrison for his support, encouragement and patience. It has been a privilege and a great pleasure to learn from him. His wonderful enthusiasm enlivened all of our interactions, both one-on-one and in our study groups, and it helped to remind me (when I was occasionally in danger of forgetting) that the reason that I study physics is because it's fun.

Thanks to Profs. Richard Hazeltine, Wendell Horton, Roger Broucke and Robert Williams for reading and commenting on my dissertation, and for judging my final defense. I am grateful for the instruction and guidance from these four men and from all of the other professors and others who have taught me over the years. Thanks especially to Dr. Jim Meiss, who guided my introduction to nonlinear dynamics. I also enjoyed the opportunity to work on research projects with Profs. Wendell Horton and Toshiki Tajima. Prof. Roger Bengtson supervised my introduction to experimental plasma physics, and I have enjoyed his continued encouragement.

I would like to especially mention Profs. Dwight Nicholson and Christoph Goertz of the University of Iowa, whose tragic deaths, along with those of several of their colleagues, in November 1991 were such a shock. I have very good memories of both of them from my undergraduate days at Iowa. They both provided much encouragement and support, and influenced the path that

I took during my graduate career. I had very much looked forward to seeing them again in the future.

Also (going way back) I would like to thank Glen Morland, whose high school physics class led me to pursue physics as a profession. While the subject matter might have won me over regardless of the teacher, "Mr. Morland" conveyed the excitement of the field in a way that was especially appealing. I remember with pleasure learning from him.

I am very grateful to the Institute for Fusion Studies and the Fusion Research Center for support under the TAERF Fellowship and Research Assistantship that made it possible to carry out this work. The working environment here has been wonderful. Especially valuable has been the support for travel to numerous conferences. These meetings provided an invaluable opportunity to meet other researchers and to learn about their work. Critical problems in my research might never have been solved but for the conversations that took place there.

Many IFS/FRC staff members were very helpful. Drs. Buff Miner and Ahmet Aydemir and Mr. Mike Sternberg provided much assistance with computing. The administrative staff was wonderful; I would like to especially thank Saralyn Stewart, Carolyn Valentine, Joyce Patton, Diane Allen and Joan Gillette for all of their help.

It was a great pleasure to know the many fellow students who have been part of my life during the past several years. I especially enjoyed the close friendship of Mark Calvin, Sylvania Pereira, Terry Rhodes, Kevin Sandusky, Xiang Ning Su and Xueqiao Xu. I have also enjoyed work and play with Raul Acevedo, Leon Ofman, Qi Chen, Xiaoling Chen, Hyungtae Kook, Martin

Prahovic, Brad Shadwick, Diego del Castillo, Andy Meigs and Mark Foster.

I am especially grateful to Dr. Huanchun Ye for many helpful discussions on my research, as well as for his friendship. I would also like to thank Dr. Ivan Gjaja of the University of Maryland for several helpful discussions and correspondences regarding the applications of Lie transformations to numerical computation.

Thanks very much to Drs. Lee Sloan and Bob Thompson of Austin Research Associates for providing me a job there for the past several years. I have enjoyed their friendship and have benefited greatly from many discussions with them, and from the opportunity to work on a number of interesting problems outside the immediate area of my dissertation research.

I have enjoyed the friendship and support of many friends outside of the academic environment, who made it possible for me to complete this work. I could never mention all of them here. You know who you are!

Finally, thanks to my family, who were a source of strength during all stages of this work. My parents, through their encouragement and support, made it possible for me to do this. I will mention especially my sister Rosemary, whose ear I talked off during many times good and bad. I am grateful for the support of all of my family.

I'm sure I've left out someone, because so many people have been involved. To everyone: Thank you!

Christopher Shane Kueny

*The University of Texas at Austin*

*May, 1993*



NONLINEAR INSTABILITY AND CHAOS IN  
PLASMA WAVE-WAVE INTERACTIONS

Publication No. \_\_\_\_\_

Christopher Shane Kueny, Ph.D.  
The University of Texas at Austin, 1993

Supervisor: Philip J. Morrison

Conventional linear stability analyses may fail for fluid systems with an indefinite free energy functional. When such a system is linearly stable, it is said to possess negative energy modes. Instability may then occur either via dissipation of the negative energy modes, or nonlinearly via resonant wave-wave coupling, which leads to explosive growth. In the dissipationless case, it is conjectured that intrinsic chaotic behavior may allow initially non-resonant systems to reach resonance by diffusion in phase space.

This is illustrated for a simple equilibrium involving cold counter-streaming ions. The system is described in the fluid approximation by a Hamiltonian functional and associated noncanonical Poisson bracket. By Fourier decomposition and appropriate coordinate transformations, the Hamiltonian for the perturbed energy is expressed in action-angle form. The normal modes

correspond to Doppler-shifted ion-acoustic waves of positive and negative energy. Nonlinear coupling leads to decay instability via two-wave interactions, which occur generically for long enough wavelengths. Three-wave interactions which occur in isolated, but numerous, regions of parameter space can drive either decay instability or explosive instability. When the resonance for explosive growth is detuned, a stable region exists around the equilibrium point in phase space, while explosive growth occurs outside of a separatrix.

These interactions may be described exactly if only one resonance is considered, while multiple nonlinear terms make the Hamiltonian nonintegrable. Simple Hamiltonians of two and three degrees of freedom are studied numerically using symplectic integration algorithms, including an explicit algorithm derived using Lie algebraic methods. Two-wave and three-wave decay interactions lead to strongly chaotic motion, which destroys the separatrix bounding the stable region for near-resonant triplets. Phase space orbits experience slow diffusive growth to amplitudes sufficient for explosive instability, thus effectively reducing the critical amplitude. For Hamiltonians with more than two degrees of freedom, there is actually no critical amplitude for growth, because small perturbations may grow to arbitrary size via Arnold diffusion. It is observed numerically that this diffusion can be very slow for the smallest perturbations, although the actual diffusion rate is probably underestimated due to the simplicity of the model.

## Table of Contents

Acknowledgments	v
Table of Contents	x
List of Tables	xiii
List of Figures	xiv
<b>1. Introduction</b>	<b>1</b>
<b>2. Background</b>	<b>5</b>
2.1 Noncanonical Hamiltonian Formalism and the Free Energy Principle . . . . .	5
2.1.1 Finite-Degree-of-Freedom Systems . . . . .	5
2.1.2 Fields . . . . .	8
2.2 Resonant Wave-Wave Interactions: Cherry's Example . . . . .	11
2.3 Implications of Chaotic Motion . . . . .	14
<b>3. Counterstreaming Ions: Basic Development</b>	<b>17</b>
3.1 Linear Analysis . . . . .	18
3.2 Hamiltonian Development . . . . .	21
3.2.1 Hamiltonian Structure . . . . .	21
3.2.2 Reduction to Normal-Mode Variables . . . . .	24
3.2.3 Nonlinear Coupling . . . . .	29

3.3	Corrections to the Fluid Theory . . . . .	31
3.3.1	Collisions . . . . .	31
3.3.2	Landau Damping . . . . .	31
<b>4.</b>	<b>Resonances and Nonlinear Instability</b>	<b>33</b>
4.1	Introduction . . . . .	33
4.2	Phase Space Structure: Single Resonance . . . . .	35
4.2.1	Two-Wave Interactions . . . . .	38
4.2.2	Three-Wave Interactions . . . . .	46
4.3	Multiple Resonances and Chaos . . . . .	55
4.3.1	General Discussion . . . . .	57
4.3.2	Multiple Resonances in the Beam Problem . . . . .	58
<b>5.</b>	<b>Numerical Method</b>	<b>60</b>
5.1	Symplectic Integration . . . . .	60
5.2	Symplectic Runge-Kutta . . . . .	61
5.3	Lie Transformations . . . . .	62
5.3.1	Introduction . . . . .	62
5.3.2	Application to a Simple Example . . . . .	67
<b>6.</b>	<b>Numerical Results: Explosive Instability and Two-Wave Inter-</b>	
	<b>actions</b>	<b>71</b>
6.1	Integrable Cases . . . . .	72
6.1.1	Positive Energy Resonance . . . . .	72
6.1.2	Negative Energy Resonance . . . . .	76
6.2	Nonintegrability: Two Degrees of Freedom . . . . .	79
6.2.1	Two Positive Energy Resonances . . . . .	79

6.2.2	One Positive Energy and One Negative Energy Resonance	84
6.3	Chaotic Transport in Three Degrees of Freedom . . . . .	89
<b>7.</b>	<b>Effect of Three-Wave Positive Energy Resonance</b>	<b>101</b>
7.1	Introduction . . . . .	101
7.2	Six-Wave Hamiltonian . . . . .	104
7.3	Two Degrees of Freedom . . . . .	107
7.3.1	Two Positive Energy Resonances . . . . .	108
7.3.2	One Positive Energy and One Negative Energy Resonance	109
7.4	Three Degrees of Freedom . . . . .	113
<b>8.</b>	<b>Conclusions</b>	<b>125</b>
<b>A.</b>	<b>Transformation of the Bracket</b>	<b>128</b>
<b>B.</b>	<b>Diagonalization of <math>\delta^2 F</math></b>	<b>130</b>
<b>C.</b>	<b>Nonlinear Stability for Three-Wave Interactions</b>	<b>135</b>
<b>D.</b>	<b>Numerical Algorithm for the Five-Wave and Six-Wave Hamil-</b>	
<b>tonians</b>		<b>140</b>
D.1	Transformation to Computational Variables . . . . .	140
D.2	Derivation of the Algorithm . . . . .	142
	<b>BIBLIOGRAPHY</b>	<b>146</b>
	Vita	

## List of Tables

5.1	Transformations of $(p, q)$ generated by $e^{f \cdot \cdot}$ for various $f$ . . . .	66
-----	--	----

## List of Figures

2.1	Surfaces of section for Cherry's Hamiltonian, for the resonant ( $2\omega_1 = \omega_2$ ) and nonresonant ( $2\omega_1 \neq \omega_2$ ) cases. (a) $q_1 = 0$ plane. (b) $q_2 = 0$ plane. . . . .	13
3.1	Dispersion relation $\omega(k)$ for the cases (a) $v < 1$ , where negative energy modes (branches 3 and 4) are linearly unstable for long wavelengths, and (b) $v > 1$ , where all modes are linearly stable.	20
4.1	Locations in $(k_1, v)$ -space of all three-wave resonances involving mode numbers up to $m = 10$ for (a) decay instability and (b) explosive instability. . . . .	36
4.2	Three modes which form two near-resonant doublets. . . . .	39
4.3	Phase space topology for two-wave decay instability described by Hamiltonian (4.12) with $\Lambda = 100$ , $v = 1.4796$ , $\bar{I}_3 = 0.01$ and (a) $L = 1000$ ; (b) $L = 5000$ . . . . .	43
4.4	Phase space topology for two-wave decay instability described by Hamiltonian (4.21) with $\Lambda = 100$ , $v = 1.4796$ , $\tilde{I}_3 = 0.02$ and (a) $L = 5000$ ; (b) $L = 10000$ . . . . .	45
4.5	Three modes which form a negative energy resonance. . . . .	46
4.6	Phase space plots for Hamiltonian (4.28) with $\bar{I}_4 = \bar{I}_5 = 0$ . $\Lambda = 100$ , $L = 5000$ , and (a) $v = 1.47959435$ ( $\bar{\Omega}_3 = 0$ ); (b) $v = 1.47959256$ ( $\bar{\Omega}_3 \neq 0$ ). . . . .	49

4.7	Phase space plots for Hamiltonian (4.28) with $\bar{I}_4 = 1.0$ and $\bar{I}_5 = 0$ . $\Lambda = 100$ , $L = 5000$ , and (a) $v = 1.47959435$ ( $\frac{\bar{\Omega}_3}{\gamma} = 0$ ); (b) $v = 1.47959256$ ( $\frac{\bar{\Omega}_3}{\gamma} = 0.2121$ ); (c) $v = 1.479591$ ( $\frac{\bar{\Omega}_3}{\gamma} = 0.4044$ ).	51
4.8	Phase space plots for Hamiltonian (4.28) with $\bar{I}_4 = \bar{I}_5 = 1.0$ . $\Lambda = 100$ , $L = 5000$ , and (a) $v = 1.47959435$ ( $\frac{\bar{\Omega}_3}{\gamma} = 0$ ); (b) $v = 1.47959256$ ( $\frac{\bar{\Omega}_3}{\gamma} = 0.2121$ ); (c) $v = 1.479589$ ( $\frac{\bar{\Omega}_3}{\gamma} = 0.6459$ ).	52
4.9	Three modes which form a positive energy resonance. . . . .	53
4.10	Phase space topology for three-wave decay instability described by Hamiltonian (4.33), with $\bar{\Omega}_4 = 0$ and (a) $\bar{I}_7 = 0$ ; (b) $\bar{I}_7 \neq 0$ .	56
6.1	Numerical results for the Hamiltonian (4.12) with $\Lambda = 100$ , $L = 5000$ , $v = 1.4796$ , using (a) Runge-Kutta, and (b) Lie transformations. . . . .	74
6.2	Long-time computation of a single invariant curve of Figure 6.1.b for timestep $dt = 1.0$ , by (a) Runge-Kutta, and (b) Lie transformations, using 14-digit algebra. In each case the left-hand figure shows the curve plotted up to $t = 2000$ , and the right-hand figure shows superimposed on this the curve plotted for $998,000 < t < 1,000,000$ . . . . .	75
6.3	Numerical results for the Hamiltonian (6.7) with $\Lambda = 100$ , $L = 5000$ and $v = 1.47959256$ ( $\bar{\Omega}_3 \neq 0$ ), using (a) Runge-Kutta, and (b) Lie transformations. . . . .	77
6.4	Numerical results for the Hamiltonian (6.7) with $\Lambda = 100$ , $L = 5000$ and $v = 1.47959435$ ( $\bar{\Omega}_3 = 0$ ) using (a) Runge-Kutta, and (b) Lie transformations. . . . .	78



6.5	$\bar{P}_2 = 0$ surface-of-section plots for Hamiltonian (6.11), with (a) $L = 2500$ ; (b) $L = 5000$ ; (c) $L = 9000$ . Each orbit was started with $\bar{Q}_2 = 10^{-6}$ , so that each corresponds to a different value of $\bar{H}$ . . . . .	83
6.6	Four modes comprising one negative energy resonance and one positive energy near-resonance. . . . .	85
6.7	Surface-of-section plots for Hamiltonian (6.16), for (a) $L = 2500$ , (b) $L = 5000$ and (c) $L = 9000$ . . . . .	88
6.8	Five modes comprising a negative energy resonance and two positive energy near-resonances. . . . .	89
6.9	Phase space diffusion in three degrees of freedom, with $L = 5000$ and $\bar{Q}_3(0) = -0.16$ . Escape occurs at $t = 1279$ . . . . .	94
6.10	Phase space diffusion with $L = 5000$ and $\bar{Q}_3(0) = -0.14$ . Escape had not yet occurred at $t = 100,000$ . . . . .	95
6.11	Phase space diffusion with $L = 10000$ and $\bar{Q}_3(0) = -0.08$ . Escape occurs at $t = 38,144$ . . . . .	96
6.12	Phase space diffusion with $L = 10000$ and $\bar{Q}_3(0) = -0.07$ . Escape occurs at $t = 59,940$ . . . . .	97
6.13	Phase space diffusion with $L = 10000$ and $\bar{Q}_3(0) = -0.06$ . Escape had not yet occurred at $t = 100,000$ . . . . .	98
7.1	Six modes which can form one explosively unstable triplet, one resonant decay triplet and one nearly resonant doublet. . . . .	102

7.2	Locations in parameter space of three-wave resonances involving the modes of Figure 7.1, with various modenumbers including (a) $m_2 = 2$ and (b) $m_2 = 3$ . Solid lines indicate resonance between $J_2, J_3$ and $J_6$ and are labelled with $m_6$ ; dashed lines indicate resonance between $J_2, J_4$ and $J_5$ and are labelled with $m_5$ . . . .	103
7.3	$\bar{P}_1 = 0$ surface-of-section plots for Hamiltonian (7.12) with $\bar{\Omega}_2 = 0$ . (a) $L = 2500$ ; (b) $L = 5000$ . . . . .	110
7.4	$\bar{P}_1 = 0$ surface-of-section plots for Hamiltonian (7.15) with $\bar{\Omega}_2 = 0$ . (a) $L = 2500$ ; (b) $L = 5000$ ; (c) $L = 9000$ . . . . .	112
7.5	Phase space diffusion with $L = 2500$ and $\bar{Q}_3(0) = 0.32$ . Escape occurs at $t = 68,439$ . . . . .	115
7.6	Phase space diffusion with $L = 2500$ and $\bar{Q}_3(0) = 0.30$ . Escape occurs at $t = 23,221$ . . . . .	116
7.7	Phase space diffusion with $L = 2500$ and $\bar{Q}_3(0) = 0.28$ . Escape occurs at $t = 53,699$ . . . . .	117
7.8	Phase space diffusion with $L = 2500$ and $\bar{Q}_3(0) = 0.26$ . No overall growth in $\bar{I}_3$ was visible at $t = 100,000$ . . . . .	118
7.9	Phase space diffusion with $L = 5000$ and $\bar{Q}_3(0) = 0.13$ . Escape occurs at $t = 13,116$ . . . . .	119
7.10	Phase space diffusion with $L = 5000$ and $\bar{Q}_3(0) = 0.12$ . Escape occurs at $t = 158,316$ . . . . .	120
7.11	Phase space diffusion with $L = 5000$ and $\bar{Q}_3(0) = 0.11$ . No overall growth in $\bar{I}_3$ was visible at $t = 500,000$ . . . . .	121

7.12	Phase space diffusion with $L = 9000$ and $\bar{Q}_3(0) = 0.08$ . Escape occurs at $t = 43,235$ . . . . .	122
7.13	Phase space diffusion with $L = 9000$ and $\bar{Q}_3(0) = 0.07$ . Escape occurs at $t = 561,316$ . . . . .	123
7.14	Phase space diffusion with $L = 9000$ and $\bar{Q}_3(0) = 0.06$ . No overall growth in $\bar{I}_3$ was visible at $t = 600,000$ . . . . .	124

# Chapter 1

## Introduction

In this paper we discuss the effect of negative energy waves and intrinsic chaos on the nonlinear stability of plasma systems. Many plasma equilibria that appear stable by a linear analysis can contain negative energy modes [1, 2, 3]. If dissipation occurs, these negative energy modes become unstable as they give up energy; in the dissipationless case, nonlinear instability may occur via resonant coupling to positive energy modes. The growth of negative energy waves from dissipation or resonant wave-wave coupling is well known in plasma and beam physics [4, 5, 6, 7, 8, 9, 10, 11]. Here we will consider wave-wave interactions in dissipationless systems, which may be described via a Hamiltonian formulation.

Analytical treatments of coherent wave-wave interactions often proceed by considering a single wave triplet, whose component waves interact via a single nonlinear term in the Hamiltonian [5, 12]. This formulation may be arrived at by averaging, where non-resonant nonlinear terms are assumed fast-varying compared to the single resonant or near-resonant term, and are therefore dropped. Such a Hamiltonian is integrable, so that the wave amplitudes and phases may be described exactly as a function of time. When appropriate resonance conditions are satisfied, coupling between waves of positive and negative energy results in explosive growth (infinite amplitude in a finite time) for arbitrarily small perturbations, while coupling between waves of

the same energy sign results in growth to a finite amplitude (decay instability), limited by energy conservation. When the resonance is “detuned”, the equilibrium becomes stable to infinitesimal perturbations, with growth occurring for modes above some critical amplitude (outside a separatrix in phase space). Growth rates and critical amplitudes for growth may be calculated exactly in the integrable case.

It is often the case that more than one nonlinear term in the Hamiltonian is nearly resonant and should be retained. This will in general result in a nonintegrable system [13, 14, 15]. In this case the motion cannot be described analytically, and some invariant surfaces in the phase space will be replaced by regions of chaotic motion. Chaos originates in the vicinity of separatrices between different types of phase space trajectories, so that in the case of a detuned resonance we expect destruction of the separatrix between stable and unstable motion, and therefore a change in the effective size of the stable region. If the system is nearly integrable, most of the invariant curves within the stable region will remain intact. For a two-degree-of-freedom Hamiltonian (i.e., some number of modes coupled by only two nonlinear terms), these invariant curves provide absolute barriers to transport in the phase space, and the system will be absolutely stable for small enough perturbations. If the system is very chaotic, most invariant curves within the stable region may be destroyed so that stability is effectively lost. For more than two degrees of freedom, the invariant surfaces are not of high enough dimensionality to partition the phase space, so that even in a nearly integrable system transport may occur across unlimited regions of phase space [16]. Thus waves whose amplitudes are initially well within a “stable” region may experience relatively slow growth until

they reach sufficient amplitude for instability to occur. This process (Arnold diffusion) is generally quite slow; faster “thick layer” diffusion will occur if most of the invariant surfaces are destroyed [17].

In general, therefore, for a system with negative energy modes, one might expect lack of long-term stability to be the rule. Our goal in this work is to see what type of transport occurs and to determine the relevant time scales for a simple example.

The paper is organized as follows. Chapter 2 contains a review of some relevant background material. Section 2.1 discusses the noncanonical Hamiltonian formalism which will be used to describe our plasma model, and describe the free energy principle which yields a generalized definition of negative energy modes and a criterion for nonlinear stability [18, 19]. In Section 2.2 we discuss a simple Hamiltonian due to Cherry, which is linearly stable but exhibits explosive instability via nonlinear wave-wave coupling [20, 21]. Section 2.3 examines the effect of chaotic motion in such a system. In Chapter 3 we describe the physical system that was studied and the fluid model that was used to describe it. In Sections 3.1 and 3.2 the system’s energy is described by a Hamiltonian functional, and the equations of motion found from the corresponding noncanonical bracket. We describe the reduction to normal-mode variables. Section 3.3 addresses the effects of collisions and Landau damping, which are not included in the fluid theory [22]. In Chapter 4 we discuss the resonance properties arising from nonlinear interactions between the normal modes, and how chaotic motion arises. In Chapter 5 we discuss the numerical method used. Section 5.1 discusses symplectic integration algorithms in general [23], Section 5.2 describes the symplectic Runge-Kutta algorithm [24] and Section 5.3 fo-

cuses on Lie transformations and on methods of obtaining explicit polynomial expressions for the time-advanced dynamical variables [25, 26, 27, 28, 29]. In Chapters 6 and 7 we present numerical results for a number of relevant systems described by Hamiltonians of one, two and three degrees of freedom. We demonstrate the role of chaotic diffusion in destabilizing such systems. Chapter 8 provides a summary and conclusions.

## Chapter 2

### Background

#### 2.1 Noncanonical Hamiltonian Formalism and the Free Energy Principle

We will be investigating a Hamiltonian system with a noncanonical Hamiltonian structure. This is the natural framework for a system described in terms of Eulerian variables. Here we will review the noncanonical formalism for both finite-degree-of-freedom systems and for fields [18], and we discuss the free energy principle and the related concept of negative energy modes [19] which will determine the stability of our system.

##### 2.1.1 Finite-Degree-of-Freedom Systems

We consider first an  $M$ -degree-of-freedom Hamiltonian system where the dynamical variables are given by the vector  $\mathbf{z} \equiv (z^1, \dots, z^M)$ . Such a system is defined by a Hamiltonian function  $H$  and a Poisson bracket  $\{, \}$  with the time evolution of the dynamical variables given by Hamilton's equations:

$$\dot{z}^i = \{z^i, H\} = J^{ij} \frac{\partial H}{\partial z^j}, \quad i = 1, \dots, M \quad (2.1)$$

where the Poisson bracket is defined by

$$\{F, G\} \equiv \frac{\partial F}{\partial z^i} J^{ij} \frac{\partial G}{\partial z^j} \quad (2.2)$$

for any functions  $F$  and  $G$  of the phase space variables. (Here we sum repeated indices from 1 to  $M$ .) The Poisson bracket must satisfy the following algebraic



properties:

$$\begin{aligned}
\{\alpha F + \beta G, K\} &= \alpha\{F, K\} + \beta\{G, K\}, \\
\{F, G\} &= -\{G, F\}, \\
\{FG, K\} &= F\{G, K\} + \{F, K\}G, \\
\{\{F, G\}, K\} + \{\{K, F\}, G\} + \{\{G, K\}, F\} &= 0,
\end{aligned} \tag{2.3}$$

where  $\alpha$  and  $\beta$  are arbitrary constants.

A special case is the canonical one [30] where the  $M$  dynamical variables split into  $N$  configuration variables and  $N$  momenta:

$$\mathbf{z} \equiv (q_1, \dots, q_N, p_1, \dots, p_N) \tag{2.4}$$

and the Poisson bracket has the form

$$[F, G] \equiv \frac{\partial F}{\partial z^i} J_c^{ij} \frac{\partial G}{\partial z^j}, \tag{2.5}$$

where the constant matrix

$$\mathbf{J}_c \equiv \begin{bmatrix} 0_N & I_N \\ -I_N & 0_N \end{bmatrix} \tag{2.6}$$

is known as the cosymplectic form. ( $I_N$  and  $0_N$  are the  $N \times N$  unit and zero matrices.) Hamilton's equations (2.1) then take the familiar form

$$\begin{aligned}
\dot{q}_i &= \frac{\partial H}{\partial p_i}, \\
\dot{p}_i &= -\frac{\partial H}{\partial q_i}.
\end{aligned} \tag{2.7}$$

In the general (noncanonical) case,  $J^{ij}$  may be odd-dimensional and may be a function of the  $z^i$ . An important property of noncanonical brackets is the existence of Casimir invariants, which commute with any function of the dynamical variables  $z^i$ :

$$\{C, F(z)\} = 0. \tag{2.8}$$

Since  $F$  is arbitrary, we see from Eq. (2.2) that

$$J^{ij} \frac{\partial C}{\partial z^j} = 0, \quad i = 1, \dots, M. \quad (2.9)$$

This linear system clearly has nontrivial (non-constant) Casimir solutions only if

$$\det(J^{ij}) = 0. \quad (2.10)$$

Since the cosymplectic form (2.6) has determinant 1, the canonical bracket has no nontrivial Casimir invariants. For noncanonical brackets, the Casimirs label “leaves” in phase space upon which trajectories are constrained to lie.

Consider perturbations about an equilibrium  $z_e$  given by  $\frac{\partial F}{\partial z^i} = 0$ . The changes in  $H$  and any  $C$  under a small perturbation  $\delta z$  are

$$\Delta H = H(z_e + \delta z) - H(z_e) = \frac{\partial H}{\partial z^i} \delta z^i + \frac{1}{2} \frac{\partial^2 H}{\partial z^i \partial z^j} \delta z^i \delta z^j + \dots, \quad (2.11)$$

$$\Delta C = C(z_e + \delta z) - C(z_e) = \frac{\partial C}{\partial z^i} \delta z^i + \frac{1}{2} \frac{\partial^2 C}{\partial z^i \partial z^j} \delta z^i \delta z^j + \dots. \quad (2.12)$$

For perturbations with  $\Delta C = 0$ , we can add  $\sum \lambda_i \Delta C_i$  (where the  $\lambda_i$  are arbitrary real constants) to  $\Delta H$  to obtain the energy change at constant Casimir:

$$\Delta H|_C = \frac{1}{2} \delta^2 (H + \sum_{i=1}^M \lambda_i \Delta C_i) \equiv \delta^2 F, \quad (2.13)$$

where we have defined the “free energy”

$$F \equiv H + \sum \lambda_i C_i. \quad (2.14)$$

We see that  $\delta^2 F$  gives the energy change under perturbations which conserve the Casimir constraints. Different values of  $\lambda_i$  label different equilibria.

If an equilibrium is such that  $\delta^2 F$  is of definite sign for all perturbations, then nearby surfaces of constant  $F$  are topologically spheres and the

equilibrium is stable. If  $\delta^2 F$  is indefinite, then the system may be spectrally unstable, or if spectrally stable, then it possesses modes of both “positive energy” and “negative energy”. This may be taken as a general definition of a negative energy mode. Note that since energy is not a covariant quantity, we must require that  $\delta^2 F$  must be indefinite in *any* reference frame.

In the theory of dielectric media the energy content of a linear wave is defined as the work done by an external agent in exciting the wave, and is given by [31]

$$\mathcal{E} = \frac{\partial}{\partial \omega}(\omega \varepsilon) |E|^2 = \omega \frac{\partial \varepsilon}{\partial \omega} |E_k|^2 \quad (2.15)$$

where  $\varepsilon(k, \omega)$  is the dielectric function,  $E_k$  is the electric field strength for the mode of wavenumber  $k$  and  $\omega(k)$  is the frequency as found from the zeroes of  $\varepsilon(k, \omega)$ . The energy signature is given by  $\text{sgn}(\omega \frac{\partial \varepsilon}{\partial \omega})$ , so that waves of both negative and positive energy are possible. A negative energy wave is one such that the total energy of the system is lower in the presence of the excitation. Our previous definition of negative energy waves via  $\delta^2 F$  agrees with the definition from dielectric theory, and provides a generalization which is valid for systems where the dielectric function is not defined or is difficult to calculate.

It is conjectured that systems with indefinite  $\delta^2 F$  are generically unstable, via either dissipation or nonlinear resonance [19]. In following sections we will examine the role of resonant wave-wave interactions in a dissipationless plasma physics example.

### 2.1.2 Fields

The ideas just discussed are readily extended to the case of fields [18]. In this case the state of the system is specified by the field variables  $\psi^i$ ,

$i = 1, \dots, M$ . The time evolution is determined by a Hamiltonian functional  $H$  and a Poisson bracket

$$\{F, G\} = \int d\tau \frac{\delta F}{\delta \psi^i} \mathcal{O}^{ij} \frac{\delta G}{\delta \psi^j}, \quad (2.16)$$

where  $\mathcal{O}$  is an operator (possibly a function of the  $\psi^i$ ) making the bracket satisfy the properties (2.3), and  $d\tau$  is the volume element. The equations of motion are

$$\dot{\psi}^i = \{\psi^i, H\} = \mathcal{O}^{ij} \frac{\delta H}{\delta \psi^j}, \quad i = 1, \dots, M. \quad (2.17)$$

For a canonical field theory the dynamical variables split into  $N$  configuration variables  $\eta^i$  and  $N$  momenta  $\pi^i$ . In this case the operator  $\mathcal{O}$  is the  $2N \times 2N$  constant matrix

$$\mathcal{O}_c = \begin{bmatrix} 0_N & I_N \\ -I_N & 0_N \end{bmatrix}, \quad (2.18)$$

giving for the Poisson bracket

$$\{F, G\} = \sum_{i=1}^N \int d^3x \left[ \frac{\delta F}{\delta \eta^i} \frac{\delta G}{\delta \pi^i} - \frac{\delta G}{\delta \eta^i} \frac{\delta F}{\delta \pi^i} \right]. \quad (2.19)$$

Hamilton's equations take the form

$$\begin{aligned} \dot{\eta}^i &= \{\eta^i, H\} = \frac{\delta H}{\delta \pi^i}, \\ \dot{\pi}^i &= \{\pi^i, H\} = -\frac{\delta H}{\delta \eta^i}. \end{aligned} \quad (2.20)$$

For the noncanonical case we again have some number  $P$  (possibly infinite) of Casimir invariants satisfying

$$\{C_k, F(\psi)\} = 0, \quad k = 1, \dots, P. \quad (2.21)$$

We can then find equilibria corresponding to extremals of the free energy functional

$$F = H + \sum_{k=1}^P \lambda_k C_k, \quad (2.22)$$

i.e., the Hamiltonian subject to the constraints of constant Casimirs. By definition, equilibria satisfy

$$\dot{\psi}^i = 0, \quad i = 1, \dots, M. \quad (2.23)$$

Since we have

$$\dot{\psi}^i = \{\psi^i, F\} = \{\psi^i, H\} = \mathcal{O}^{ij} \frac{\delta F}{\delta \psi^j}, \quad (2.24)$$

we see that the equilibrium equations are

$$\frac{\delta F}{\delta \psi^i} = 0, \quad i = 1, \dots, M. \quad (2.25)$$

Now suppose that  $\psi_e^i$  are solutions of (2.25). Then the first variation of  $F$  in the direction  $\phi = (\phi^1, \dots, \phi^M)$ , denoted  $DF \cdot \phi$ , is given by

$$\delta F \equiv \frac{d}{d\epsilon} F(\psi + \epsilon\phi)|_{\epsilon=0} \equiv DI \cdot \phi \equiv \int d\tau \frac{\delta F}{\delta \psi^i} \phi^i. \quad (2.26)$$

Eq. (2.25) implies that  $DF \cdot \phi = 0$  for all  $\phi$ . A second variation at fixed  $\phi$  yields

$$\delta^2 F \equiv \frac{d}{d\epsilon} DF(\psi + \epsilon\phi)|_{\epsilon=0} \equiv D^2 F(\psi) \cdot \phi^2 \equiv \int d\tau \phi^i \frac{\delta^2 F}{\delta \psi^i \delta \psi^j} \phi^j. \quad (2.27)$$

Now analogous to the finite-dimensional case, definite  $\delta^2 F$  implies stability, while indefinite  $\delta^2 F$  implies either linear instability or the existence of negative energy modes.

## 2.2 Resonant Wave-Wave Interactions: Cherry's Example

When a linearly stable system has indefinite  $\delta^2 F$ , then it contains (by the definition in Section 2.1) negative energy modes. These negative energy modes may lead to instability by way of nonlinear mode coupling. A simple example for which this occurs is described by Cherry's Hamiltonian [20, 21]:

$$\begin{aligned} H &= \frac{\omega_1}{2}(p_1^2 + q_1^2) - \frac{\omega_2}{2}(p_2^2 + q_2^2) + \alpha [2q_1 p_1 p_2 - q_2(q_1^2 - p_1^2)] \\ &= \omega_1 J_1 - \omega_2 J_2 + \alpha J_1 \sqrt{J_2} \sin(2\theta_1 + \theta_2) \end{aligned} \quad (2.28)$$

where the second form comes from the transformation  $q_i = \sqrt{2J_i} \sin \theta_i$ ,  $p_i = \sqrt{2J_i} \cos \theta_i$ . This Hamiltonian describes, for example, a particle in an inverted harmonic potential  $V = -(x^2 + y^2)/2$  whose motion is stabilized by a uniform magnetic field  $B_z$  [19]. We will see in Section 4.2 that a Hamiltonian describing three-wave interactions in a plasma,

$$H = \omega_1 J_1 - \omega_2 J_2 - \omega_3 J_3 + \alpha \sqrt{J_1 J_2 J_3} \sin(\theta_1 + \theta_2 - \theta_3), \quad (2.29)$$

may also be written in the form (2.28) by a canonical transformation of variables.

The system (2.28) has an equilibrium point at  $q_1 = p_1 = q_2 = p_2 = 0$ , satisfying  $\frac{\partial H}{\partial z_i} = 0$ . Linear stability is guaranteed by the  $\omega_i$  being real; this linear motion is just that of two harmonic oscillators. Nonlinear stability requires definiteness of the matrix  $\frac{\partial^2 H}{\partial z_i \partial z_j}$  evaluated at the equilibrium. This matrix has the (doubly degenerate) eigenvalues  $(\omega_1, -\omega_2)$ ; since there are both positive and negative eigenvalues, the stability is indefinite. It turns out that

an explosive instability arises from the nonlinear coupling term when the third-order resonance condition  $2\omega_1 = \omega_2$  is satisfied (the case studied by Cherry). Cherry found the two-parameter solution set

$$\begin{aligned} q_1 &= \frac{\sqrt{2}}{\epsilon - \alpha t} \sin(\omega_1 t + \gamma), \\ p_1 &= \frac{\sqrt{2}}{\epsilon - \alpha t} \cos(\omega_1 t + \gamma), \\ q_2 &= \frac{1}{\epsilon - \alpha t} \sin(2\omega_1 t + 2\gamma), \\ p_2 &= \frac{1}{\epsilon - \alpha t} \cos(2\omega_1 t + 2\gamma), \end{aligned}$$

where  $\epsilon$  and  $\gamma$  are constants determined by the initial conditions. Thus the amplitudes go to infinity at a finite time  $t_0 = \epsilon/\alpha$ .

What happens when the resonance condition is not satisfied? Since the Hamiltonian (2.28) is integrable (possessing the constant of motion  $I = J_1 - 2J_2$ ), we can describe the motion exactly. When  $2\omega_1 \neq \omega_2$ , the nonlinear coupling term leads to explosive instability only for waves above some critical amplitude. This can be illustrated graphically by surface-of-section plots of the phase space, which consists of plotting two of the dynamical variables for a fixed value of one of the others. (The value of the remaining variable is fixed by the constancy of  $H$ .) For example, we can plot (analytically)  $q_1$  vs.  $p_1$  for the surface  $q_2 = 0$ , or  $q_2$  vs.  $p_2$  for the surface  $q_1 = 0$ . (Equivalently, a canonical transformation could be used to reduce the Hamiltonian to one degree of freedom, so that there would be only two variables left to plot.) The  $q_1 = 0$  and  $q_2 = 0$  surfaces are shown in Figure 2.1, for both the resonant ( $2\omega_1 = \omega_2$ ) and nonresonant ( $2\omega_1 \neq \omega_2$ ) cases. When the resonance is detuned we see the

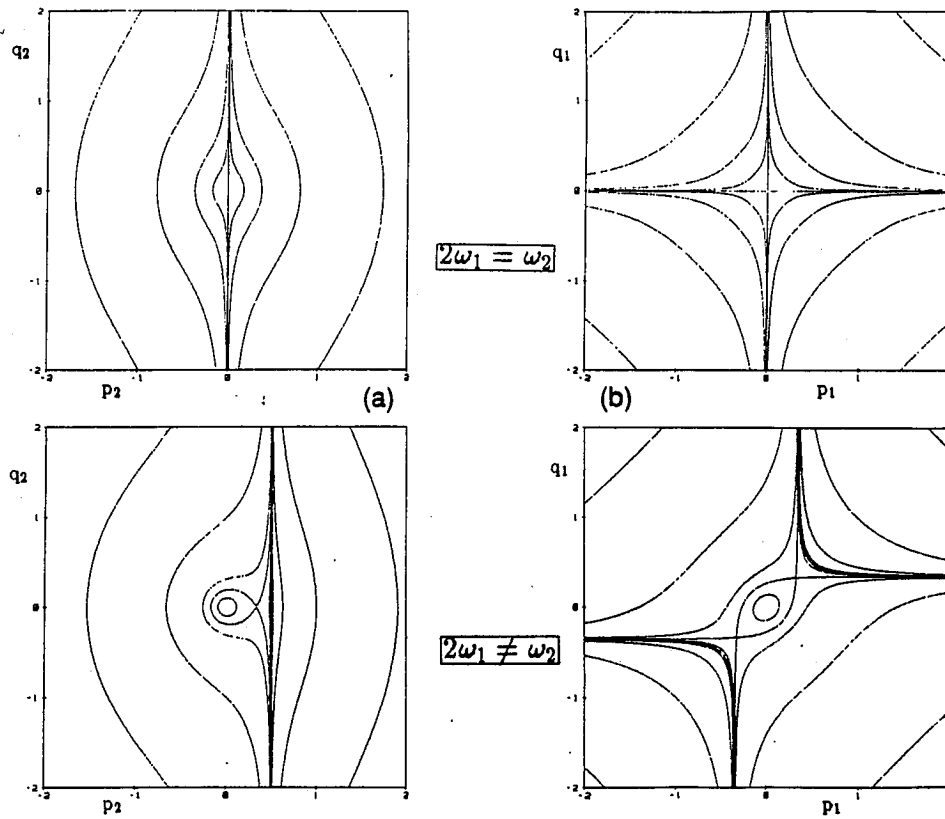


Figure 2.1: Surfaces of section for Cherry's Hamiltonian, for the resonant ( $2\omega_1 = \omega_2$ ) and nonresonant ( $2\omega_1 \neq \omega_2$ ) cases. (a)  $q_1 = 0$  plane. (b)  $q_2 = 0$  plane.



opening of a stable islet, bounded by a separatrix. For this integrable system, motion within the separatrix is absolutely stable.

### 2.3 Implications of Chaotic Motion

If Hamiltonian (2.28) is perturbed by adding other nonlinear terms, then the integrability will in general be destroyed [32]. Using the constant of motion  $I$ , the Hamiltonian (2.28) can be reduced to a one-degree-of-freedom system. One additional nonlinear term will in general result in a system that can be reduced to two degrees of freedom, with  $I \neq$  constant. In this case we can again employ surface-of-section plots, like those of Figure 2.1. While the curves of Figure 2.1 were calculated analytically, in a nonintegrable system the orbits must be followed numerically, and points plotted as the orbits pass through the desired plane.

The nonintegrable Hamiltonian would yield surfaces-of-section like those of Figure 2.1, but with invariant curves replaced by chaotic orbits in some regions of the phase space. These chaotic orbits will occur in the vicinity of separatrices that separate different types of motion [13, 14, 15]. The portion of the phase space containing these chaotic orbits may range from very large to very small, depending on the perturbation. Even in a nearly integrable system, most of whose invariant surfaces are intact, the chaotic layers are found arbitrarily close to any point, but their extent vanishes exponentially with the perturbation.

If the perturbation is very strong, then most of the invariant curves within the stable islet may be destroyed, so that an orbit starting within that region is not prevented from increasing in amplitude until it is of sufficient

size for explosive instability to occur. For a two-degree-of-freedom system, the remaining invariant curves will provide boundaries for the motion, so that any surviving invariant curve around the equilibrium point will ensure stability for all orbits within it. If the perturbation is weak enough, then most of the invariant surfaces will survive, and the (very thin) chaotic layers within the stable islet will be bounded by the invariant surfaces that surround them.

If the perturbation is such that the reduced Hamiltonian has three or more degrees of freedom, then the situation is much different. Again, depending upon the form of the nonlinear terms, the motion may be either very regular or very chaotic. However, the high dimensionality of the phase space now allows a new type of behavior. For a two-degree-of-freedom Hamiltonian, we have a four-dimensional phase space. By the constancy of  $H$ , the motion is confined to a three-dimensional "energy surface" in phase space. The invariant surfaces for an  $N$ -degree-of-freedom Hamiltonian are also  $N$ -dimensional, so that the two-dimensional surfaces around the equilibrium point can partition the three-dimensional energy surface into an "inside" and an "outside", bounding the small-amplitude motion. For a three-degree-of-freedom Hamiltonian, the motion is on a five-dimensional energy surface, while the invariant surfaces are only three-dimensional. Three-dimensional surfaces do not partition a five-dimensional space (just as a one-dimensional line does not partition a three-dimensional space) and therefore chaotic orbits near the equilibrium point are not necessarily confined there. In fact, it is conjectured that the chaotic layers in any Hamiltonian system of more than three degrees of freedom are interconnected in an "Arnold web", so that an orbit may get from any part of the energy surface to any other point on the energy surface by chaotic diffusion

along this web [33, 16, 17]. Therefore any trajectory not exactly on an invariant surface may eventually escape from the stable islet. This process is known as “Arnold diffusion”, and is a universal property of many-dimensional Hamiltonian systems. Arnold diffusion has been studied, for example, in connection with particle losses in high-energy accelerators [34], magnetic mirror machines [35] and tokamaks [36], and in the Earth’s geomagnetic field [37]. While the diffusion rate can be significant [36], in many situations it may be slower than any time scales of interest [38]. In some cases, additional phenomena (such as collisions) may combine with Arnold diffusion to increase its impact [35]. Of course, Arnold diffusion is a limiting case; while it can eliminate absolute stability in a Hamiltonian system, there may be much faster processes occurring in a very chaotic system, as we shall see.

## Chapter 3

### Counterstreaming Ions: Basic Development

As a physical example we now consider a simple one-dimensional plasma configuration consisting of two cold counterstreaming ion beams in a neutralizing isothermal electron background [8]. The system supports ion-acoustic oscillations of both positive and negative energy. While exponentially growing disturbances are possible, we will consider the case in which all modes are linearly stable. In this case we find the possibility of explosive instability due to resonant three-wave interactions. We will then examine the role of chaotic diffusion processes in enhancing the likelihood of these instabilities.

We begin by describing the fluid equations governing the system, and the characteristic modes of oscillation that arise from the linearized equations. Next we describe the Hamiltonian structure of the system, and from the energy functional we derive a Hamiltonian in action-angle variables for the lowest-order perturbed energy, which again yields the characteristic modes that were found in the linear analysis. We then calculate the next-order terms in the Hamiltonian, which provide the coupling between modes that leads to explosive instability. Finally we describe the phase space topology that results from the nonlinear interactions and indicate how chaotic diffusive processes arise, and how they are expected to influence the stability of the system.

### 3.1 Linear Analysis

The dimensionless equations of motion for the two ion streams are

$$\frac{\partial v_\alpha}{\partial t} + v_\alpha \frac{\partial v_\alpha}{\partial x} + \frac{\partial \phi}{\partial x} = 0, \quad (3.1)$$

$$\frac{\partial n_\alpha}{\partial t} + \frac{\partial}{\partial x} (n_\alpha v_\alpha) = 0, \quad (3.2)$$

where  $\alpha = \pm$  labels each ion stream with the sign of its velocity relative to the center-of-mass frame. Here the  $n_\alpha$  are normalized to the total unperturbed ion density  $n_0$ ,  $v_\alpha$  is in units of the ion sound speed  $c_s \equiv \sqrt{\frac{T}{m_i}}$ , the electric potential  $\phi$  is in units of  $T_e/e$  where  $T$  is the electron temperature in energy units,  $x$  is in units of the electron Debye length  $\lambda_d \equiv \sqrt{\frac{T_e}{4\pi n_0 e^2}}$  and time is in units of the inverse ion plasma frequency  $\omega_p^{-1} \equiv \sqrt{\frac{m_i}{4\pi n_0 e^2}}$ . These equations are supplemented with the isothermal ( $\frac{m_e}{m_i} \rightarrow 0$ ) approximation for the electron motion and Poisson's equation:

$$n_e = e^\phi, \quad (3.3)$$

$$-\frac{\partial^2 \phi}{\partial x^2} = n_+ + n_- - n_e, \quad (3.4)$$

where  $n_e$  is normalized to  $n_0$ . Through the latter two equations we can in principle solve for  $\phi(n_+, n_-)$  so that the entire system is described in terms of the dynamical variables  $n_\pm$  and  $v_\pm$ .

For simplicity we consider an equilibrium of ion streams of equal density and speed:

$$n_+ = n_- = \frac{1}{2},$$

$$v_+ = -v_- = v, \quad (3.5)$$

$$E = \phi = 0,$$

where the ion drift speed  $v$  is normalized to  $c_s$ . If we assume that perturbations have the dependence  $e^{i(kx-\omega t)}$  and linearize Eqs. (3.1)-(3.4), the condition for the resulting system to have non-trivial solutions is the vanishing of the dielectric function, given by

$$\varepsilon(k, \omega) \equiv 1 + \frac{1}{k^2} - \frac{1}{2} \left[ \frac{1}{(\omega - kv)^2} + \frac{1}{(\omega + kv)^2} \right] = 0. \quad (3.6)$$

(Here  $k$  is normalized to  $\lambda_d^{-1}$  and  $\omega$  to  $\omega_{pi}$ .) Solving for  $\omega$  we obtain

$$\omega^2 = k^2 \left[ \frac{1}{2(1+k^2)} + v^2 \pm \sqrt{\frac{1}{4(1+k^2)^2} + \frac{2v^2}{(1+k^2)}} \right]. \quad (3.7)$$

A plot of the four branches of  $\omega(k)$  is shown in Fig. 3.1 for the cases  $v > 1$  and  $v < 1$ . Taking the “+”-sign in Eq. (3.7) yields “fast modes”, with phase speed  $\omega/k$  greater than the drift speed  $v$ . These modes are always linearly stable ( $\omega$  real). The “-”-sign yields “slow modes” with  $\omega/k < v$ , which are linearly stable when  $v > \frac{1}{1+k^2}$ . (Recall that  $v$  is the ratio of the equilibrium ion drift speed to the ion sound speed, which is also the ratio of the equilibrium ion kinetic energy to the electron temperature). For  $v < 1$ , the slow modes become linearly unstable, via the well-known ion-ion two-stream instability, for small  $k$ . It should be noted that the linear stability criterion  $v > 1$  would be replaced by the more stringent criterion  $|v| \cos \theta > 1$  in a two-dimensional model, where  $\theta$  is the angle between  $\mathbf{k}$  and  $\mathbf{v}$ .

As discussed earlier, the energy signature of a wave is given by  $\omega \frac{\partial \varepsilon}{\partial \omega}$ . It is easily shown from Eqs. (3.6) and (3.7) that the fast modes have positive energy, while the slow modes are negative energy waves.

Before further discussing these characteristic modes, we examine the noncanonical Hamiltonian structure of this system, and re-derive the normal modes in the Hamiltonian formalism.

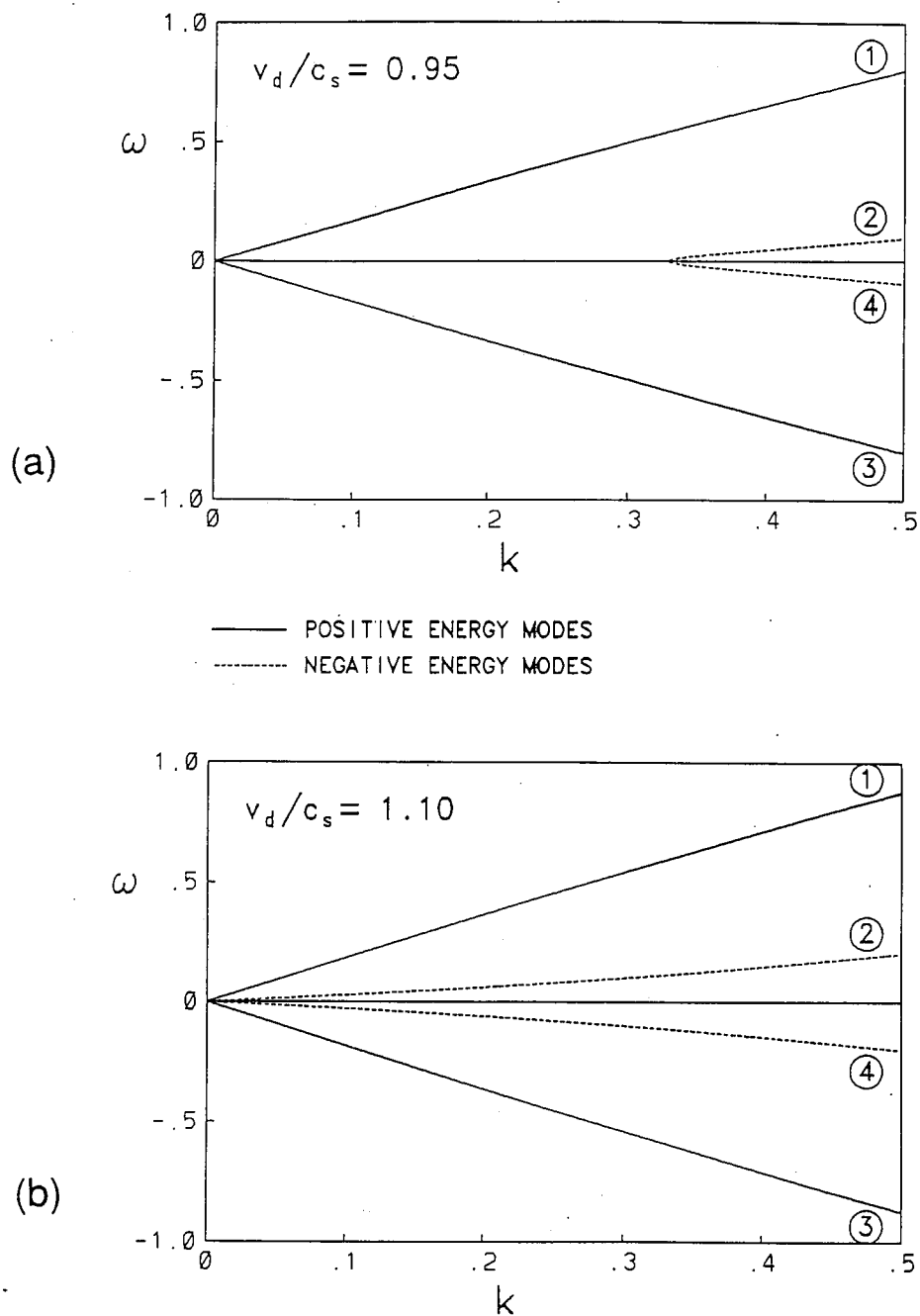


Figure 3.1: Dispersion relation  $\omega(k)$  for the cases (a)  $v < 1$ , where negative energy modes (branches 3 and 4) are linearly unstable for long wavelengths, and (b)  $v > 1$ , where all modes are linearly stable.

## 3.2 Hamiltonian Development

### 3.2.1 Hamiltonian Structure

The energy of this system can be written as the functional

$$H = \Lambda \int_0^L dx \left[ \frac{1}{2} n_+ v_+^2 + \frac{1}{2} n_- v_-^2 + \int_0^\phi d\phi \phi e^\phi + \frac{1}{2} \left( \frac{\partial \phi}{\partial x} \right)^2 \right] \quad (3.8)$$

where  $\Lambda = n_0 \lambda_d \gg 1$  is the (one-dimensional) plasma parameter,  $L$  is the size of the system in Debye lengths and  $H$  is normalized to the electron temperature. The first two terms are the ion kinetic energy densities, the third is the internal energy function for the electrons [39] and the fourth is the electric field energy. The electrons can be envisioned as supplying an effective ion pressure.

The appropriate Poisson bracket is given by [39]

$$\{\mathcal{F}, \mathcal{G}\} = \Lambda^{-1} \sum_{\alpha=\pm} \int_0^L dx \left[ \frac{\delta \mathcal{G}}{\delta v_\alpha} \frac{\partial}{\partial x} \frac{\delta \mathcal{F}}{\delta n_\alpha} - \frac{\delta \mathcal{F}}{\delta v_\alpha} \frac{\partial}{\partial x} \frac{\delta \mathcal{G}}{\delta n_\alpha} \right] \quad (3.9)$$

where  $\mathcal{F}$  and  $\mathcal{G}$  are functions of the  $n_\alpha$  and  $v_\alpha$ , and  $\frac{\delta f}{\delta u}$  denotes the variational derivative of  $f$  with respect to  $u$ . The Poisson bracket has units of  $(\text{energy} \times \text{time})^{-1} = \text{action}^{-1}$ ; consistent with our earlier normalizations we have written it in units of  $\omega_{pi} T_e^{-1}$ . The equations of motion (3.1) and continuity equations (3.2) are obtained from the usual formulae for time derivatives in terms of Poisson brackets:

$$\begin{aligned} \dot{n}_\alpha &= \{n_\alpha(x, t), H\} \\ &= \Lambda^{-1} \sum_{\alpha'=\pm} \int_0^L dx' \frac{\delta H}{\delta v_{\alpha'}} \frac{\partial}{\partial x'} \frac{\delta n_\alpha(x)}{\delta n_{\alpha'}(x')} \\ &= - \int_0^L dx' \frac{\partial}{\partial x'} (n_{\alpha'} v_{\alpha'}) \frac{\delta n_\alpha(x)}{\delta n_{\alpha'}(x')} \end{aligned}$$



$$\begin{aligned}
&= - \int_0^L dx' \frac{\partial}{\partial x'} (n_\alpha v_\alpha) \delta(x - x') \\
&= - \frac{\partial}{\partial x} (n_\alpha v_\alpha), \tag{3.10}
\end{aligned}$$

$$\begin{aligned}
\dot{v}_\alpha &= \{v_\alpha, H\} \\
&= -\Lambda^{-1} \int_0^L dx' \frac{\delta v_\alpha(x)}{\delta v_\alpha(x')} \frac{\partial}{\partial x'} \frac{\delta H}{\delta n_\alpha} \\
&= - \int_0^L dx' \delta(x - x') \frac{\partial}{\partial x'} \left( \frac{1}{2} v_\alpha^2 + \phi \right) \\
&= - \frac{\partial}{\partial x} \left( \frac{1}{2} v_\alpha^2 + \phi \right), \tag{3.11}
\end{aligned}$$

where we have used Poisson's equation (3.4) and the Boltzmann relation (3.3) in evaluating  $\frac{\delta H}{\delta n_\alpha}$  for the last equation.

The Poisson bracket has the Casimir invariants

$$\begin{aligned}
C_1^\pm &= \int_0^L dx n_\pm, \\
C_2^\pm &= \int_0^L dx v_\pm. \tag{3.12}
\end{aligned}$$

The physical significance of these Casimirs may be traced back to the kinetic theory describing this system. The basic (dimensionless) equations are the Vlasov-Poisson equations:

$$\begin{aligned}
\frac{\partial f}{\partial t} &= -v \frac{\partial f}{\partial x} + \frac{\partial \phi(f; x)}{\partial x} \frac{\partial f}{\partial v}, \\
\frac{\partial^2 \phi}{\partial x^2} &= - \int f dv \tag{3.13}
\end{aligned}$$

where  $f(x, v, t)$  is the phase space density for a single species. This system has the invariant

$$C = \int \mathcal{F}(f) dx dv \tag{3.14}$$

where  $\mathcal{F}$  is an arbitrary function; this invariant corresponds to conservation of phase space volume for a given value of  $f$  [40]. The correspondence between the fluid model and the Vlasov-Poisson system is made via the water-bag model [10]. This assumes the following form for  $f$ :

$$f(x, v) = \begin{cases} A & \text{for } v_- < v < v_+, \\ 0 & \text{otherwise} \end{cases} \quad (3.15)$$

where  $A = \text{constant}$ , and  $v_+$  and  $v_-$  are single-valued functions of  $x$  and  $t$ . We then obtain

$$\begin{aligned} n &= \int_{-\infty}^{\infty} f \, dv = A(v_+ - v_-), \\ v &= \frac{\int_{-\infty}^{\infty} v f \, dv}{\int_{-\infty}^{\infty} f \, dv} = \frac{1}{2}(v_+ + v_-) \end{aligned} \quad (3.16)$$

and

$$C = \int \mathcal{F}(A)[v_+ - v_-] \, dx. \quad (3.17)$$

Eq. (3.12) is implied by Eqs. (3.16) and (3.17). Thus the Casimir invariants correspond to the conservation of phase space volume that is required by Liouville's theorem in the Vlasov theory [41].

We now look at variations of the free energy functional

$$F = H + \lambda_1^+ C_1^+ + \lambda_1^- C_1^- + \lambda_2^+ C_2^+ + \lambda_2^- C_2^-. \quad (3.18)$$

The equilibrium (3.5) is obtained from the first variation of  $F$ :

$$\delta F = 0 \Rightarrow \left\{ \begin{array}{l} \frac{\delta F}{\delta n_{\pm}} = 0 \\ \frac{\delta F}{\delta v_{\pm}} = 0 \end{array} \right\} \Rightarrow \left\{ \begin{array}{l} \lambda_1^{\pm} = -\frac{1}{2}v^2 \\ \lambda_2^{\pm} = \mp \frac{1}{2}v \end{array} \right. \quad (3.19)$$

The Lagrange multipliers may be recognized as the kinetic energy and momentum of the two streams.

Stability is determined from the second variation, evaluated on the equilibrium:

$$\begin{aligned} \delta^2 F = \Lambda \frac{1}{2} \int_0^L dx & \left[ \frac{1}{2} (\delta v^+)^2 + \frac{1}{2} (\delta v^-)^2 \right. \\ & \left. + 2v \delta n^+ \delta v^+ - 2v \delta n^- \delta v^- + (\delta \phi_x)^2 + (\delta \phi)^2 \right] \end{aligned} \quad (3.20)$$

where  $\delta \phi_x$  denotes  $\frac{\partial}{\partial x} \delta \phi$ . Here we have expanded the exponential in the internal energy function, keeping second-order terms. The sign of  $\delta^2 F$  may be either positive or negative, depending on the perturbation; thus we may have either positive or negative energy waves in the system. It is important to note that, for this system,  $\delta^2 F$  is indefinite regardless of reference frame.

### 3.2.2 Reduction to Normal-Mode Variables

We now Fourier decompose the perturbations:

$$\begin{aligned} \delta n^\pm &= \sum_{m=-\infty}^{\infty} n_m^\pm e^{ik_m x}, \\ \delta v^\pm &= \sum_{m=-\infty}^{\infty} v_m^\pm e^{ik_m x}, \\ \delta \phi &= \sum_{m=-\infty}^{\infty} \phi_m e^{ik_m x}, \end{aligned} \quad (3.21)$$

where  $k_m \equiv mk_1$ , and  $k_1 \equiv \frac{2\pi}{L}$ . If we linearize Eqs. (3.3) and (3.4) about the equilibrium (expanding the exponential) and insert the Fourier expansions for  $\delta n^\pm$  and  $\delta \phi$ , we can solve for  $\phi_m(n_m^+, n_m^-)$ :

$$\begin{aligned} \phi_m = \frac{N_m}{1 + k_m^2} - \frac{1}{2} \sum_{l=1}^{\infty} & \left[ \frac{N_l N_{m-l}}{(1 + k_l^2)(1 + k_m^2)(1 + k_{m-l}^2)} \right. \\ & \left. + \frac{N_{-l} N_{m+l}}{(1 + k_{-l}^2)(1 + k_m^2)(1 + k_{m+l}^2)} \right] \end{aligned}$$

$$+ \mathcal{O}(N^3), \quad (3.22)$$

where  $N_m \equiv n_m^+ + n_m^-$ . In terms of Fourier coefficients we then have

$$\begin{aligned} \delta^2 F &= \frac{1}{2} \Lambda L \sum_{m=1}^{\infty} \left[ \left( |v_m^+|^2 + |v_m^-|^2 \right) \right. \\ &\quad \left. + 2v \left( n_m^+ v_{-m}^+ - n_m^- v_{-m}^- + C.C. \right) + 2 \frac{|N_m|^2}{1 + k_m^2} \right] \\ &\quad + \mathcal{O}(|N_m|^3) \end{aligned} \quad (3.23)$$

where  $C.C.$  denotes complex conjugate. Here we have dropped terms of order  $|N_m|^3$  which came from evaluating  $|\phi_m|^2$ ; we shall reclaim them when we evaluate the cubic terms in the Hamiltonian.

The Poisson bracket (3.9) now takes the form (see Appendix A)

$$\begin{aligned} \{\mathcal{F}, \mathcal{G}\} &= \sum_{\alpha=\pm} \sum_{m=1}^{\infty} \frac{v k_m}{\Lambda L} \left[ \frac{\delta \mathcal{G}}{\delta n_m^\alpha} \frac{\delta \mathcal{F}}{\delta v_{-m}^\alpha} - \frac{\delta \mathcal{F}}{\delta n_m^\alpha} \frac{\delta \mathcal{G}}{\delta v_{-m}^\alpha} \right. \\ &\quad \left. + \frac{\delta \mathcal{G}}{\delta n_{-m}^\alpha} \frac{\delta \mathcal{F}}{\delta v_m^\alpha} - \frac{\delta \mathcal{F}}{\delta n_{-m}^\alpha} \frac{\delta \mathcal{G}}{\delta v_m^\alpha} \right]. \end{aligned} \quad (3.24)$$

This can be put into the familiar form via the transformation

$$\begin{aligned} n_m^+ &= \frac{\sqrt{\pi v k_m}}{\sqrt{\Lambda L}} (p_2 - i q_1), & n_{-m}^+ &= (n_m^+)^*, \\ v_m^+ &= \frac{1}{2\sqrt{\Lambda}\sqrt{\pi v}} (p_1 - i q_2), & v_{-m}^+ &= (v_m^+)^*, \\ n_m^- &= \frac{\sqrt{\pi v k_m}}{\sqrt{\Lambda L}} (p_4 - i q_3), & n_{-m}^- &= (n_m^-)^*, \\ v_m^- &= \frac{1}{2\sqrt{\Lambda}\sqrt{\pi v}} (p_3 - i q_4), & v_{-m}^- &= (v_m^-)^*, \end{aligned} \quad (3.25)$$

where the  $p_i$  and  $q_i$  are labeled by the mode number  $m$ . (Here the  $p_i$  and  $q_i$  would have dimensions of  $action^{\frac{1}{2}} = (energy \times time)^{\frac{1}{2}}$  and have been normalized to  $(T_e/\omega_{p_i})^{\frac{1}{2}}$ .) The bracket then becomes

$$\{\mathcal{F}, \mathcal{G}\} = \sum_{m=1}^{\infty} \sum_{i=1}^4 \left( \frac{\partial \mathcal{F}}{\partial q_i} \frac{\partial \mathcal{G}}{\partial p_i} - \frac{\partial \mathcal{G}}{\partial q_i} \frac{\partial \mathcal{F}}{\partial p_i} \right). \quad (3.26)$$

Using the transformation (3.25) our expression (3.23) for the perturbed energy becomes

$$\begin{aligned}\delta^2 F &= \frac{1}{2} \sum_{m=1}^{\infty} \sum_{i,j=1}^4 (q_i A_{ij} q_j + p_i B_{ij} p_j)_m \\ &= \frac{1}{2} \sum_{m=1}^{\infty} (\tilde{q} \mathbf{A} \mathbf{q} + \tilde{p} \mathbf{B} \mathbf{p})_m\end{aligned}\quad (3.27)$$

where

$$\mathbf{A} = \begin{bmatrix} \frac{k_m^2 k_1 v}{1+k_m^2} & k_m v & \frac{k_m^2 k_1 v}{1+k_m^2} & 0 \\ k_m v & \frac{1}{2k_1 v} & 0 & 0 \\ \frac{k_m^2 k_1 v}{1+k_m^2} & 0 & \frac{k_m^2 k_1 v}{1+k_m^2} & -k_m v \\ 0 & 0 & -k_m v & \frac{1}{2k_1 v} \end{bmatrix}\quad (3.28)$$

$$\mathbf{B} = \begin{bmatrix} \frac{1}{2k_1 v} & k_m v & 0 & 0 \\ k_m v & \frac{k_m^2 k_1 v}{1+k_m^2} & 0 & \frac{k_m^2 k_1 v}{1+k_m^2} \\ 0 & 0 & \frac{1}{2k_1 v} & -k_m v \\ 0 & \frac{k_m^2 k_1 v}{1+k_m^2} & -k_m v & \frac{k_m^2 k_1 v}{1+k_m^2} \end{bmatrix}$$

(The tilde denotes transpose.) The subscript "m" in Eq. (3.27) is a shorthand indicating that each quantity inside the parantheses is labelled with this mode number.

The wave momentum is given by

$$P = \Lambda \int_0^L dx (n^+ v^+ + n^- v^-). \quad (3.29)$$

The total momentum for our equilibrium is zero; the perturbed momentum is

$$\begin{aligned}\delta^2 P &= \Lambda L \sum_{m=1}^{\infty} (n_m^+ v_{-m}^+ + n_m^- v_{-m}^- + C.C.) \\ &= \sum_{m=1}^{\infty} k_m (p_1 p_2 + q_1 q_2 + p_3 p_4 + q_3 q_4)_m \\ &= \frac{1}{2} \sum_{m=1}^{\infty} (\tilde{q} \mathbf{C} \mathbf{q} + \tilde{p} \mathbf{C} \mathbf{p})_m\end{aligned}\quad (3.30)$$

where

$$\mathbf{C} = \begin{bmatrix} 0 & k_m & 0 & 0 \\ k_m & 0 & 0 & 0 \\ 0 & 0 & 0 & k_m \\ 0 & 0 & k_m & 0 \end{bmatrix}. \quad (3.31)$$

We now seek a canonical transformation to diagonalize both  $\delta^2 F$  and  $\delta^2 P$ . The appropriate transformation, derived in Appendix B, is given by

$$\mathbf{q} = \mathbf{S}\mathbf{Q}, \quad \mathbf{p} = \mathbf{T}\mathbf{P}, \quad (3.32)$$

where the matrices  $\mathbf{S}$  and  $\mathbf{T}$  are given by

$$\mathbf{S} = \begin{bmatrix} -b_3 & -b_4 & -b_1 & -b_2 \\ a_1 & a_2 & a_3 & a_4 \\ b_1 & b_2 & b_3 & b_4 \\ a_3 & a_4 & a_1 & a_2 \end{bmatrix} \quad \mathbf{T} = \begin{bmatrix} a_1 & -a_2 & -a_3 & a_4 \\ -b_3 & b_4 & b_1 & -b_2 \\ a_3 & -a_4 & -a_1 & a_2 \\ b_1 & -b_2 & -b_3 & b_4 \end{bmatrix} \quad (3.33)$$

where

$$a_i \equiv \hat{a}_i \sqrt{\hat{k}_m \hat{k}_1 \hat{v}}, \quad (3.34)$$

$$b_i \equiv \hat{b}_i / \sqrt{\hat{k}_m \hat{k}_1 \hat{v}}, \quad (3.35)$$

and

$$\begin{aligned} \hat{a}_1 &\equiv \frac{\hat{\omega}_+ + \hat{v}}{\sqrt{4R\hat{\omega}_+}}, & \hat{b}_1 &\equiv \sqrt{\frac{(\hat{\omega}_+ - \hat{v})^2 - \frac{1}{2}}{8R\hat{\omega}_+}}, \\ \hat{a}_2 &\equiv \frac{\hat{\omega}_- + \hat{v}}{\sqrt{4R\hat{\omega}_-}}, & \hat{b}_2 &\equiv -\sqrt{\frac{(\hat{\omega}_- - \hat{v})^2 - \frac{1}{2}}{8R\hat{\omega}_-}}, \\ \hat{a}_3 &\equiv \frac{\hat{\omega}_+ - \hat{v}}{\sqrt{4R\hat{\omega}_+}}, & \hat{b}_3 &\equiv -\sqrt{\frac{(\hat{\omega}_+ + \hat{v})^2 - \frac{1}{2}}{8R\hat{\omega}_+}}, \\ \hat{a}_4 &\equiv \frac{\hat{\omega}_- - \hat{v}}{\sqrt{4R\hat{\omega}_-}}, & \hat{b}_4 &\equiv \sqrt{\frac{(\hat{\omega}_- + \hat{v})^2 - \frac{1}{2}}{8R\hat{\omega}_-}}, \end{aligned} \quad (3.36)$$

and where we have defined

$$\hat{k}_m \equiv \frac{k_m}{\sqrt{1 + k_m^2}}, \quad (3.37)$$

$$\hat{k}_1 \equiv \frac{k_1}{\sqrt{1 + k_m^2}}, \quad (3.38)$$

$$\hat{v} \equiv v\sqrt{1 + k_m^2}. \quad (3.39)$$

(Note that  $\hat{k}_1$  and  $\hat{v}$  both depend on the mode number  $m$  whereas  $k_1$  and  $v$  do not; since the former are occurring only inside matrices that depend upon a single  $m$ , this will not lead to confusion.) The utility of introducing  $\hat{a}_i$  and  $\hat{b}_i$  is that these variables are of order unity and depend relatively weakly on  $k_1$  and  $v$ . In terms of the new variables we find

$$\delta^2 F = \sum_{m=1}^{\infty} \left[ \omega_+ \frac{P_1^2 + Q_1^2}{2} - \omega_- \frac{P_2^2 + Q_2^2}{2} + \omega_+ \frac{P_3^2 + Q_3^2}{2} - \omega_- \frac{P_4^2 + Q_4^2}{2} \right]_m \quad (3.40)$$

and

$$\delta^2 P = \sum_{m=1}^{\infty} k_m \left[ \frac{P_1^2 + Q_1^2}{2} - \frac{P_2^2 + Q_2^2}{2} - \frac{P_3^2 + Q_3^2}{2} + \frac{P_4^2 + Q_4^2}{2} \right]_m \quad (3.41)$$

where

$$\omega_{\pm} = k_m \left[ \frac{1}{2(1 + k_m^2)} + v^2 \pm \sqrt{\frac{1}{4(1 + k_m^2)^2} + \frac{2v^2}{(1 + k_m^2)}} \right]^{\frac{1}{2}} > 0. \quad (3.42)$$

Making one further canonical transformation to action-angle variables

$$Q_i = \sqrt{2J_i} \sin \theta_i \quad (3.43)$$

$$P_i = \sqrt{2J_i} \cos \theta_i,$$

we arrive at

$$\delta^2 F = \sum_{m=1}^{\infty} [\omega_+ J_1 - \omega_- J_2 + \omega_+ J_3 - \omega_- J_4]_m \quad (3.44)$$

$$\delta^2 P = \sum_{m=1}^{\infty} k_m [J_1 - J_2 - J_3 + J_4]_m. \quad (3.45)$$

The  $J_{i(m)}$  will be recognized as corresponding to the four eigenmodes of Fig. 3.1, and the negative energy character of branches 2 and 4 is now explicit in the Hamiltonian. To further illustrate the correspondence, let us write the perturbed energy (3.23) and momentum (3.30) in terms of the Fourier coefficients for the electric field  $E_m \equiv -ik_m \phi_m$ . We obtain

$$\delta^2 F = \sum_{m=1}^{\infty} \omega(k_m) \left( L \frac{\partial \varepsilon(k_m, \omega)}{\partial \omega} |E_m|^2 \right), \quad (3.46)$$

$$\delta^2 P = \sum_{m=1}^{\infty} k_m \left( L \frac{\partial \varepsilon(k_m, \omega)}{\partial \omega} |E_m|^2 \right), \quad (3.47)$$

where  $\omega(k_m)$  is one of the four roots (positive or negative) of the dispersion relation  $\varepsilon(k_m, \omega) = 0$ . We immediately identify the wave action as

$$J = N \frac{\partial \varepsilon}{\partial \omega} |E_m|^2. \quad (3.48)$$

Again we see that the sign of the wave energy is given by  $\omega \frac{\partial \varepsilon}{\partial \omega}$ .

### 3.2.3 Nonlinear Coupling

We now consider cubic terms of the perturbed energy. Taking the third variation of  $F$ , inserting the Fourier expansions and carrying out the integration we obtain

$$\begin{aligned} \delta^3 F = \sum_{l,m=1}^{\infty} \left\{ \frac{\Lambda L}{2} \sum_{\alpha=\pm} [n_m^\alpha v_l^\alpha v_{-(m+l)}^\alpha + n_m^\alpha v_{-l}^\alpha v_{-(m-l)}^\alpha + C.C.] \right. \\ \left. - \frac{\Lambda L}{6} \left[ \frac{N_m N_l N_{-(m+l)}}{(1+k_m^2)(1+k_l^2)(1+k_{m+l}^2)} \right. \right. \\ \left. \left. + \frac{N_m N_{-l} N_{-(m-l)}}{(1+k_m^2)(1+k_l^2)(1+k_{m-l}^2)} + C.C. \right] \right\} \end{aligned}$$



$$\begin{aligned}
&= \sum_{l,m=1}^{\infty} \left\{ \alpha_m \left[ (p_2 - \imath q_1)_m (p_1 - \imath q_2)_l (p_1 + \imath q_2)_{m+l} \right. \right. \\
&\quad + (p_2 - \imath q_1)_m (p_1 - \imath q_2)_{-l} (p_1 + \imath q_2)_{m-l} \\
&\quad + (p_4 - \imath q_3)_m (p_3 - \imath q_4)_l (p_3 + \imath q_4)_{m+l} \\
&\quad \left. \left. + (p_4 - \imath q_3)_m (p_3 - \imath q_4)_{-l} (p_3 + \imath q_4)_{m-l} \right] \right. \\
&\quad + \beta_{l,m} \left[ (p_2 - \imath q_1 + p_4 - \imath q_3)_m (p_2 - \imath q_1 + p_4 - \imath q_3)_l (p_2 + \imath q_1 + p_4 + \imath q_3)_{m+l} \right] \\
&\quad + \beta_{-l,m} \left[ (p_2 - \imath q_1 + p_4 - \imath q_3)_m (p_2 - \imath q_1 + p_4 - \imath q_3)_{-l} (p_2 + \imath q_1 + p_4 + \imath q_3)_{m-l} \right] \\
&\quad \left. + C.C. \right\} \tag{3.49}
\end{aligned}$$

where

$$\begin{aligned}
\alpha_m &= \frac{k_m}{8\pi^{\frac{1}{2}} \Lambda^{\frac{1}{2}} v^{\frac{1}{2}}} \\
\beta_{\pm l,m} &= \frac{k_1^2 v^{\frac{3}{2}}}{24\pi^{\frac{1}{2}} \Lambda^{\frac{1}{2}}} \frac{k_m k_{\pm l} k_{m \pm l}}{(1+k_m^2)(1+k_{\pm l}^2)(1+k_{m \pm l}^2)}. \tag{3.50}
\end{aligned}$$

We can now substitute the transformations used earlier in Eqs. (3.32) and (3.43):

$$\begin{aligned}
q_i &= \sum_{j=1}^4 S_{ij} Q_j = \sum_{j=1}^4 S_{ij} \sqrt{2J_j} \sin \theta_j \\
p_i &= \sum_{j=1}^4 T_{ij} P_j = \sum_{j=1}^4 T_{ij} \sqrt{2J_j} \cos \theta_j. \tag{3.51}
\end{aligned}$$

Rather than attempt to write the general expression, we simply note for now that the general cubic term will have the form (up to a constant phase)

$$\alpha J_a^{|m_a|/2} J_b^{|m_b|/2} J_c^{|m_c|/2} \sin(m_a \theta_a + m_b \theta_b + m_c \theta_c) \tag{3.52}$$

where  $|m_a| + |m_b| + |m_c| = 3$  and where  $\alpha$  here represents some combination of the  $\alpha_m$  and  $\beta_{\pm l,m}$  and the matrix elements  $S_{ij}$  and  $T_{ij}$ .

For later reference we note how the coefficients of the cubic terms scale with the equilibrium quantities. Using the  $S_{ij}$  and  $T_{ij}$  defined in Appendix B, we find that for wavenumbers of order  $mk_1$ ,

$$\delta^3 F \sim \frac{m^{\frac{3}{2}} k_1^2}{\Lambda}. \quad (3.53)$$

### 3.3 Corrections to the Fluid Theory

A number of approximations are inherent in our fluid model. The most important of these are the neglect of both collisions and Landau damping. We now consider on what time scales these effects will become important.

#### 3.3.1 Collisions

In high-temperature plasmas it is often a very good approximation to neglect collisions. Since we will be considering slow diffusive processes, we will want to consider how valid this is. The typical ion-electron collision frequency is given roughly by [22]

$$\nu \sim \frac{\omega_{pe}}{\Lambda^3} \sim \sqrt{\frac{m_i}{m_e}} \frac{\omega_p}{\Lambda^3}. \quad (3.54)$$

We will evaluate this for parameters of interest in Chapter 6. While a large collision frequency would invalidate the fluid approximation used in our model, collisions may also enhance some of the diffusive processes that are of interest [35].

#### 3.3.2 Landau Damping

We have assumed delta-function distributions for our ion beams. If we consider beams with finite thermal spreads, then the waves in the system may

exchange energy with the background particles via Landau damping or growth [41, 22]. Considering a broad Maxwellian distribution for the electrons and narrow Maxwellians for the ion streams, a straightforward calculation yields the growth or damping rate  $\omega^{(I)}$ :

$$\begin{aligned} \frac{\omega^{(I)}}{\omega^{(R)}} \sim \frac{\omega^{(I)}}{k} = & -\sqrt{\pi} \left( \frac{\omega^{(R)}}{k} - v \right)^4 \left( \frac{T_e}{T_i} \right)^{\frac{3}{2}} e^{-\frac{T_e}{T_i} \left( \frac{\omega^{(R)}}{k} - v \right)^2} \\ & - \sqrt{\pi} \frac{\omega^{(R)}}{k} \left( \frac{\omega^{(R)}}{k} - v \right)^3 \sqrt{\frac{m_e}{m_i}} \end{aligned} \quad (3.55)$$

where  $\omega^{(I)}$  is in units of the the ion plasma frequency  $\omega_p$ , and we have assumed  $|\omega^{(I)}| \ll \omega^{(R)}$ . The first term on the right-hand side describes energy exchange with the ions, and the second term with the electrons. We see that energy exchange between the waves and the ions decreases rapidly with the ratio  $T_i/T_e$ . If  $T_i/T_e$  is small enough, then ion Landau damping (or growth) may be negligible on the time scales of interest. However, energy exchange with the electrons then approaches a constant value proportional to  $\sqrt{\frac{m_e}{m_i}}$ . As the electron temperature is made very large, the distribution becomes more and more broad and flat. However, the phase speeds of the waves also increase with the electron temperature, so that the rate of damping or growth stays constant. This type of energy exchange can dominate other processes such as the diffusive processes that we will be interested in; however, it may be suppressed if there is a local flat spot in the particle distribution function, as described by quasilinear theory [42].

## Chapter 4

### Resonances and Nonlinear Instability

#### 4.1 Introduction

Our interest is in resonant interactions between linearly stable modes; we therefore consider only sets of modes that interact resonantly (or near-resonantly) via the cubic terms of Eq. (3.49). Other modes in the infinite sum yield nonlinear terms with rapidly varying phase, which may be removed by averaging. The third-order resonance conditions to be satisfied are

$$n_1 k^{(1)} + n_2 k^{(2)} + n_3 k^{(3)} = 0 \quad (4.1)$$

$$n_1 \sigma_1 \omega^{(1)} + n_2 \sigma_2 \omega^{(2)} + n_3 \sigma_3 \omega^{(3)} = 0 \quad (4.2)$$

where  $\omega^{(i)} = \omega(k^{(i)})$ , the  $n_i$  are integers satisfying  $|n_1| + |n_2| + |n_3| = 3$ , and the  $\sigma_i$  are all equal to  $\pm 1$ .

One important case is that of two-wave interactions, where two modes from the same branch of the dispersion relation satisfy

$$2k^{(1)} = k^{(2)}$$

$$2\omega^{(1)} \approx \omega^{(2)}.$$

This situation is generic for long wavelengths (small  $k$ ), where we have  $\omega_{\pm} \approx k_m \left[ \frac{1}{2} + v^2 \pm \sqrt{\frac{1}{4} + 2v^2} \right]^{\frac{1}{2}}$ , so that for all pairs of waves with  $2k_1 = k_2$  we will also have  $\omega_1 \approx 2\omega_2$ . The frequency matching condition cannot be satisfied

exactly, but is approached in the limit  $k \rightarrow 0$ . For a large system ( $k_1 \ll 1$ ) there may be many such nearly resonant pairs of modes. We will see that this can be a strong source of stochasticity.

A large number of three-wave resonances is also possible in our system. This may be seen graphically from Figure 3.1. If the point ( $k = 0, \omega = 0$ ) on one of the negative- $\omega$  branches 3 or 4 is translated along branch 1, then its intersection with branch 2 defines a three-wave resonance. In the continuum limit such resonances occur regardless of the equilibrium parameters; for a finite system only special values of the parameters will yield exact resonances.

For our symmetric equilibrium there are only two physically distinct possibilities: a resonance involving two slow modes and one fast mode (where branch 4 connecting branches 1 and 2), or two fast modes and one slow one (where branch 3 connecting branches 1 and 2). Note that if the equilibrium parameters are such as to allow a resonance of either type, then there is another resonance given by the reflection of these modes about the  $k$ -axis (i.e., a resonance involving branches 1, 2 and 3 will be accompanied by a resonance involving branches 3, 4 and 1.) This degeneracy is a result of the symmetry which was included for analytical simplicity; general equilibria will yield isolated resonances.

Resonances involving modes of different energy signature result in explosive instability. As stated earlier, the presence of negative energy modes (the slow modes) in the system is independent of reference frame; the energy signature of a particular mode, however, is not. If we go to a reference frame moving with speed  $u$ , the signed frequencies  $\omega$  go to  $\omega - ku$ . (This does not affect the resonance conditions (4.1).) The quantity  $\frac{\partial \varepsilon(k, \omega - ku)}{\partial \omega}$  is invariant under

frame shift, but the energy signature  $(\omega - ku) \frac{\partial \varepsilon(k, \omega - ku)}{\partial \omega}$  is not. Thus if  $\omega - ku$  has opposite sign from  $\omega$  (i.e., the branch crosses the  $k$ -axis) then the energy signature of the mode changes. If there exists a reference frame where all modes of a triplet have the same energy signature, then conservation of momentum and energy imply nonlinear stability (i.e., only limited growth is possible) [10]. It can be shown for general three-wave interactions that if and only if the wave of highest frequency has energy signature opposite in sign to that of the other two waves, then no such reference frame exists [11]. (The proofs of both of these statements are outlined in Appendix C.) It is easily seen from the dispersion diagram for our system that this frequency relation holds if and only if the coupling is between one positive energy wave and two negative energy waves. These resonances therefore lead to explosive instability, while those involving two positive energy modes and one of negative energy will exhibit only decay instability and limited growth.

A particular three-wave resonance condition (4.2) will be satisfied only along some curve in the two-dimensional  $(k_1, v)$  parameter space. In Figure 4.1 we illustrate all three-wave resonances involving mode numbers up to  $m = 10$ . Fig. 4.1.a shows “positive energy” resonances (involving two positive energy modes and one of negative energy) and Fig. 4.1.b shows “negative energy” resonances (two negative energy modes and one of positive energy).

## 4.2 Phase Space Structure: Single Resonance

If we are near only one resonance in parameter space and need therefore keep only one resonant nonlinear term in the Hamiltonian, then the system is integrable. We first consider two-wave interactions involving modes from the

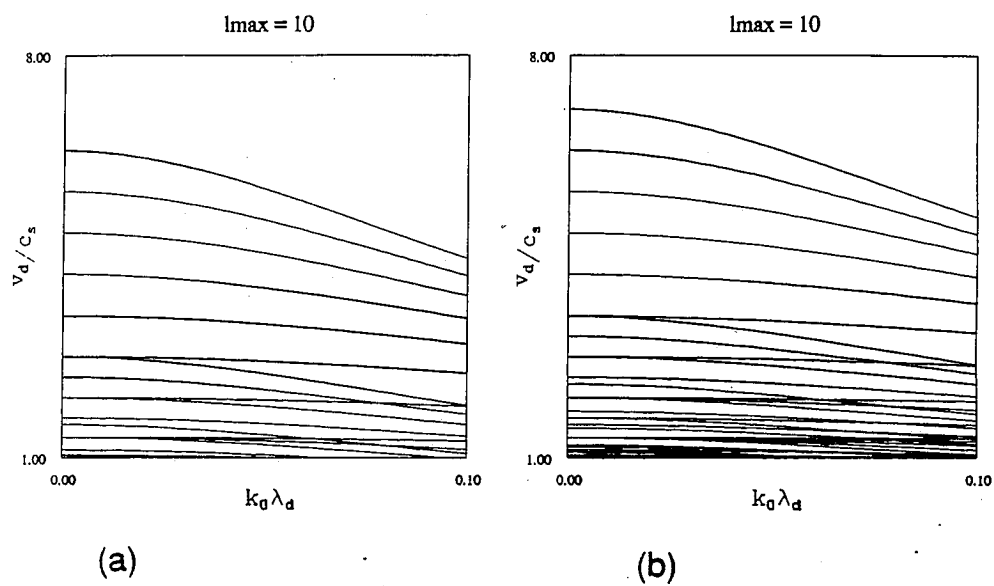


Figure 4.1: Locations in  $(k_1, v)$ -space of all three-wave resonances involving mode numbers up to  $m = 10$  for (a) decay instability and (b) explosive instability.

same branch of the dispersion diagram, and then look at three-wave resonances involving modes from different branches.

Before discussing these situations, we should note the standard form of the Hamiltonians that will occur. The Hamiltonian for a general three-wave resonance will take the form

$$H = \omega_1 J_1 - \omega_2 J_2 + \sigma \omega_3 J_3 + \alpha \sqrt{J_1 J_2 J_3} \sin(\theta_1 + \theta_2 - \sigma \theta_3) \quad (4.3)$$

where  $\sigma = 1$  denotes a positive energy resonance, and  $\sigma = -1$  a negative energy resonance. (Now the subscripts on the  $J_i$  will be used to label single modes, rather than labelling the branch of the dispersion relation on which the mode lies.) This can actually be re-written in the form of a two-wave resonance by employing a canonical transformation to a new set of coordinates. We will employ canonical transformations repeatedly in this work in order to obtain coordinate systems that help to illuminate some properties of the Hamiltonians. One source of such transformations is a mixed-variable generating function [30]. We will use the “type 2” generating function which is a function of the new actions and the old angles:

$$F(I_1, I_2, \theta_1, \theta_2) = \frac{1}{2} I_1 (\theta_1 + \theta_2) + I_2 \theta_2 + I_3 \theta_3. \quad (4.4)$$

The transformation from  $(J_1, J_2, \theta_1, \theta_2)$  to  $(I_1, I_2, \psi_1, \psi_2)$  is then given by

$$\begin{aligned} J_1 &= \frac{\partial F}{\partial \theta_1} = \frac{1}{2} I_1, & \psi_1 &= \frac{\partial F}{\partial I_1} = \frac{1}{2} (\theta_1 + \theta_2), \\ J_2 &= \frac{\partial F}{\partial \theta_2} = I_2 + \frac{1}{2} I_1, & \psi_2 &= \frac{\partial F}{\partial I_2} = \theta_2, \\ J_3 &= \frac{\partial F}{\partial \theta_3} = I_3, & \psi_3 &= \frac{\partial F}{\partial I_3} = \theta_3. \end{aligned} \quad (4.5)$$

The Hamiltonian then takes the form

$$h = H + \omega_2 I_2$$



$$= \frac{1}{2}(\omega_1 - \omega_2)I_1 + \sigma\omega_3I_3 + \frac{\alpha}{2}\sqrt{I_1(I_1 + 2I_2)I_3} \sin(2\psi_1 - \sigma\psi_3).$$

If we set the constant  $I_2 \equiv J_2 - J_1 = 0$ , this becomes

$$h = \hat{\omega}_1 I_1 + \sigma\omega_3 I_3 + \frac{\alpha}{2} I_1 \sqrt{I_3} \sin(2\psi_1 - \sigma\psi_3), \quad (4.6)$$

where  $\hat{\omega}_1 = \frac{1}{2}(\omega_1 - \omega_2)$ . For  $\sigma = 1$  this has the form of the Hamiltonian for two-wave interactions to be discussed in the next section, and for  $\sigma = -1$  it has the form of Cherry's Hamiltonian, discussed earlier.

The motion for the Hamiltonian (4.3) (and consequently for the two-wave Hamiltonians) may be solved exactly in terms of elliptic integrals [5, 8]. Our further discussion of the integrable cases will focus primarily on graphical representations of the phase space to understand the motion. For nonintegrable systems to be considered later, there is of course no exact solution, and numerical methods will be used.

#### 4.2.1 Two-Wave Interactions

We now consider the case of a two-wave near-resonance involving modes from a single branch. Some modes for which this could occur are shown in Figure 4.2. Here modes  $J_1$ ,  $J_2$  and  $J_3$  have wavenumbers  $k_1$ ,  $2k_1$  and  $4k_1$  respectively. For  $k_1 \ll 1$  we will simultaneously have near-resonance between modes  $J_1$  and  $J_2$  and between modes  $J_2$  and  $J_3$ . Later we will see that three waves coupled in this way will exhibit strongly chaotic motion. For now we consider the single near-resonance formed by modes  $J_1$  and  $J_2$ . The Hamiltonian is

$$H = \omega_1 J_1 + \omega_2 J_2 + \alpha J_1 \sqrt{J_2} \sin(2\theta_1 - \theta_2), \quad (4.7)$$

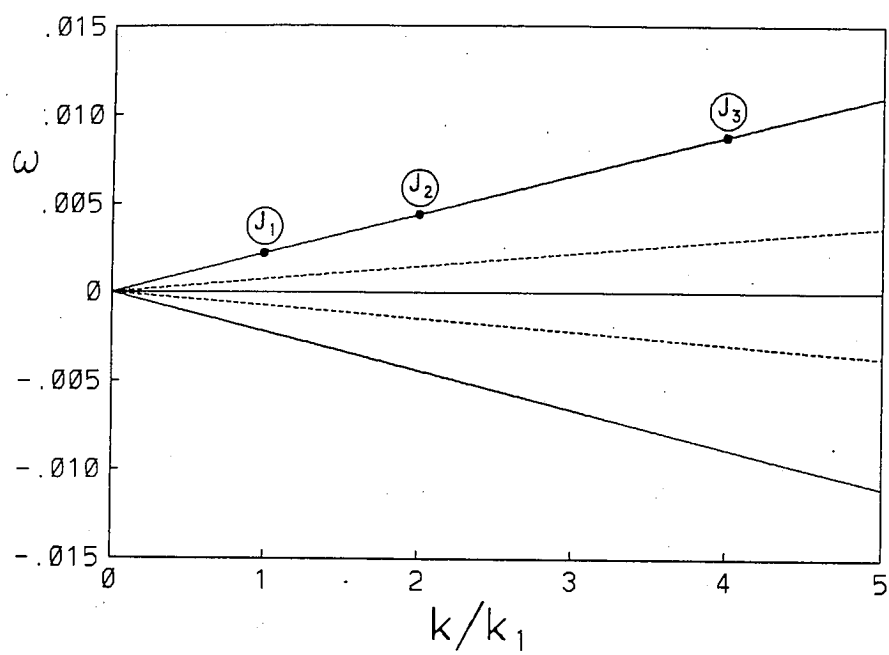


Figure 4.2: Three modes which form two near-resonant doublets.

where

$$\omega = \hat{k} \sqrt{\frac{1}{2} + \hat{v}^2 + \sqrt{\frac{1}{4} + 2\hat{v}^2}} \quad (4.8)$$

and

$$\begin{aligned} \alpha = \frac{k_1^2}{\sqrt{8\pi\Lambda}} & \left[ \hat{a}_{3(k_1)} \left( 2\hat{a}_{3(2k_1)} \hat{b}_{1(k_1)} + \hat{a}_{3(k_1)} \hat{b}_{1(2k_1)} \right) \right. \\ & - \hat{a}_{1(k_1)} \left( 2\hat{a}_{1(2k_1)} \hat{b}_{3(k_1)} + \hat{a}_{1(k_1)} \hat{b}_{3(2k_1)} \right) \\ & \left. + \frac{\left( \hat{b}_{1(k_1)} - \hat{b}_{3(k_1)} \right)^2 \left( \hat{b}_{1(2k_1)} - \hat{b}_{3(2k_1)} \right)}{(1 + k_1^2)^2 (1 + 4k_1^2)} \right]. \quad (4.9) \end{aligned}$$

(The subscripts in parentheses are the values of  $k$  at which the  $\hat{a}_i$  and  $\hat{b}_i$  are evaluated.) Since the angles  $\theta_1, \theta_2$  occur only in one combination, this can be reduced to a one-degree-of-freedom system. We therefore eliminate one degree of freedom by employing a canonical transformation to a new set of variables, which we call "resonance variables". One such transformation is provided by the generating function

$$F = \bar{I}_1(2\theta_1 - \theta_2) + \bar{I}_3\theta_2, \quad (4.10)$$

which yields

$$\begin{aligned} J_1 = \frac{\partial F}{\partial \theta_1} &= 2\bar{I}_1, & \bar{\psi}_1 = \frac{\partial F}{\partial \bar{I}_1} &= 2\theta_1 - \theta_2, \\ J_2 = \frac{\partial F}{\partial \theta_2} &= \bar{I}_3 - \bar{I}_1, & \bar{\psi}_3 = \frac{\partial F}{\partial \bar{I}_3} &= \theta_2. \end{aligned} \quad (4.11)$$

The Hamiltonian becomes

$$\begin{aligned} \bar{H} &= H - \omega_2 \bar{I}_3 \\ &= \bar{\Omega}_1 \bar{I}_1 + 2\alpha \bar{I}_1 \sqrt{\bar{I}_3 - \bar{I}_1} \sin \bar{\psi}_1, \end{aligned} \quad (4.12)$$

where

$$\bar{\Omega}_1 \equiv 2\omega_1 - \omega_2 \quad (4.13)$$

is the “detuning” of the resonance and

$$\bar{I}_3 \equiv J_2 + \frac{1}{2}J_1 = \text{constant}. \quad (4.14)$$

(The choice of the labels “1,3” rather than “1,2” was made for later convenience.) Note that the constant of the motion  $\bar{I}_3$  is just proportional to the wave momentum  $k_1(J_1 + 2J_2)$ .

For arbitrary pairs of waves, the phase space topology is determined by the “effective detuning”  $\left|\frac{\Omega_{\pm}}{\alpha}\right|$ , where “ $\pm$ ” denotes waves of positive or negative energy. Expanding  $\Omega_{\pm}$  for small  $k$ , we find

$$\begin{aligned} \Omega_{\pm} &\equiv \omega_{\pm}(2k) - 2\omega_{\pm}(k) \\ &= k^3 \frac{3}{\sqrt{2}} \frac{\mp(1 + 4v^2 \pm \sqrt{1 + 8v^2})}{\sqrt{1 + 8v^2}\sqrt{1 + 2v^2 \pm \sqrt{1 + 8v^2}}} + \mathcal{O}(k^5). \end{aligned} \quad (4.15)$$

The detunings  $\Omega_+$  and  $\Omega_-$  are nearly equal for most  $v$ , differing in magnitude only for  $v$  near 1 (since  $\Omega_-$  diverges as  $v \rightarrow 1$ ). Recalling from Eq. (3.53) that  $\alpha \sim \frac{k^2}{\Lambda}$  for small  $k$ , we find for the effective detuning

$$\left|\frac{\Omega_{\pm}}{\alpha}\right| \sim \frac{m^3 k_1^3 \Lambda}{m^{\frac{3}{2}} k_1^2} \sim m^{\frac{3}{2}} k_1 \Lambda \sim m^{\frac{3}{2}} \frac{\Lambda}{L} \quad (4.16)$$

with a weaker dependence on  $v$ . We will therefore have the strongest resonance for the smallest  $\Lambda$  (dense plasma); however, we have seen in Section 3.3 that this also results in a larger collision frequency, which will invalidate our fluid approximation. We will also obtain stronger resonance by considering smaller  $k_1$  (larger  $L$ ); however, since  $k_1$  enters into both  $\Omega$  and  $\alpha$ , this also increases the time scales required for the system to evolve. For a given pair of modes (fixed  $m$ ), simultaneously increasing  $\Lambda$  and  $L$  while keeping their ratio constant will decrease the collisionality of the plasma while maintaining the strength of the

two-wave resonance; the modes under consideration will, however, become of lower and lower frequency.

We will see later that the behavior of the system is most strongly influenced by the most nearly resonant sets of modes; therefore, the physical parameters that lead to interesting phenomena will be determined by some compromise between these competing effects. Whatever the values of the physical parameters, we see that the strongest two-wave interactions will occur for long-wavelength modes such as  $J_1$  and  $J_2$  of Hamiltonian (4.7).

We now examine the phase space structure for the Hamiltonian (4.12). For graphical representations of this and other systems it is convenient to use the cartesian form of the resonance variables:

$$\begin{aligned}\bar{P}_i &= \sqrt{2\bar{I}_i} \cos \bar{\psi}_i \\ \bar{Q}_i &= \sqrt{2\bar{I}_i} \sin \bar{\psi}_i.\end{aligned}$$

In Figure 4.3 we display constant-energy contours for two values of  $L$  and fixed  $\Lambda$  and  $\nu$ .  $\bar{I}_3$  was chosen to be 0.01. The motion is confined to the region  $\bar{P}_1^2 + \bar{Q}_1^2 \leq 2I_3$ . When  $|\frac{\bar{\Omega}_1}{\alpha}| < \sqrt{\bar{I}_3}$  there is an unstable fixed point at the origin and two stable fixed points on the positive and negative  $\bar{Q}_1$ -axis. As  $|\frac{\bar{\Omega}_1}{\alpha}|$  passes through  $\sqrt{\bar{I}_3}$ , one of the stable fixed points merges with the origin, which then becomes stable for  $|\frac{\bar{\Omega}_1}{\alpha}| > \sqrt{\bar{I}_3}$ .

Recall that in the Hamiltonian (4.12),  $\bar{I}_1 = \frac{1}{2}J_1$ , so that in Figure 4.3 we are examining the behavior of  $J_1$ . We could equally well have eliminated  $J_1$  in order to examine the behavior of  $J_2$ . Equivalent to this, and more useful for later reference, is looking at the behavior of  $J_2$  when coupled to the mode

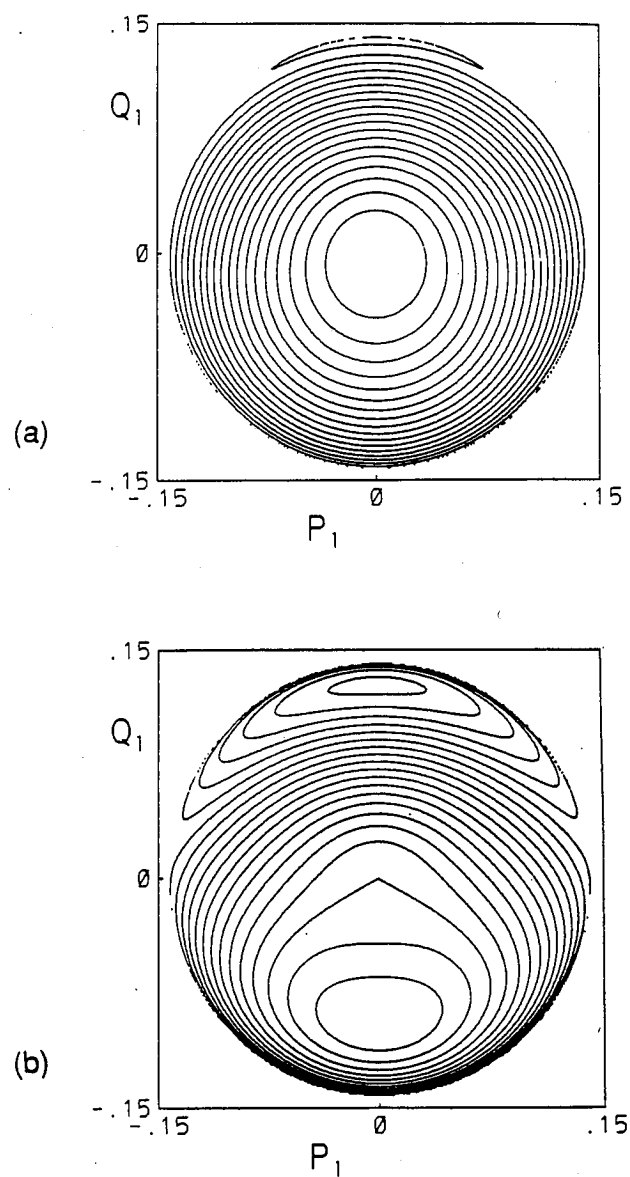


Figure 4.3: Phase space topology for two-wave decay instability described by Hamiltonian (4.12) with  $\Lambda = 100$ ,  $\nu = 1.4796$ ,  $\bar{I}_3 = 0.01$  and (a)  $L = 1000$ ; (b)  $L = 5000$ .

$J_3$  of Figure 4.2. (In either case we will be considering the behavior of the high-frequency mode of a pair.) The Hamiltonian for this system is given by

$$H = \omega_2 J_2 + \omega_3 J_3 + \beta J_2 \sqrt{J_3} \sin(2\theta_2 - \theta_3), \quad (4.17)$$

where

$$\begin{aligned} \beta = \frac{k_1^2}{\sqrt{\pi\Lambda}} & \left[ \hat{a}_{3(2k_1)} \left( 2\hat{a}_{3(4k_1)} \hat{b}_{1(2k_1)} + \hat{a}_{3(2k_1)} \hat{b}_{1(4k_1)} \right) \right. \\ & - \hat{a}_{1(2k_1)} \left( 2\hat{a}_{1(4k_1)} \hat{b}_{3(2k_1)} + \hat{a}_{1(2k_1)} \hat{b}_{3(4k_1)} \right) \\ & \left. + \frac{\left( \hat{b}_{1(2k_1)} - \hat{b}_{3(2k_1)} \right)^2 \left( \hat{b}_{1(4k_1)} - \hat{b}_{3(4k_1)} \right)}{(1 + 4k_1^2)^2 (1 + 16k_1^2)} \right]. \end{aligned} \quad (4.18)$$

We now use the generating function

$$F = \tilde{I}_2(\theta_3 - 2\theta_2) + \tilde{I}_3\theta_2 \quad (4.19)$$

to obtain

$$\begin{aligned} J_2 = \frac{\partial F}{\partial \theta_2} = \tilde{I}_3 - 2\tilde{I}_2, & \quad \tilde{\psi}_2 = \frac{\partial F}{\partial \tilde{I}_2} = \theta_3 - 2\theta_2, \\ J_3 = \frac{\partial F}{\partial \theta_3} = \tilde{I}_2, & \quad \tilde{\psi}_3 = \frac{\partial F}{\partial \tilde{I}_3} = \theta_2. \end{aligned} \quad (4.20)$$

The Hamiltonian becomes

$$\begin{aligned} \tilde{H} &= H - \omega_2 \tilde{I}_3 \\ &= \tilde{\Omega}_2 \tilde{I}_2 - \beta (\tilde{I}_3 - 2\tilde{I}_2) \sqrt{\tilde{I}_2} \sin \tilde{\psi}_2 \end{aligned} \quad (4.21)$$

where

$$\tilde{\Omega}_2 \equiv \omega_3 - 2\omega_2, \quad (4.22)$$

and

$$\tilde{I}_3 \equiv J_2 + 2J_3 = \text{constant} \quad (4.23)$$

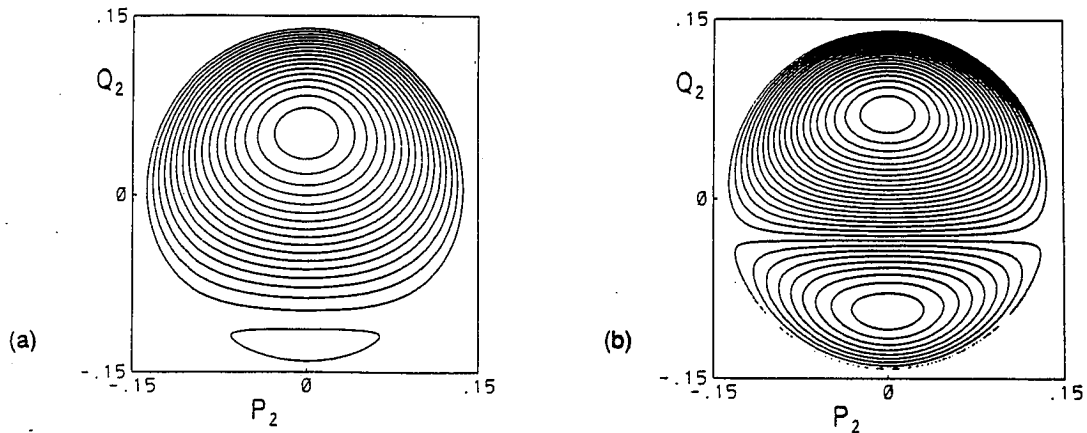


Figure 4.4: Phase space topology for two-wave decay instability described by Hamiltonian (4.21) with  $\Lambda = 100$ ,  $\nu = 1.4796$ ,  $\tilde{I}_3 = 0.02$  and (a)  $L = 5000$ ; (b)  $L = 10000$ .

is again just proportional to the momentum. This Hamiltonian describes the behavior of the high-frequency wave of a near-resonant doublet, whereas Hamiltonian (4.12) describes the behavior of the low-frequency wave. Figure 4.4 displays the phase space variables  $\tilde{P}_2, \tilde{Q}_2$  for two values of  $L$ . We find that the origin is no longer a fixed point, no unstable fixed point ever occurs, and the two stable fixed points on the positive and negative  $\tilde{P}_2$ -axis always exist, changing only in position as  $\tilde{\Omega}_2$  is varied.



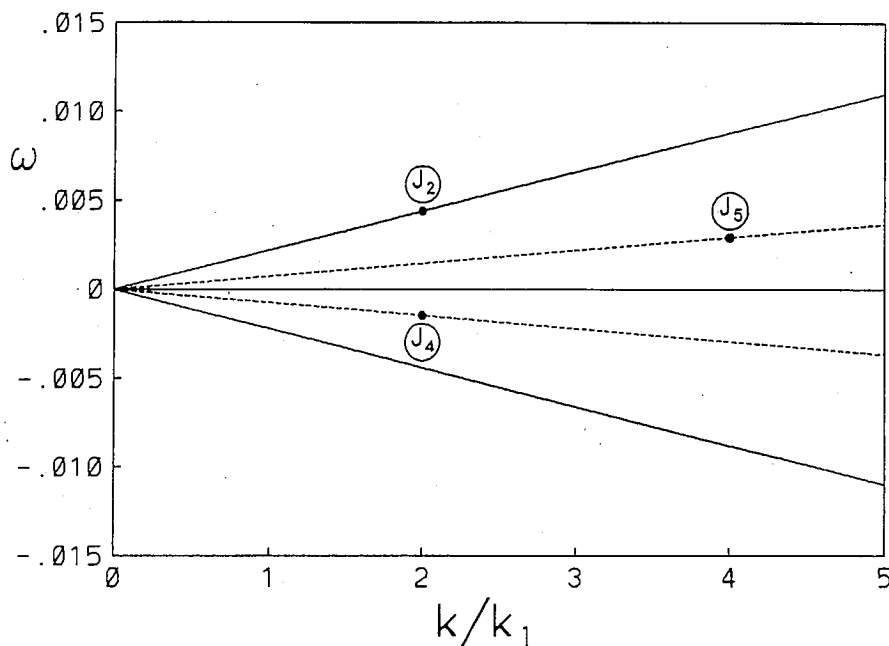


Figure 4.5: Three modes which form a negative energy resonance.

#### 4.2.2 Three-Wave Interactions

We now discuss three-wave resonances involving modes from different branches of the dispersion relation. We first look at “negative energy resonances” (involving two negative energy modes and one of positive energy) and then at “positive energy resonances” (two positive energy modes and one of negative energy).

**Negative Energy Resonance** We now consider a three-wave negative energy resonance, involving the modes shown in Figure 4.5. Modes  $J_2$ ,  $J_4$  and  $J_5$  have wavenumbers  $2k_0$ ,  $2k_0$  and  $4k_0$ , respectively. (The numbering convention is

chosen so that we may later couple these modes to those of Figure 4.2 without changing numbers.) The Hamiltonian is given by

$$H = \omega_2 J_2 - \omega_4 J_4 - \omega_5 J_5 + \gamma \sqrt{J_2 J_4 J_5} \sin(\theta_2 + \theta_4 + \theta_5), \quad (4.24)$$

where

$$\begin{aligned} \gamma = \frac{2k_1^2}{\sqrt{\pi\Lambda}} & \left[ -\hat{a}_{2(2k_1)} \hat{a}_{4(4k_1)} \hat{b}_{1(2k_1)} + \hat{a}_{1(2k_1)} \hat{a}_{2(4k_1)} \hat{b}_{2(2k_1)} \right. \\ & - \hat{a}_{2(2k_1)} \hat{a}_{3(2k_1)} \hat{b}_{2(4k_1)} + \hat{a}_{2(4k_1)} \hat{a}_{4(2k_1)} \hat{b}_{3(2k_1)} \\ & - \hat{a}_{3(2k_1)} \hat{a}_{4(4k_1)} \hat{b}_{4(2k_1)} + \hat{a}_{1(2k_1)} \hat{a}_{4(2k_1)} \hat{b}_{4(4k_1)} \\ & \left. + \frac{(\hat{b}_{1(2k_1)} - \hat{b}_{3(2k_1)}) (\hat{b}_{2(2k_1)} - \hat{b}_{4(2k_1)}) (\hat{b}_{2(4k_1)} - \hat{b}_{4(4k_1)})}{(1 + 4k_1^2)^2 (1 + 16k_1^2)} \right]. \quad (4.25) \end{aligned}$$

We recall that by eliminating one degree of freedom, this can be reduced to the form of Cherry's Hamiltonian (2.28), so that all of the comments made there apply also here. We will, however, go directly to the resonance variables which reduce this to a one-degree-of-freedom system. The transformation from the variables  $(J_2, J_4, J_5, \theta_2, \theta_4, \theta_5)$  to the resonance variables  $(\bar{I}_3, \bar{I}_4, \bar{I}_5, \bar{\psi}_3, \bar{\psi}_4, \bar{\psi}_5)$  comes from the generating function

$$F = \bar{I}_3(\theta_2 + \theta_4 + \theta_5) + \bar{I}_4\theta_4 + \bar{I}_5\theta_5, \quad (4.26)$$

which gives us

$$\begin{aligned} J_2 &= \frac{\partial F}{\partial \theta_2} = \bar{I}_3, & \bar{\psi}_3 &= \frac{\partial F}{\partial \bar{I}_3} = \theta_2 + \theta_4 + \theta_5, \\ J_4 &= \frac{\partial F}{\partial \theta_4} = \bar{I}_4 + \bar{I}_3, & \bar{\psi}_4 &= \frac{\partial F}{\partial \bar{I}_4} = \theta_4, \\ J_5 &= \frac{\partial F}{\partial \theta_5} = \bar{I}_5 + \bar{I}_3, & \bar{\psi}_5 &= \frac{\partial F}{\partial \bar{I}_5} = \theta_5. \end{aligned} \quad (4.27)$$

The Hamiltonian then becomes

$$\begin{aligned}\bar{H} &= H + \omega_4 \bar{I}_4 + \omega_5 \bar{I}_5 \\ &= \bar{\Omega}_3 \bar{I}_3 + \gamma \sqrt{\bar{I}_3(\bar{I}_4 + \bar{I}_3)(\bar{I}_5 + \bar{I}_3)} \sin \bar{\psi}_3,\end{aligned}\quad (4.28)$$

where

$$\bar{\Omega}_3 = \omega_2 - \omega_4 - \omega_5,$$

$$\bar{I}_4 = J_4 - J_2 = \text{constant},$$

$$\bar{I}_5 = J_5 - J_2 = \text{constant}.$$

(The wave momentum is just  $-2k_1(\bar{I}_4 + \bar{I}_5)$ .)

The negative energy resonance condition  $\omega_2 - \omega_4 - \omega_5 = 0$  is relatively insensitive to the value of  $L$ ; the main control parameter is now  $v$ . For a given  $L$ , we may calculate the value of  $v$  which yields either exact resonance or a stable region of a desired size.

In Figure 4.6 we plot  $\bar{Q}_3$  vs.  $\bar{P}_3$  for  $L = 5000$  and two values of  $v$ , for the special case  $\bar{I}_4 = \bar{I}_5 = 0$  (corresponding to equal mode amplitudes  $J_2 = J_4 = J_5$ ). Figure 6.3.a corresponds to  $v = 1.47959435$  which yields exact resonance for this value of  $L$ . All orbits are seen to go to infinity. Figure 6.3.b corresponds to  $v = 1.47959256$ , which yields  $\bar{\Omega}_3 \neq 0$ . In this case the resonance is slightly detuned, opening up a small stable region around the equilibrium point, with an accompanying unstable fixed point on the  $\bar{Q}_3$ -axis. The value of  $v$  was chosen so the the separatrix goes through the point  $\bar{P}_3 = 0, \bar{Q}_3 = 0.1$ . Orbits outside the separatrix still experience explosive growth, while those inside execute stable oscillations. The size of the stable region increases with

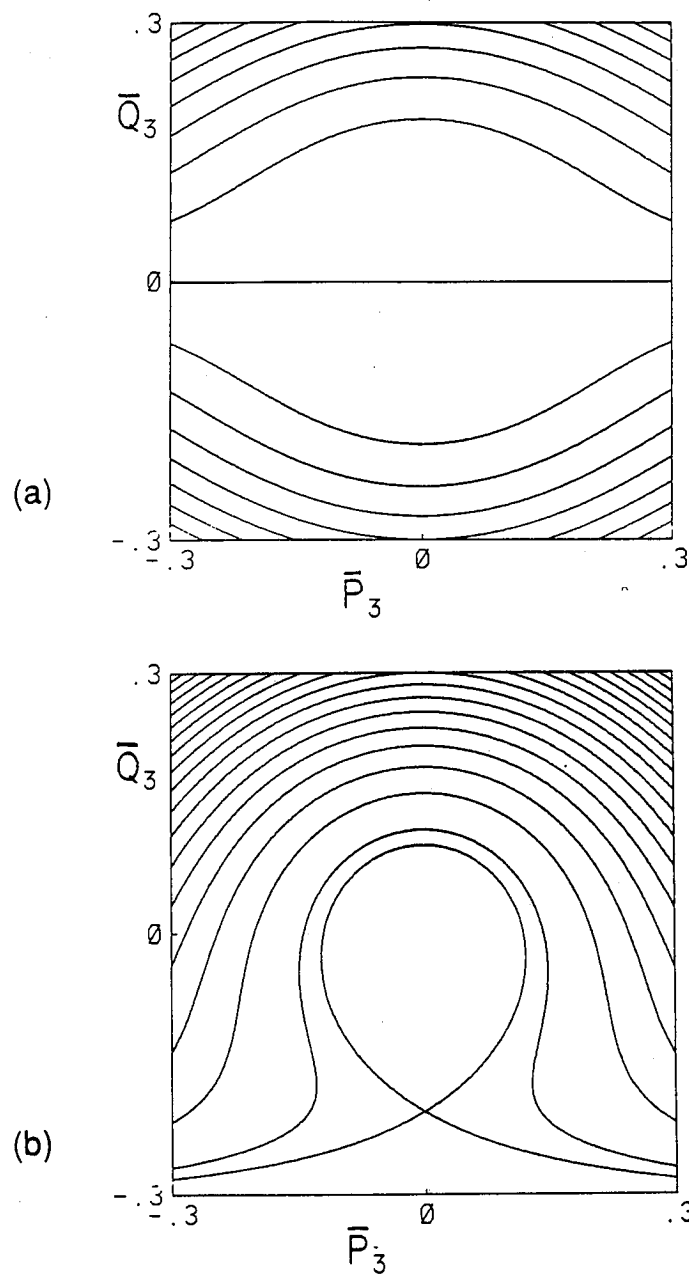


Figure 4.6: Phase space plots for Hamiltonian (4.28) with  $\bar{I}_4 = \bar{I}_5 = 0$ ,  $\Lambda = 100$ ,  $L = 5000$ , and (a)  $v = 1.47959435$  ( $\bar{\Omega}_3 = 0$ ); (b)  $v = 1.47959256$  ( $\bar{\Omega}_3 \neq 0$ ).

$\left|\frac{\bar{\Omega}_3}{\gamma}\right|$ . These phase space plots are of course essentially identical to those for Cherry's Hamiltonian in Figure 2.1.b. We could have chosen other coordinates in which the phase portraits would look like those in Figure 2.1.a.

When one of the constants  $\bar{I}_4$  or  $\bar{I}_5$  is non-zero (i.e., either  $J_4$  or  $J_5$  has amplitude different from  $J_2$ ), the origin  $\bar{I}_3 = 0$  will still be a fixed point, but will only become stable for  $|\bar{\Omega}_3| > \sqrt{\bar{I}_4}$  or  $\sqrt{\bar{I}_5}$ . Thus there is a range of non-zero  $\bar{\Omega}_3$  that yields instability at the origin. This situation is illustrated in Figure 4.7. If both  $\bar{I}_4$  and  $\bar{I}_5$  are non-zero, (i.e., neither  $J_4$  nor  $J_5$  is equal to  $J_2$ ), then no fixed points exist for small  $\bar{\Omega}_3$ . When  $|\bar{\Omega}_3|$  is large enough, a pair of fixed points (stable and unstable) appear, but the stable point is shifted off of the origin  $\bar{I}_3 = 0$  (Figure 4.8).

**Positive Energy Resonance** We now consider a three-wave resonance involving two positive energy waves and one negative energy wave. This resonance will lead to decay instability just as in the case of two-wave interactions. An important difference is that a given wave triplet can be in *exact* resonance for some  $v$ ; however, the resonance condition is strongly dependent on  $v$ . (Figure 4.1).

We consider the modes shown in Figure 4.9. The wavenumbers of  $J_2$ ,  $J_6$  and  $J_7$  are  $2k_0$ ,  $k_0$  and  $3k_0$ , respectively. Mode  $J_2$  is the same one featured in Figures 4.2 and 4.5; the numbering of the other two modes was chosen to avoid confusion with modes already discussed. The Hamiltonian is given by

$$H = \omega_2 J_2 + \omega_6 J_6 - \omega_7 J_7 + \delta \sqrt{J_2 J_6 J_7} \sin(\theta_2 - \theta_6 + \theta_7), \quad (4.29)$$

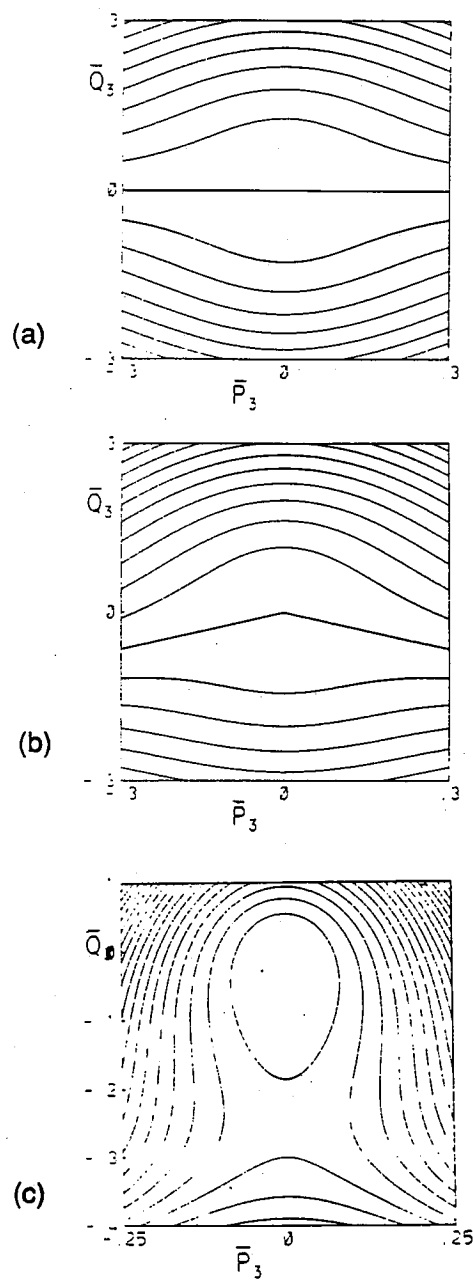


Figure 4.7: Phase space plots for Hamiltonian (4.28) with  $\bar{I}_4 = 1.0$  and  $\bar{I}_5 = 0$ .  $\Lambda = 100$ ,  $L = 5000$ , and (a)  $v = 1.47959435$  ( $\frac{\bar{\Omega}_3}{\gamma} = 0$ ); (b)  $v = 1.47959256$  ( $\frac{\bar{\Omega}_3}{\gamma} = 0.2121$ ); (c)  $v = 1.479591$  ( $\frac{\bar{\Omega}_3}{\gamma} = 0.4044$ ).

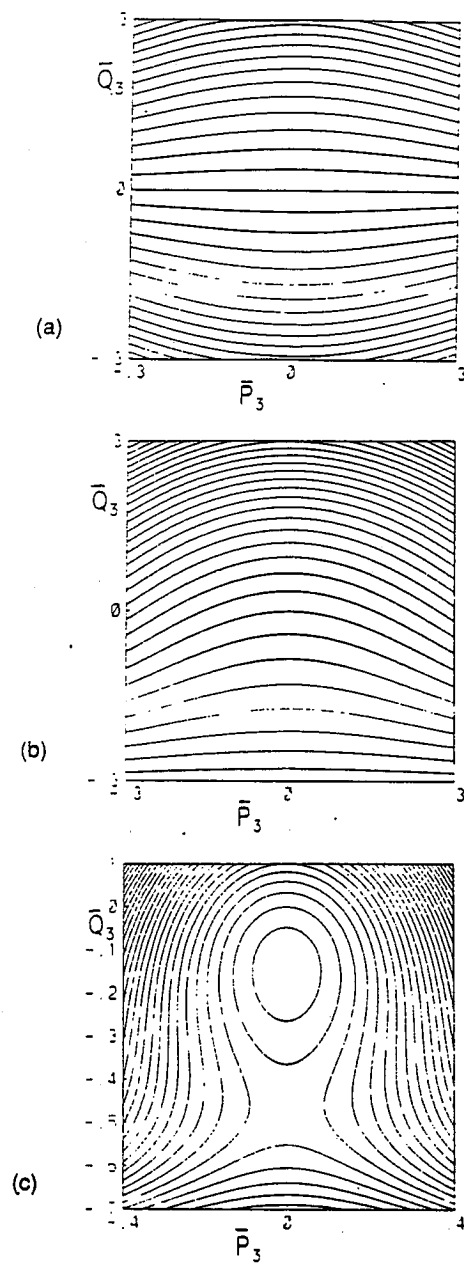


Figure 4.8: Phase space plots for Hamiltonian (4.28) with  $\bar{I}_4 = \bar{I}_5 = 1.0$ .  $\Lambda = 100$ ,  $L = 5000$ , and (a)  $v = 1.47959435$  ( $\frac{\bar{\Omega}_3}{\gamma} = 0$ ); (b)  $v = 1.47959256$  ( $\frac{\bar{\Omega}_3}{\gamma} = 0.2121$ ); (c)  $v = 1.479589$  ( $\frac{\bar{\Omega}_3}{\gamma} = 0.6459$ ).

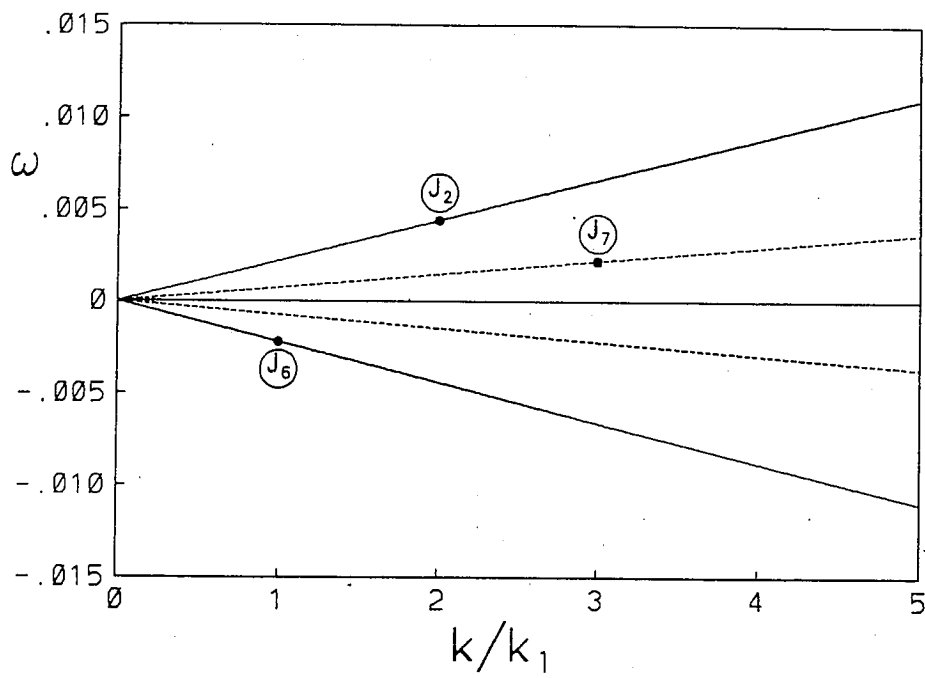


Figure 4.9: Three modes which form a positive energy resonance.



where

$$\begin{aligned}
\delta = & \frac{\sqrt{6}k_1^2}{2\sqrt{\pi\lambda}} \left( \hat{a}_{3(2k_1)} \hat{a}_{4(3k_1)} \hat{b}_{3(k_1)} - \hat{a}_{1(2k_1)} \hat{a}_{2(3k_1)} \hat{b}_{1(k_1)} \right. \\
& + \hat{a}_{1(k_1)} \hat{a}_{4(3k_1)} \hat{b}_{1(2k_1)} - \hat{a}_{2(k_3)} \hat{a}_{3(k_1)} \hat{b}_{3(2k_1)} \\
& + \hat{a}_{1(k_1)} \hat{a}_{3(2k_1)} \hat{b}_{2(3k_1)} - \hat{a}_{1(2k_1)} \hat{a}_{3(k_1)} \hat{b}_{4(3k_1)} \\
& \left. + \frac{(\hat{b}_{3(k_1)} - \hat{b}_{1(k_1)}) (\hat{b}_{3(2k_1)} - \hat{b}_{1(2k_1)}) (\hat{b}_{4(3k_1)} - \hat{b}_{2(3k_1)})}{(1+k_1^2)(1+4k_1^2)(1+9k_1^2)} \right). \quad (4.30)
\end{aligned}$$

Analysis of this Hamiltonian proceeds exactly as in the three-wave negative energy case. Employing the generating function

$$F = \bar{I}_2(\theta_2 - \theta_6 + \theta_7) + \bar{I}_6\theta_6 + \bar{I}_7\theta_7, \quad (4.31)$$

we obtain the transformation

$$\begin{aligned}
J_2 &= \frac{\partial F}{\partial \theta_2} = \bar{I}_2, & \bar{\psi}_2 &= \frac{\partial F}{\partial \bar{I}_2} = \theta_2 - \theta_6 + \theta_7, \\
J_6 &= \frac{\partial F}{\partial \theta_6} = \bar{I}_6 - \bar{I}_2, & \bar{\psi}_6 &= \frac{\partial F}{\partial \bar{I}_6} = \theta_6, \\
J_7 &= \frac{\partial F}{\partial \theta_7} = \bar{I}_7 + \bar{I}_2, & \bar{\psi}_7 &= \frac{\partial F}{\partial \bar{I}_7} = \theta_7,
\end{aligned} \quad (4.32)$$

yielding the Hamiltonian

$$\begin{aligned}
h &= H + \omega_6 \bar{I}_6 - \omega_7 \bar{I}_7 \\
&= \bar{\Omega}_4 \bar{I}_2 + \delta \sqrt{\bar{I}_2(\bar{I}_6 - \bar{I}_2)(\bar{I}_7 + \bar{I}_2)} \sin \bar{\psi}_2
\end{aligned} \quad (4.33)$$

where

$$\bar{\Omega}_4 \equiv \omega_2 - \omega_6 - \omega_7 \quad (4.34)$$

and

$$\bar{I}_6 = J_6 + J_2 = \text{constant},$$

$$\bar{I}_7 = J_7 - J_2 = \text{constant}.$$

The motion will be bounded by  $\bar{I}_2 < \bar{I}_6$ . If  $\bar{I}_7 = 0$  ( $J_2 = J_7$ ), then the Hamiltonian has exactly the form of Hamiltonian (4.12), and the same analysis applies, except that we may now have exactly  $\bar{\Omega}_4 = 0$ . When  $\bar{I}_7 \neq 0$ , we find the same behavior as that of Hamiltonian (4.21). The phase space is shown in Figure 4.10. The topologies of Figures 4.10.a and 4.10.b look similar, but for  $\bar{I}_7 \neq 0$  there is no fixed point at the origin. We could also have  $\bar{I}_7 < 0$ , corresponding to  $J_2 > J_7$ , but this would imply a forbidden region around the origin of the  $\bar{P}_2$ - $\bar{Q}_2$  plane, and so will not be considered.

### 4.3 Multiple Resonances and Chaos

For the integrable systems just considered, small-amplitude motion about the stable fixed points will be stable for all time. Thus when a negative energy resonance is detuned, only motions with large enough amplitude (outside the separatrix of Figures 4.6-4.8) will exhibit explosive instability. However, if we consider coupling to other modes via other nonlinear terms in our Hamiltonian, then chaotic motion will generally arise. In its mildest manifestation, this chaotic behavior will occur in thin layers near separatrices. Thus the separatrix between the stable and unstable orbits will presumably be “smeared out”. When chaotic motion is more widespread, many of the invariant curves within the stable region may be destroyed, effectively decreasing the size of the region. Moreover, as discussed in Section 2.3, in any chaotic system of more than two degrees of freedom, trajectories can make their way across the “stable” islets, so that a small perturbation may grow until it reaches the separatrix. The speed of this transport may vary widely depending on how nearly resonant the various waves are. We now examine this phenomenon in

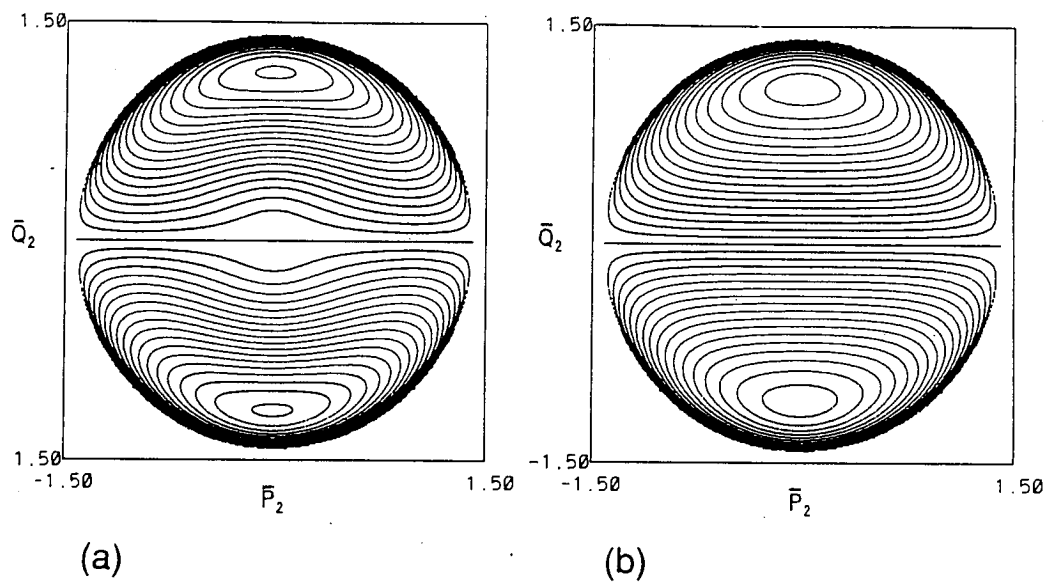


Figure 4.10: Phase space topology for three-wave decay instability described by Hamiltonian (4.33), with  $\bar{\Omega}_4 = 0$  and (a)  $\bar{I}_7 = 0$ ; (b)  $\bar{I}_7 \neq 0$ .

detail.

### 4.3.1 General Discussion

Hamiltonians of the form

$$\begin{aligned}
 H &= \omega_1 J_1 + \omega_2 J_2 + \omega_3 J_3 \\
 &+ \epsilon [\alpha F(J_1, J_2, J_3) \cos(m_1 \theta_1 + m_2 \theta_2 + m_3 \theta_3) \\
 &+ \beta G(J_1, J_2, J_3) \cos(n_1 \theta_1 + n_2 \theta_2 + n_3 \theta_3)], \tag{4.35}
 \end{aligned}$$

where  $F$  and  $G$  are higher-than-linear functions of the  $J_i$ , have been discussed by Contopoulos [43]. A particular case involving exact resonance in both non-linear terms (i.e.,  $m_1 \omega_1 + m_2 \omega_2 + m_3 \omega_3 = n_1 \omega_1 + n_2 \omega_2 + n_3 \omega_3 = 0$ ) was studied numerically by Ford and Lunsford [44] and analytically by Kummer [45]. It was shown that, in general, globally chaotic motion occurs for arbitrarily small but non-zero  $\alpha$  and  $\beta$ . This involves the breaking of most invariant surfaces and the consequent wandering of orbits over most of the energy surface. Contopoulos examined the transition to this situation from the non-resonant case. One exact constant of the motion besides  $H$  clearly exists since there are only two combinations of angles in the Hamiltonian. If only one resonance condition is satisfied (e.g.,  $\Omega_1 \equiv m_1 \omega_1 + m_2 \omega_2 + m_3 \omega_3 = 0$ ), then another approximate constant can be constructed, indicating the existence of invariant curves over most of the phase space. In this case chaotic motion will be confined to thin layers around broken separatrices. Very slow diffusion may occur along these thin layers; general estimates of the diffusion rate by Nekhoroshev [46] have been specialized by others [47] to the simpler case of coupled linear oscillators that we are considering. As the other resonance condition is approached

( $\Omega_2 \equiv n_1\omega_1 + n_2\omega_2 + n_3\omega_3 \rightarrow 0$ ) and the “effective perturbation”  $\epsilon/\Omega_2$  becomes large enough, then the approximate constant cannot be constructed, and the widespread dissolution of invariant surfaces occurs. This allows very fast transport in phase space.

### 4.3.2 Multiple Resonances in the Beam Problem

We now consider what sort of multiple resonances occur in our counterstreaming ion problem. We have seen that exact three-wave resonances are possible, involving either decay instability (“positive energy resonance”) or explosive instability (“negative energy resonance”). In addition, long-wavelength modes from the same branch of the dispersion relation will interact strongly due to the near-resonance that will always exist between them. Whenever we include more than one nonlinear term in the Hamiltonian, we will expect to find chaotic behavior originating in thin layers near separatrices. One result is that the well-defined stability boundary associated with a single negative energy resonance will be destroyed. We then expect that perturbations that were within the unperturbed separatrix may now become explosively unstable by crossing the chaotic layer. Another important consequence involves the breaking of separatrices associated with the positive energy resonances. Since these separatrices involve confined motion, the chaotic orbits that replace them can provide a long-time driver for chaotic transport through the phase space. When the system includes a negative energy triplet coupled to one or more such positive energy resonances, this chaotic motion may allow orbits that are initially deep within the “stable” negative energy islet to grow in amplitude until explosive instability occurs.

The extent of these chaotic regions may range from very thin layers to the entire phase space, depending on how many positive energy resonances or near-resonances occur. The two-wave near-resonance conditions may be arbitrarily well-satisfied depending only on the wavelengths, so that we would expect the possibility of approaching global chaos as was just described. This effect may be even stronger if a three-wave positive energy resonance condition is satisfied, which can occur for modes of any wavelength. With most or all invariant surfaces destroyed, orbits may reach any point in phase space via "thick-layer" diffusion. If positive energy resonance conditions are not nearly enough satisfied, then stochasticity will be confined to thin layers. Transport across large distances in the phase space may then be expected via Arnold diffusion (although on slow time scales) if the Hamiltonian has three or more degrees of freedom. We will now investigate these issues numerically.

We will study two simple systems that illustrate the phenomena we have discussed. For both systems the Hamiltonians have three nonlinear coupling terms, one of which can drive the explosive instability, and the other two of which describe positive energy resonances. In the first system both positive energy resonances arise from two-wave interactions; in the second system one of these terms describes a three-wave interaction.

## Chapter 5

### Numerical Method

#### 5.1 Symplectic Integration

As discussed earlier, chaotic motion in a system of waves may allow phase space diffusion that can have dramatic consequences for long-term stability. At the same time, invariant surfaces in phase space will often place strict limits on the motion. In doing numerical work, therefore, we must ensure that invariant structures are properly reproduced, as well as ensuring that the observed chaotic motion and phase space diffusion are true properties of the Hamiltonian under consideration and not spurious results of the numerical method.

In an  $N$ -degree-of-freedom Hamiltonian system, the evolution of the  $2N$  dynamical variables  $\mathbf{z} \equiv (q_1, \dots, q_N, p_1, \dots, p_N)$  during a time  $\Delta t$  is given by a canonical, or symplectic, transformation [14, 48]. Defining the  $2N \times 2N$  Jacobian matrix  $\mathbf{M}$  for this transformation

$$M_{ij}(\mathbf{z}) = \frac{\partial z'_i}{\partial z_j}, \quad (5.1)$$

the symplectic condition is stated as

$$\tilde{\mathbf{M}}\mathbf{M} = \mathbf{J} \quad (5.2)$$

where  $\mathbf{J}$  is the cosymplectic form (2.6). Such a transformation preserves the hierarchy of Poincare invariants [49], placing strict limits on the possible motion.

A consequence of this is the conservation of phase space volume as required by Liouville's theorem. A number of symplectic integration schemes have been developed which rigorously satisfy the symplectic requirement (see [23] and references therein). We employ two such approaches. The first is a symplectic Runge-Kutta algorithm [24, 50] which is applied to our Hamiltonian written in cartesian coordinates  $(P_i, Q_i)$ . While this provides an exactly symplectic transformation for the time advance of the dynamical variables, a major drawback is that the equations providing this transformation are implicit in the time-advanced variables  $z'_i$ . In general, this necessitates numerical solution of the implicit equations. It turns out that for the systems of interest in this work, this numerical solution is sometimes very difficult to achieve. A second approach that provides an algorithm in explicit form involves the application of Lie transformations [26]. In Section 5.3 we show how this method is used to obtain an explicit small-timestep integrator.

## 5.2 Symplectic Runge-Kutta

The Runge-Kutta method is one of the most commonly used techniques for integration of ordinary differential equations [51]. Less well known is the fact that this method, in implicit form, is symplectic [50]. For a Hamiltonian  $H$ , the symplectic transformation for the second-order Runge-Kutta timestep is given by [24]

$$z' = z + \Delta t \mathbf{J} \cdot \nabla H(z + \mathbf{y}, t + \Delta t/2) \quad (5.3)$$

where  $\mathbf{y}$  is the solution of the implicit equation

$$\mathbf{y} - \frac{\Delta t}{2} \mathbf{J} \cdot \nabla H(z + \mathbf{y}, t + \Delta t/2) = 0. \quad (5.4)$$



A fourth-order timestep is also possible [24]; in this paper only second-order was used. The complete FORTRAN subroutine used was written by H. Ye [52], based on the work in [24]. Numerical results obtained using this method will be described in the next chapter.

## 5.3 Lie Transformations

### 5.3.1 Introduction

Like most symplectic integration methods, the Runge-Kutta algorithm just described is an implicit method, requiring numerical solution of the implicit equations at each timestep. Besides being time-consuming, this numerical solution can sometimes be difficult to achieve. This turns out to be the case for some of the highly chaotic systems considered later in this paper. We therefore turn to another method which overcomes this difficulty, and in addition yields a much faster algorithm. This is the method of Lie transformations.

Given a time-independent Hamiltonian  $H$ , the evolution of the  $2N$  dynamical variables  $z_i$  during time  $\Delta t$  may be described in terms of an exponential operator

$$z'_i = e^{[-\Delta t H, \cdot]} z_i. \quad (5.5)$$

Such an operator  $e^{[f, \cdot]}$ , for any function  $f$ , is evaluated by expanding the exponential:

$$e^{[f, \cdot]} z_i \equiv z_i + [f, z_i] + \frac{1}{2!} [f, [f, z_i]] + \frac{1}{3!} [f, [f, [f, z_i]]] + \dots \quad (5.6)$$

where  $[f, g]$  is just the Poisson bracket

$$[f, g] = \sum_{i,j=1}^N \frac{\partial f}{\partial z_i} J^{ij} \frac{\partial g}{\partial z_j}$$

$$= \sum_{i,j=1}^N \left( \frac{\partial f}{\partial q_i} \frac{\partial g}{\partial p_i} - \frac{\partial g}{\partial q_i} \frac{\partial f}{\partial p_i} \right) \quad (5.7)$$

for any functions  $f$  and  $g$  of the dynamical variables. A transformation of the form (5.6) is known as a Lie transformation.

The evolution of the dynamical variables during time  $\Delta t$  under the action of the polynomial Hamiltonian  $H$  is then given by

$$\begin{aligned} z'_i &= e^{[-\Delta t H, \cdot]} z_i \\ &= z_i - \Delta t [H, z_i] + \frac{(\Delta t)^2}{2!} [H, [H, z_i]] \\ &\quad - \frac{(\Delta t)^3}{3!} [H, [H, [H, z_i]]] + \dots \end{aligned} \quad (5.8)$$

Note that for vanishing  $\Delta t$ , this just yields Hamilton's equations

$$\begin{aligned} \dot{q}_i &= -[H, q_i] = \frac{\partial H}{\partial p_i}, \\ \dot{p}_i &= -[H, p_i] = -\frac{\partial H}{\partial q_i}. \end{aligned}$$

It turns out that any (symplectic) transformation of the phase space variables  $z_i$  that may be written as a power series

$$z'_i = a_0 + a_j z_j + a_{jk} z_j z_k + a_{jkl} z_j z_k z_l + \dots \quad (5.9)$$

(where repeated indices imply summation) may be uniquely expressed in the form of an infinite product of Lie transformations of the form

$$\begin{aligned} z'_i &= \mathcal{M} z_i \\ &= \prod_{n=1}^{\infty} e^{[f_n, \cdot]} z_i \\ &= \dots e^{[f_4, \cdot]} e^{[f_3, \cdot]} e^{[f_2, \cdot]} e^{[f_1, \cdot]} z_i \end{aligned} \quad (5.10)$$

where  $f_n$  is a homogeneous polynomial of degree  $n$ . Each  $n$ -th order operator  $e^{[f_n, \cdot]}$  reproduces the corresponding  $n$ -th order terms in the series (5.9). The Hamiltonians that we will consider may all be written as polynomials, so that the resulting transformations will be of the form (5.9). Each operator in the product (5.10) describes a symplectic transformation, and the transformation described by the product of any number of such operators is likewise symplectic. If this infinite product is truncated at any order  $n$ , then the remaining finite product of operators will describe the motion accurately up to order  $n$  in the dynamical variables.

It is possible to combine a product of two or more operators into a single operator, or to decompose a single operator into a product. In general, two operators  $e^{[f, \cdot]}$  and  $e^{[g, \cdot]}$  will not commute with one another; i.e., the action of  $e^{[f, \cdot]}e^{[g, \cdot]}$  is not the same as the action of  $e^{[g, \cdot]}e^{[f, \cdot]}$ ; therefore the combination of two Lie operators into one is not trivial. However, a result known as the Campbell-Baker-Hausdorff theorem tells us how to relate these operators in terms of simple commutators of  $f$  and  $g$ . For Lie operators the commutators are very simply defined in terms of Poisson brackets involving  $f$  and  $g$ . The theorem gives us the following form for the combination of two operators:

$$e^{[\alpha f, \cdot]}e^{[\beta g, \cdot]} = e^{[h, \cdot]} \quad (5.11)$$

where

$$\begin{aligned} h = & \alpha f + \beta g + \frac{\alpha\beta}{2}[f, g] + \frac{\alpha^2\beta}{12}[f, [f, g]] + \frac{\alpha\beta^2}{12}[g, [g, f]] \\ & + \frac{\alpha^2\beta^2}{24}[f, [g, [g, f]]] + \mathcal{O}(\alpha^4\beta, \alpha^3\beta^2, \alpha^2\beta^3, \alpha\beta^4). \end{aligned} \quad (5.12)$$

Note that if  $\alpha$  and  $\beta$  are small parameters, then the higher-order commutators in  $h$  are progressively smaller, and in some cases may therefore be discarded above some desired order.

Any Lie transformation such as (5.6) or (5.8) has the required virtue of being exactly symplectic, but the infinite series unfortunately cannot be truncated at any finite order without destroying this symplecticity [28]. It turns out, however, that closed-form expressions exist for the general series [29]. For some special functions  $f$  the series actually terminates at finite order. For example, in one degree of freedom, if  $f = f(q)$  (no  $p$ -dependence) then we have  $[f, q] = 0$  and  $[f, p] = \frac{\partial f}{\partial q}$  so that we get

$$q' = q$$

$$p' = p + \frac{\partial f}{\partial q}.$$

A number of such results are summarized in Table 5.1 for various functions  $\alpha g(p, q)$  in one degree of freedom, where  $\alpha$  is an arbitrary constant. The extension to more degrees of freedom is trivial; in that case  $\alpha$  would be either a constant or a function of dynamical variables other than the  $(p_i, q_i)$  being operated on. The two formulas before the last one, for  $f = \alpha p^m q^n$ , are due to I. Gजा [29]. Along with the preceding expressions, and in conjunction with the Campbell-Baker-Hausdorff theorem, they provide explicit expressions for the action of any operator  $e^{[f, \cdot]}$ . The last formula provides the basis for a method due to Irwin, known as kick-factorization. This involves decomposing an arbitrary operator into a product of operators that yield terminating series (describing a “kick” of the dynamical variable). This is the method that was

$f = \alpha g(q)$	$q' = q$ $p' = p + \alpha \frac{\partial g}{\partial q}$
$f = \alpha g(p)$	$q' = q - \alpha \frac{\partial g}{\partial p}$ $p' = p$
$f = \alpha p^2$	$q' = q - 2\alpha p$ $p' = p$
$f = \alpha q^2$	$q' = q$ $p' = p + 2\alpha q$
$f = \alpha pq$	$q' = e^{-\alpha} q$ $p' = e^{\alpha} p$
$f = \alpha \frac{p^2 + q^2}{2}$	$q' = q \cos \alpha + p \sin \alpha$ $p' = -q \sin \alpha + p \cos \alpha$
$f = \alpha \frac{p^2 - q^2}{2}$	$q' = q \cosh \alpha - p \sinh \alpha$ $p' = -q \sinh \alpha + p \cosh \alpha$
$f = \alpha p^m q^n, m \neq n, m + n \geq 3$	$q' = q [1 + \alpha(n - m)q^{n-1}p^{m-1}]^{\frac{m}{m-n}}$ $p' = p [1 + \alpha(n - m)q^{n-1}p^{m-1}]^{\frac{n}{n-m}}$
$f = \alpha p^n q^n, n \geq 1$	$q' = q e^{-\alpha n q^{n-1} p^{n-1}}$ $p' = p e^{\alpha n q^{n-1} p^{n-1}}$
$f = \alpha (ap + bq)^n, n \geq 1$	$q' = q - \alpha a n (ap + bq)^{n-1}$ $p' = p + \alpha b n (ap + bq)^{n-1}$

Table 5.1: Transformations of  $(p, q)$  generated by  $e^{[f, \cdot]}$  for various  $f$ .

employed in our studies of wave-wave interaction. In the next section we describe the derivation of a numerical algorithm in terms of Lie transformations, and the reduction to explicit form by kick-factorization.

### 5.3.2 Application to a Simple Example

We now apply the methods of Dragt and Forest and of Irwin to derive an explicit, small time step integrator for the two-wave Hamiltonian (4.7), correct to third order in the dynamical variables  $z_i \equiv (Q_i, P_i)$  and in the timestep  $\Delta t$ . This will serve to illustrate the method and will provide us with one of the algorithms to be used later. (These methods may be used to obtain operators accurate to any desired order; for our purposes, however, third order is sufficient.)

That Hamiltonian for the interaction of two positive energy waves was given by

$$\begin{aligned} H &= \omega_1 J_1 + \omega_2 J_2 + \alpha J_1 \sqrt{J_2} \sin(2\theta_1 - \theta_2) \\ &= \frac{\omega_1}{2} (P_1^2 + Q_1^2) + \frac{\omega_2}{2} (P_2^2 + Q_2^2) + \alpha [2Q_1 P_1 P_2 - Q_2 (P_1^2 - Q_1^2)] \end{aligned} \quad (5.13)$$

where  $P_1 = \sqrt{2J_1} \cos \theta_1$ ,  $Q_1 = \sqrt{2J_1} \sin \theta_1$ . We seek expressions for the time advance in terms of second- and third-order polynomials  $f_2$  and  $f_3$ :

$$z'_i = e^{[f_3, \cdot]} e^{[f_2, \cdot]} z_i. \quad (5.14)$$

Let us write the Hamiltonian as  $H = H_2 + H_3$  where  $H_2$  is the part quadratic in  $P_1$  and  $Q_1$  (linear in  $J_1$ ) and  $H_3$  is the part cubic in  $P_1$  and  $Q_1$  (nonlinear in  $J_1$ ). Then  $f_2$  is given simply by

$$f_2 = -H_2 \Delta t. \quad (5.15)$$

When  $e^{[f_2, \cdot]}$  operates on the  $z_i$ , the resulting series may be summed to give the linear motion:

$$\begin{bmatrix} Q'_i \\ P'_i \end{bmatrix} = \begin{bmatrix} \cos(\omega_i \Delta t) & \sin(\omega_i \Delta t) \\ -\sin(\omega_i \Delta t) & \cos(\omega_i \Delta t) \end{bmatrix} \begin{bmatrix} Q_i \\ P_i \end{bmatrix}. \quad (5.16)$$

It is easily shown from the Campbell-Baker-Hausdorff formula (5.12) that our algorithm can be made accurate to order  $\Delta t^3$  rather than  $\Delta t^2$  by splitting the linear transformation into two parts:

$$z'_i = e^{[f_2/2, \cdot]} e^{[f_3, \cdot]} e^{[f_2/2, \cdot]} z_i. \quad (5.17)$$

This was done in our computations.

The polynomial  $f_3$  is given by the negative of the integral of  $H_3$  over the lowest-order orbits

$$f_3 \equiv - \int_0^{\Delta t} dt H_3(z'_i), \quad (5.18)$$

where  $H_3(z'_i)$  means the polynomial  $H_3$  evaluated at  $z'_i = e^{[f_2, \cdot]} z_i$ . Carrying out the operations, we obtain

$$\begin{aligned} f_3 = & -\frac{\alpha}{\sqrt{8\bar{\Omega}_1}} \left\{ \sin(\bar{\Omega}_1 \Delta t) [Q_2(Q_1^2 - P_1^2) + 2Q_1 P_1 P_2] \right. \\ & \left. + 2 \sin^2(\bar{\Omega}_1 \Delta t / 2) [P_2(Q_1^2 - P_1^2) - 2Q_1 P_1 Q_2] \right\}, \quad (5.19) \end{aligned}$$

where

$$\bar{\Omega}_1 \equiv 2\omega_1 - \omega_2. \quad (5.20)$$

Again from the Campbell-Baker-Hausdorff formula, we see that any operator  $e^{[f_3, \cdot]}$  involving a cubic polynomial  $f_3$  may be approximately re-expressed as a product of operators involving the constituent monomials:

$$\begin{aligned} e^{[f_3, \cdot]} & \equiv e^{[\sum_{i=1}^N f_3^{(i)}, \cdot]} \\ & \approx \prod_{i=1}^N e^{[f_3^{(i)}, \cdot]}, \quad (5.21) \end{aligned}$$

where the error is fourth order in the  $\hat{z}_i$ . Each operator  $e^{[f_3^{(i)}, \cdot]}$  yields an infinite series that may be written in closed form. We choose, however, to express the operators in polynomial form using the kick-factorization method of Irwin. This consists of replacing the operator  $e^{[f_3, \cdot]}$ , which couples two degrees of freedom, with a new operator  $e^{[g_3, \cdot]}$  where

$$g_3 = \sum_{i=1}^6 \rho_i (Q_1 \cos \phi_x^{(i)} + P_1 \sin \phi_y^{(i)})^2 (Q_2 \cos \phi_x^{(i)} + P_2 \sin \phi_y^{(i)}). \quad (5.22)$$

From the last formula in Table 1 we see that the action of the operator  $e^{[g_3, \cdot]}$  on any  $z_i$  yields an expression that terminates at second order, so that each time advance is now done in terms of compositions of quadratic polynomial mappings.

The angles comprising the linearly independent pairs  $(\phi_x, \phi_y)$  are chosen to be evenly spaced in the interval  $(0, 2\pi)$ . The coefficients  $\rho_i$  are found by simply solving the systems of equations  $f_3 = g_3$ , which comprise six linear equations in the six unknowns  $\rho_i$ . This system is most conveniently solved numerically.

In implementing the algorithm, we actually decomposed the polynomial operator  $e^{[g_3, \cdot]}$  into a product of operators involving the constituent monomials. To advance the dynamical variables by a single timestep we then



apply the six consecutive mappings

$$\begin{aligned}
 Q'_1 &= Q_1 - \rho_i 2(Q_1 \cos \phi_x^{(i)} + P_1 \sin \phi_x^{(i)})(Q_2 \cos \phi_y^{(i)} + P_2 \sin \phi_y^{(i)}) \sin \phi_x^{(i)}, \\
 Q'_2 &= Q_2 - \rho_i (Q_1 \cos \phi_x^{(i)} + P_1 \sin \phi_x^{(i)})^2 \sin \phi_y^{(i)}, \\
 P'_1 &= P_1 + \rho_i 2(Q_1 \cos \phi_x^{(i)} + P_1 \sin \phi_x^{(i)})(Q_2 \cos \phi_y^{(i)} + P_2 \sin \phi_y^{(i)}) \cos \phi_x^{(i)}, \\
 P'_2 &= P_2 + \rho_i (Q_1 \cos \phi_x^{(i)} + P_1 \sin \phi_x^{(i)})^2 \cos \phi_y^{(i)}, \\
 i &= 1, \dots, 6.
 \end{aligned}$$

(5.23)

The angles  $\phi_{x,y}^{(i)}$  were chosen as follows:

$$\left. \begin{array}{ll}
 \phi_x^{(1)} = 0 & \phi_y^{(1)} = \pi/3 \\
 \phi_x^{(2)} = 0 & \phi_y^{(2)} = 2\pi/3 \\
 \phi_x^{(3)} = \pi/3 & \phi_y^{(3)} = 0 \\
 \phi_x^{(4)} = \pi/3 & \phi_y^{(4)} = 2\pi/3 \\
 \phi_x^{(5)} = 2\pi/3 & \phi_y^{(5)} = 0 \\
 \phi_x^{(6)} = 2\pi/3 & \phi_y^{(6)} = \pi/3.
 \end{array} \right\} \quad (5.24)$$

We now have an explicit symplectic algorithm to follow the time evolution of Hamiltonian (5.13). For some situations discussed later, it is difficult to solve implicit equations for the time-advanced variables, so that explicitness is an important strength of the Lie method. Moreover, the simplicity of this algorithm results in an increase in speed by roughly a factor of 6 (for the systems considered in this paper) over the second-order Runge-Kutta method. For some of the more time-consuming calculations described later, this too will be an important virtue.

## Chapter 6

### Numerical Results: Explosive Instability and Two-Wave Interactions

We now present numerical results for several simple systems of interest. Results are grouped according to the number of degrees of freedom, which is determined by the number of resonances included in the Hamiltonian. Three cases are considered: one degree of freedom (to see how well our algorithm reproduces the known integrable motion); two degrees of freedom (to examine the effect of nonintegrability and resultant separatrix breaking in the simplest case); and three degrees of freedom (to study the effect of high dimensionality).

The only positive energy resonances considered in this chapter will be the near-resonances that occur for pairs of long-wavelength modes. The next chapter addresses the special case of an additional three-wave positive energy resonance.

The normalization introduced in Chapter 3 was such that time is in units of the inverse ion plasma frequency  $\omega_p^{-1}$ . In these units the constant coefficients in the Hamiltonian are extremely small, and the time scales over which the system evolution occurs are correspondingly long. The actual characteristic frequency of an ion-acoustic oscillation with wavenumber  $k_1$  is  $k_1 c_s$  in physical variables, or  $k_1$  in our dimensionless variables. For computations we therefore re-normalize by dividing the Hamiltonian by  $k_1$  and multiplying the time by  $k_1$ , so that one unit of time now corresponds to one ion-acoustic oscillation time

$k^{-1}$ . To make the Hamiltonian's coefficients even closer to unity, it is divided again by a factor of  $10^4$ , so that the unit of time finally used in computations is therefore ten thousand ion-acoustic oscillation times,  $10^4/k_1$ .

## 6.1 Integrable Cases

Before looking at numerical studies of chaos, we first check that our algorithm properly reproduces the known behavior of the integrable, single-resonance systems. We consider both a two-wave positive energy resonance and a three-wave negative energy resonance, comparing the performance of the second-order implicit Runge-Kutta algorithm and the explicit polynomial algorithm.

### 6.1.1 Positive Energy Resonance

The numerical methods are first applied to the single two-wave doublet described by Hamiltonian (4.7):

$$H = \omega_1 J_1 + \omega_2 J_2 + \alpha J_1 \sqrt{J_2} \sin(2\theta_1 - \theta_2). \quad (6.1)$$

We have seen that in terms of the resonance variables

$$\begin{aligned} \bar{I}_1 &= \frac{1}{2} J_1, & \bar{\psi}_1 &= 2\theta_1 - \theta_2, \\ \bar{I}_3 &= \frac{1}{2} J_1 + J_2, & \bar{\psi}_3 &= \theta_2, \end{aligned} \quad (6.2)$$

this takes the form

$$\bar{H} = \bar{\Omega}_1 \bar{I}_1 + 2\alpha \bar{I}_1 \sqrt{\bar{I}_3 - \bar{I}_1} \sin \bar{\psi}_1 \quad (6.3)$$

with  $\bar{\Omega}_1 \equiv 2\omega_1 - \omega_2$  and  $\bar{I}_3 = \text{constant}$ .

The resonance variables (or their cartesian counterparts) are convenient ones in which to view the phase space topology, but they are not good for numerical computations, due mainly to the difficulty of evaluating  $\sqrt{\bar{I}_3 - \bar{I}_1}$  when the argument is near zero. Numerical computations are therefore done in the original coordinates  $(P_i, Q_i)$ , using both second-order Runge-Kutta and Lie transformations; the Lie algorithm used is exactly that derived in Section 5.3.2. For the discussion here we need refer only to the resonance variables; the transformations between these and the  $(P_i, Q_i)$  were done internally by the computer.

In Figure 6.1 we plot  $\bar{Q}_1$  vs.  $\bar{P}_1$  for two values of  $L$ ; the parameters used here are the same as those used in Figure 4.3. Results are shown for both numerical algorithms; in both cases the timestep was  $dt = 1.0$ . Even for this rather large timestep, both algorithms show good agreement with the analytical curves of Figure 4.3. Both sets of curves were generated from the same set of initial conditions; it will be noted that due to some distortion of the curves by the numerical algorithms, these initial conditions do not yield exactly the same curves.

It is important also to consider the long-time effects of numerical error on the invariant curves. Figure 6.2 shows one curve of Figure 6.1.b with  $dt = 1.0$ , plotted for the first 2000 and last 2000 time units of the interval  $0 < t < 10^6$ . As with all work to be described in this paper, computations were done using 14-digit precision. In neither case is any numerical diffusion of the orbit observed.

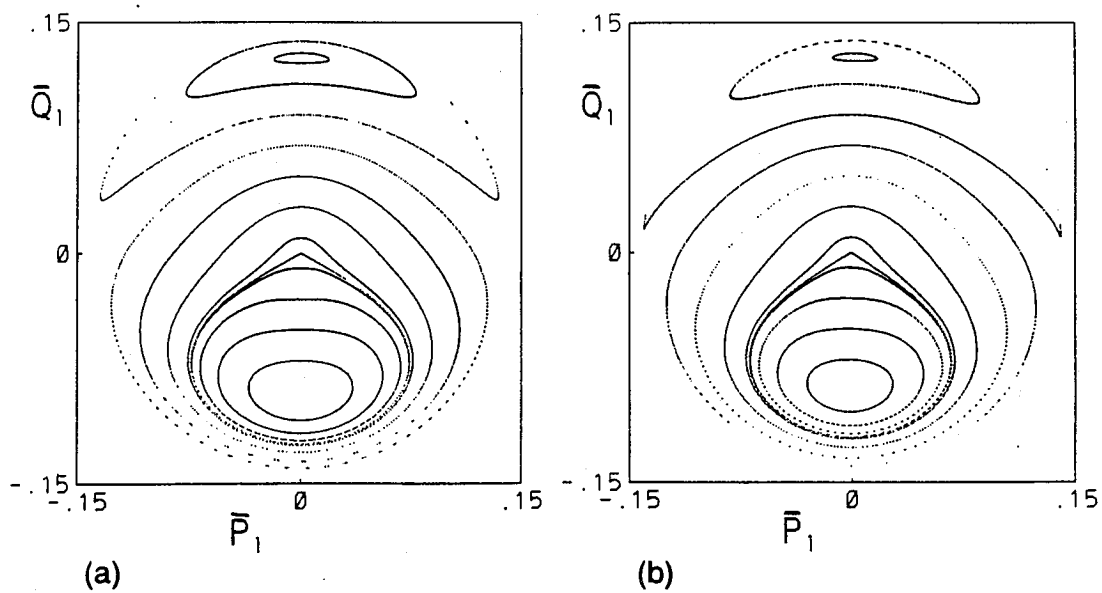


Figure 6.1: Numerical results for the Hamiltonian (4.12) with  $\Lambda = 100$ ,  $L = 5000$ ,  $v = 1.4796$ , using (a) Runge-Kutta, and (b) Lie transformations.

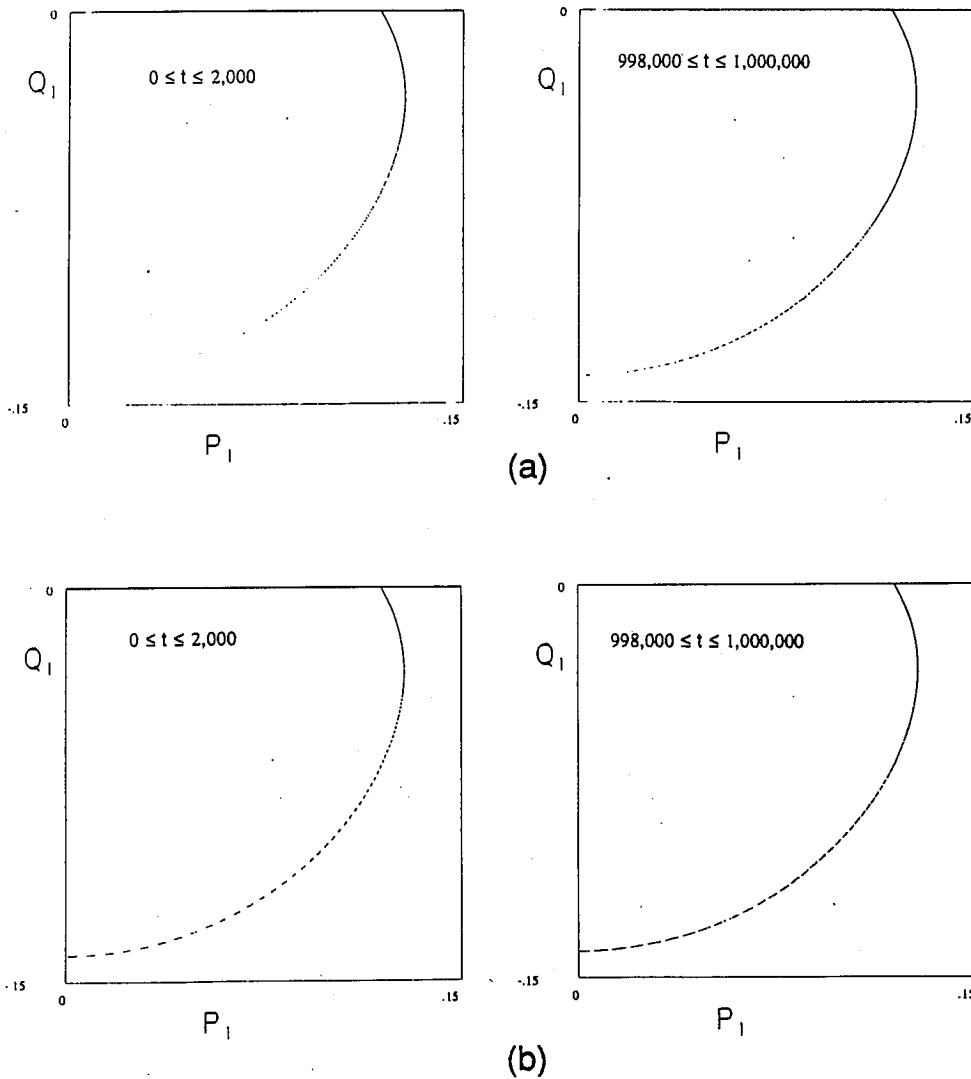


Figure 6.2: Long-time computation of a single invariant curve of Figure 6.1.b for timestep  $dt = 1.0$ , by (a) Runge-Kutta, and (b) Lie transformations, using 14-digit algebra. In each case the left-hand figure shows the curve plotted up to  $t = 2000$ , and the right-hand figure shows superimposed on this the curve plotted for  $998,000 < t < 1,000,000$ .

### 6.1.2 Negative Energy Resonance

We now consider the three-wave negative energy resonance described by Hamiltonian (4.24):

$$H = \omega_2 J_2 - \omega_4 J_4 - \omega_5 J_5 + \gamma \sqrt{J_2 J_4 J_5} \sin(\theta_2 + \theta_4 + \theta_5). \quad (6.4)$$

In terms of the resonance coordinates

$$\begin{aligned} \bar{I}_3 &= J_2, & \bar{\psi}_3 &= \theta_2 + \theta_4 + \theta_5, \\ \bar{I}_4 &= J_4 - J_2, & \bar{\psi}_4 &= \theta_4, \\ \bar{I}_5 &= J_5 - J_2, & \bar{\psi}_5 &= \theta_5 \end{aligned} \quad (6.5)$$

introduced earlier, this Hamiltonian takes the form

$$\bar{H} = \bar{\Omega}_3 \bar{I}_3 + \gamma \sqrt{\bar{I}_3 (\bar{I}_4 + \bar{I}_3) (\bar{I}_5 + \bar{I}_3)} \sin \bar{\psi}_3, \quad (6.6)$$

where  $\bar{\Omega}_3 = \omega_2 - \omega_4 - \omega_5$  and  $\bar{I}_4 = \text{constant}$ ,  $\bar{I}_5 = \text{constant}$ . For the special case  $\bar{I}_4 = \bar{I}_5 = 0$  (corresponding to  $J_2 = J_4 = J_5$ ), the Hamiltonian reduces to the polynomial form

$$\begin{aligned} \bar{H} &= \bar{\Omega}_3 \bar{I}_3 + \gamma \bar{I}_3^{\frac{3}{2}} \sin \bar{\psi}_3 \\ &= \frac{\bar{\Omega}_3}{2} (\bar{P}_3^2 + \bar{Q}_3^2) + \frac{\gamma}{2\sqrt{2}} \bar{Q}_3 (\bar{P}_3^2 + \bar{Q}_3^2). \end{aligned} \quad (6.7)$$

In this form the Hamiltonian is now amenable to the Lie transformation methods of Section 5.3.2. It will be noted that the nonlinear term in (6.7) is of a different form than that considered earlier, in that it involves only one degree of freedom rather than two. This leads to some difference in the application of kick-factorization. The treatment of this situation is deferred to Appendix D; here we just look at the results.

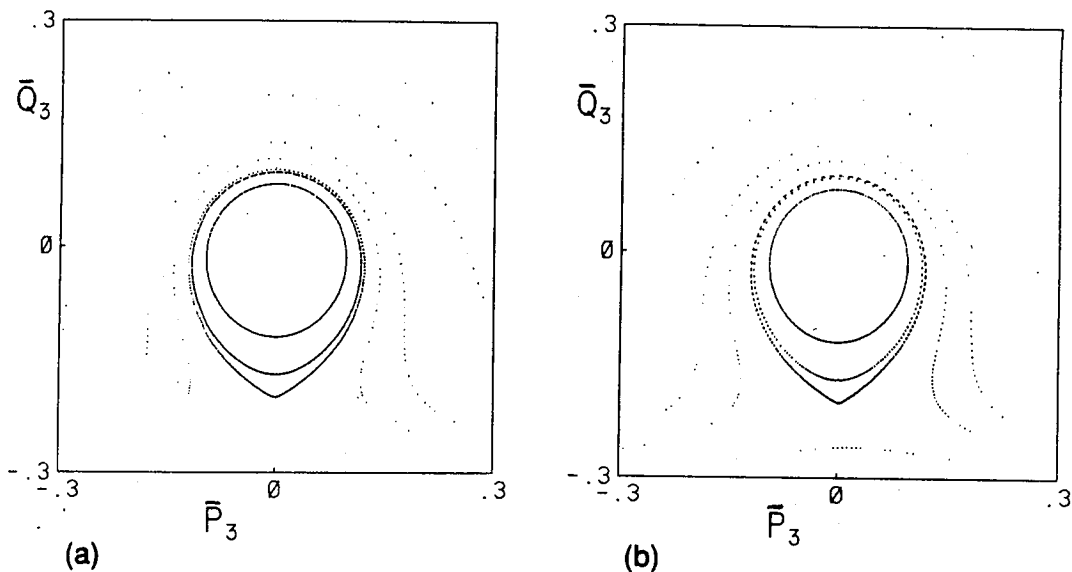


Figure 6.3: Numerical results for the Hamiltonian (6.7) with  $\Lambda = 100$ ,  $L = 5000$  and  $\nu = 1.47959256$  ( $\bar{\Omega}_3 \neq 0$ ), using (a) Runge-Kutta, and (b) Lie transformations.

As discussed in Section 4.2.2, the value of the detuning  $\bar{\Omega}_3$  depends strongly on  $\nu$  and relatively weakly on  $L$ . For a given  $L$ , the value of  $\nu$  which yields either exact resonance or a stable region of a desired size may be determined numerically.

In Figure 6.3 numerical results from both algorithms are displayed for the case  $\nu = 1.47959256$  ( $\bar{\Omega}_3 \neq 0$ ) and in Figure 6.4 for  $\nu = 1.47959435$  ( $\bar{\Omega}_3 = 0$ ). The analytical curves for the parameters considered here were shown in Figure 4.6. Again both algorithms show good qualitative agreement with the analytical curves. The only visible distortion occurs in Figure 6.4.b.



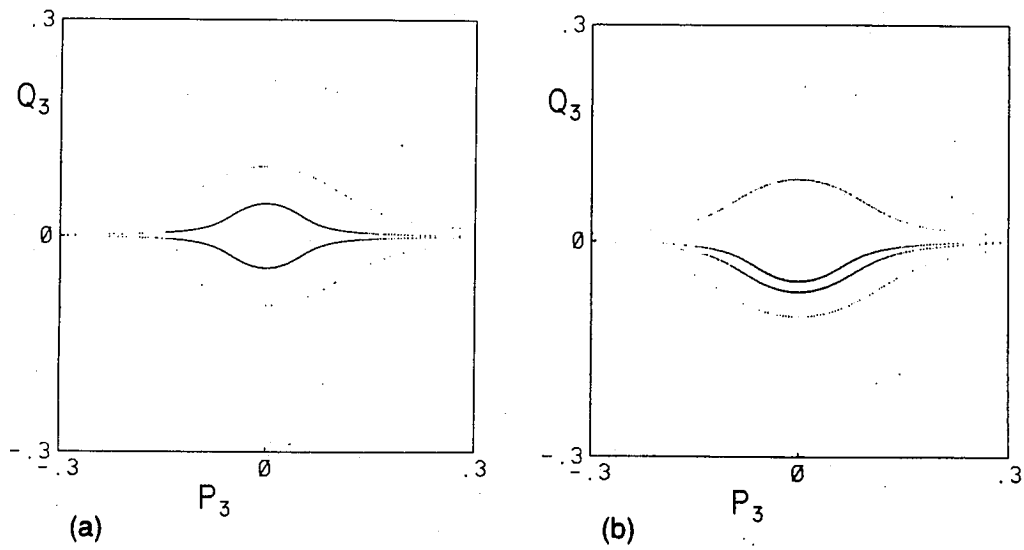


Figure 6.4: Numerical results for the Hamiltonian (6.7) with  $\Lambda = 100$ ,  $L = 5000$  and  $\nu = 1.47959435$  ( $\bar{\Omega}_3 = 0$ ) using (a) Runge-Kutta, and (b) Lie transformations.

The initial conditions were chosen symmetric about the  $\bar{Q}_3 = 0$  axis; distortion of the curves by the Lie algorithm results in these initial conditions yielding orbits not symmetric with respect to this axis.

## 6.2 Nonintegrability: Two Degrees of Freedom

We now examine two Hamiltonians involving two degrees of freedom. The two cases of interest are that of two positive energy resonances and that of one positive energy and one negative energy resonance.

### 6.2.1 Two Positive Energy Resonances

Consider first the Hamiltonian describing the interaction of all three modes of Figure 4.2:

$$\begin{aligned}
 H = \omega_1 J_1 + \omega_2 J_2 + \omega_3 J_3 + \alpha J_1 \sqrt{J_2} \sin(2\theta_1 - \theta_2) \\
 + \beta J_2 \sqrt{J_3} \sin(2\theta_2 - \theta_3),
 \end{aligned}
 \tag{6.8}$$

where  $\alpha$  is given in Eq. (4.9) and  $\beta$  in Eq. (4.18). The transformation to resonance variables comes from

$$F = \bar{I}_1(2\theta_1 - \theta_2) + \bar{I}_2(\theta_3 - 2\theta_2) + \bar{I}_3\theta_2 + \bar{I}_4\theta_4 + \bar{I}_5\theta_5,
 \tag{6.9}$$

which gives us

$$\begin{aligned}
 J_1 = \frac{\partial F}{\partial \theta_1} = 2\bar{I}_1, & \quad \bar{\psi}_1 = \frac{\partial F}{\partial \bar{I}_1} = 2\theta_1 - \theta_2, \\
 J_2 = \frac{\partial F}{\partial \theta_2} = \bar{I}_3 - 2\bar{I}_2 - \bar{I}_1, & \quad \bar{\psi}_2 = \frac{\partial F}{\partial \bar{I}_2} = \theta_3 - 2\theta_2, \\
 J_3 = \frac{\partial F}{\partial \theta_3} = \bar{I}_2, & \quad \bar{\psi}_3 = \frac{\partial F}{\partial \bar{I}_3} = \theta_2.
 \end{aligned}
 \tag{6.10}$$

The Hamiltonian then becomes

$$\begin{aligned}
 \bar{H} &= H - \omega_2 \bar{I}_3 \\
 &= \bar{\Omega}_1 \bar{I}_1 + \bar{\Omega}_2 \bar{I}_2 + \alpha 2 \bar{I}_1 \sqrt{\bar{I}_3 - 2 \bar{I}_2 - \bar{I}_1} \sin \bar{\psi}_1 \\
 &\quad - \beta (\bar{I}_3 - 2 \bar{I}_2 - \bar{I}_1) \sqrt{\bar{I}_2} \sin \bar{\psi}_2
 \end{aligned} \tag{6.11}$$

where

$$\bar{\Omega}_1 = 2\omega_1 - \omega_2$$

$$\bar{\Omega}_2 = \omega_3 - 2\omega_2$$

$$\bar{I}_3 = \frac{1}{2} J_1 + J_2 + 2J_3 = \text{constant.}$$

Again, computations were done in the original variables  $P_i, Q_i$  (in three degrees of freedom). All results displayed in this section were obtained using Lie transformations; as in Section 6.1, these agree well with the results from Runge-Kutta.

Note that the first and second nonlinear terms of Hamiltonian (6.11) have the forms that occur in Hamiltonians (4.12) and (4.21), respectively. These would individually produce the phase space structure seen in Figures 4.3 and 4.4.

We have been studying the phase space topology of single-resonance Hamiltonians with the help of phase space plots, which is trivial for one-degree-of-freedom systems. As discussed in Sections 2.2 and 2.3, Poincare surface-of-section plots can be used to obtain similar visualizations for two-degree-of-freedom systems. Thus we examine the plane  $\bar{\psi}_2 = \frac{\pi}{2}$  ( $\bar{P}_2 = 0$ ) in phase

space. That is, each time that  $\bar{P}_2 = 0$  goes through 0 (with the same sign time derivative) we plot  $\bar{Q}_1$  vs.  $\bar{P}_1$ . (The actual points plotted are determined by linear interpolation between the values immediately before and after  $\bar{\psi}_2$  goes through  $\frac{\pi}{2}$ .)

Typically, a surface-of-section plot is made by considering a fixed value of the energy  $\bar{H}$ . For the Hamiltonian (6.11), given any initial condition  $\bar{\psi}_1, \bar{I}_1$  on the  $\bar{\psi}_2 = \text{constant}$  plane, the initial value of  $\bar{I}_2$  is automatically determined by the constancy of the energy (unless the initial conditions are incompatible with the specified value of  $H$ , in which case no real solution for  $\bar{I}_2$  would be found).

Here a slightly different approach will be used, in order to facilitate comparison with the constant-energy contours plotted for the single-resonance cases in Section 4.2. For the Hamiltonian (6.11), we consider a series of orbits starting with various values of  $(\bar{\psi}_1, \bar{I}_1)$ , but some fixed, very small value of  $\bar{I}_2$  (i.e., a very small value of  $J_3$ ). These orbits will all correspond to different values of  $\bar{H}$ , which will be very nearly equal to the values of  $\bar{H}$  for the contours plotted in Figure 4.3 for the Hamiltonian (4.12), for which the mode  $J_3$  was absent. Now, however, the resonant interaction between modes  $J_2$  and  $J_3$  will lead to growth of  $J_3$  via decay instability, with a strong perturbing effect on the system. By plotting the resulting orbits we can then observe directly the perturbation to the constant-energy surfaces of Figure 4.3 caused by coupling to  $J_3$ .

In a surface-of-section plot corresponding to a two-degree-of-freedom Hamiltonian with a fixed value of  $\bar{H}$ , invariant curves cannot cross one another since that would violate the invariance. Note that this does not apply to the

plots considered here, since we are actually displaying orbits corresponding to different values of the Hamiltonian, plotted on the same page.

The phase space topology is determined primarily by the effective detunings  $\frac{\bar{\Omega}_1}{\alpha}$  and  $\frac{\bar{\Omega}_2}{\beta}$ . If we had  $\beta = 0$ , then we know that the origin ( $\bar{I}_1 = 0$ ) of that one-degree-of-freedom system would become unstable for  $|\frac{\bar{\Omega}_1}{\alpha}| < \sqrt{\bar{I}_3}$ . For the two-degree-of-freedom system this criterion will be shifted due to the non-zero  $\bar{I}_2$ . When  $|\frac{\bar{\Omega}_1}{\alpha}|$  is small then  $|\frac{\bar{\Omega}_2}{\beta}|$  will also be small (although not quite as small), and the smaller these two values are, the more chaotic the system's behavior will be.

In Figure 6.5 results are shown for  $\Lambda = 100$  and  $\nu = 1.4796$ , with  $L$  ranging from 2500 to 9000. For every orbit, the initial value of  $\bar{Q}_2$  is  $10^{-6}$  (corresponding to  $\bar{I}_2 = 5 \times 10^{-13}$ ).  $\bar{I}_3$  was set to 0.01. While very large timesteps were used in plotting the phase space for one-degree-of-freedom systems, in order to obtain good surface-of-section plots here a smaller value is required; we used  $dt = 0.1$ . For  $L = 2500$  ( $\frac{\bar{\Omega}_1}{\alpha} \approx .19$ ,  $\frac{\bar{\Omega}_2}{\beta} \approx -.53$ ) there is an unstable fixed point at the origin. A very thin stochastic layer exists along the separatrix through this fixed point; the chaotic motion is not observable in this picture. For  $L = 5000$  ( $\frac{\bar{\Omega}_1}{\alpha} \approx .09$ ,  $\frac{\bar{\Omega}_2}{\beta} \approx -.27$ ) the stochastic layer through the origin has become more prominent, and when  $L = 9000$  ( $\frac{\bar{\Omega}_1}{\alpha} \approx .05$ ,  $\frac{\bar{\Omega}_2}{\beta} \approx -.15$ ) a majority of the accessible phase plane is occupied by chaotic orbits.

Here we have considered a fixed value of the constant  $\bar{I}_3$ . A different value of  $\bar{I}_3$  would mean that a different value of the effective detuning  $\frac{\bar{\Omega}_1}{\alpha}$  would be required in order to have instability at the origin of the  $\bar{P}_1$ - $\bar{Q}_1$  plane.

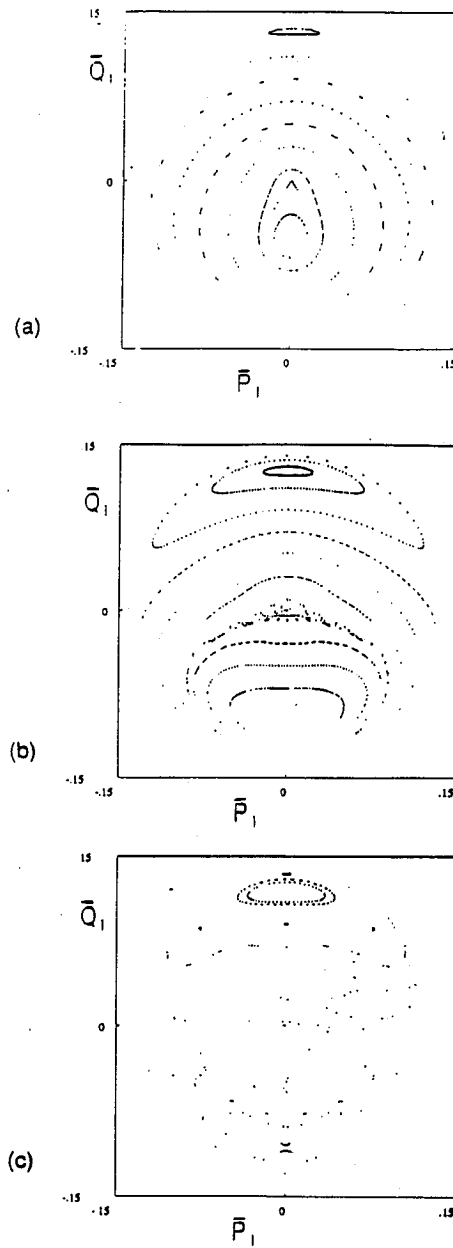


Figure 6.5:  $\bar{P}_2 = 0$  surface-of-section plots for Hamiltonian (6.11), with (a)  $L = 2500$ ; (b)  $L = 5000$ ; (c)  $L = 9000$ . Each orbit was started with  $\bar{Q}_2 = 10^{-6}$ , so that each corresponds to a different value of  $\bar{H}$ .

### 6.2.2 One Positive Energy and One Negative Energy Resonance

We have seen that wave-wave coupling involving multiple positive energy resonances can lead to strongly chaotic motion. We expect that when one of these waves is also involved in a negative energy resonance, then the occurrence of explosive instability may be strongly influenced by this chaotic motion. The many-dimensional nature (three degrees of freedom) of such a system may be particularly critical. However, before considering the effect of coupling a negative energy triplet to two positive energy resonances with their attendant strong chaos, we first consider the effect of coupling to a single positive energy resonance. While unlikely to be so strongly chaotic, such a system will exhibit some interesting effects.

We therefore consider the four modes shown in Figure 6.6. These are the same modes of Figure 4.5 with mode  $J_3$  of Figure 4.2 added. The Hamiltonian is

$$\begin{aligned}
 H = & \omega_2 J_2 + \omega_3 J_3 - \omega_4 J_4 - \omega_5 J_5 \\
 & + \beta J_2 \sqrt{J_3} \sin(2\theta_2 - \theta_3) \\
 & + \gamma \sqrt{J_2 J_4 J_5} \sin(\theta_2 + \theta_4 + \theta_5). \tag{6.12}
 \end{aligned}$$

The generating function

$$\begin{aligned}
 F = & \bar{I}_2(\theta_3 - 2\theta_2) + \bar{I}_3(\theta_2 + \theta_4 + \theta_5) \\
 & + \bar{I}_4\theta_4 + \bar{I}_5\theta_5 \tag{6.13}
 \end{aligned}$$

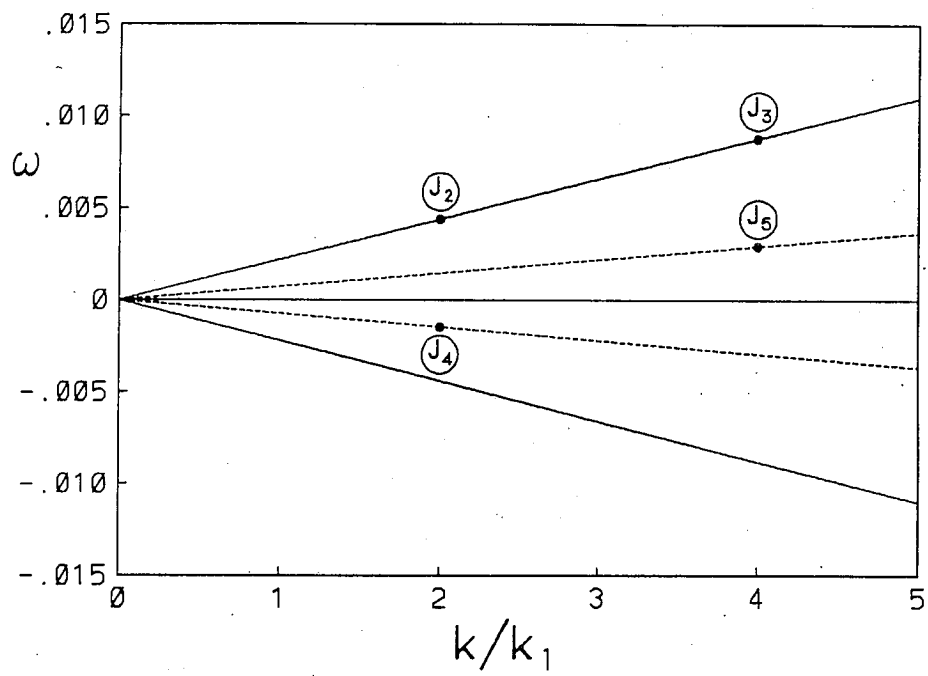


Figure 6.6: Four modes comprising one negative energy resonance and one positive energy near-resonance.



yields the transformation

$$\begin{aligned}
J_2 &= \frac{\partial F}{\partial \theta_2} = \bar{I}_3 - 2\bar{I}_2, & \bar{\psi}_2 &= \frac{\partial F}{\partial \bar{I}_2} = \theta_3 - 2\theta_2, \\
J_3 &= \frac{\partial F}{\partial \theta_3} = \bar{I}_2, & \bar{\psi}_3 &= \frac{\partial F}{\partial \bar{I}_3} = \theta_2 + \theta_4 + \theta_5, \\
J_4 &= \frac{\partial F}{\partial \theta_4} = \bar{I}_4 + \bar{I}_3, & \bar{\psi}_4 &= \frac{\partial F}{\partial \bar{I}_4} = \theta_4, \\
J_5 &= \frac{\partial F}{\partial \theta_5} = \bar{I}_5 + \bar{I}_3, & \bar{\psi}_5 &= \frac{\partial F}{\partial \bar{I}_5} = \theta_5,
\end{aligned} \tag{6.14}$$

so that the Hamiltonian becomes

$$\begin{aligned}
\bar{H} &= H + \omega_4 \bar{I}_4 + \omega_5 \bar{I}_5 \\
&= \bar{\Omega}_2 \bar{I}_2 + \bar{\Omega}_3 \bar{I}_3 - \beta (\bar{I}_3 - 2\bar{I}_2) \sqrt{\bar{I}_2} \sin \bar{\psi}_2 \\
&\quad + \gamma \sqrt{(\bar{I}_3 - 2\bar{I}_2)(\bar{I}_4 + \bar{I}_3)(\bar{I}_5 + \bar{I}_3)} \sin \bar{\psi}_3
\end{aligned} \tag{6.15}$$

where

$$\bar{\Omega}_2 \equiv \omega_3 - 2\omega_2,$$

$$\bar{\Omega}_3 \equiv \omega_2 - \omega_4 - \omega_5,$$

$$\bar{I}_4 = J_4 - (J_2 + 2J_3) = \text{constant},$$

$$\bar{I}_5 = J_5 - (J_2 + 2J_3) = \text{constant}.$$

For  $\bar{I}_4 = \bar{I}_5 = 0$  this reduces to

$$\begin{aligned}
\bar{H} &= \bar{\Omega}_2 \bar{I}_2 + \bar{\Omega}_3 \bar{I}_3 - \beta (\bar{I}_3 - 2\bar{I}_2) \sqrt{\bar{I}_2} \sin \bar{\psi}_2 \\
&\quad + \gamma \bar{I}_3 \sqrt{\bar{I}_3 - 2\bar{I}_2} \sin \bar{\psi}_3.
\end{aligned} \tag{6.16}$$

Rather than carrying out computations in the original four-degree-of-freedom Hamiltonian, this time a special set of computational coordinates are employed,

which reduce the Hamiltonian to a three-degree-of-freedom polynomial. It is convenient to defer discussion of these coordinates until later (Section 6.3 and Appendix D). For now we need only refer to the resonance variables  $(\bar{I}_i, \bar{\psi}_i)$  or  $(\bar{P}_i, \bar{Q}_i)$  that will be used for displaying our results. The results of this section were obtained from the second-order Runge-Kutta algorithm; this was the one case where Lie transformations did not give satisfactory results. (That method yielded results that depended strongly on the timestep, while Runge-Kutta results did not display this dependence. The Lie method agreed with Runge-Kutta only for exceedingly small timesteps.)

In Figure 6.7, we again see a  $\bar{P}_2 = 0$  surface-of-section, plotting  $\bar{Q}_3$  vs.  $\bar{P}_3$  for various values of  $L$ . As in the last section,  $\bar{Q}_2(0) = 10^{-6}$  for each orbit, so that each orbit corresponds to a different value of  $\bar{H}$ . The timestep was  $dt = 0.1$ . These orbits may then be thought of the energy contours of Section 4.2.2, perturbed by the near-resonant coupling between modes  $J_2$  and  $J_3$ . For each value of  $L$ ,  $v$  was chosen so that, in the absence of mode  $J_3$ , the separatrix around the stable region would be of the same size (passing through the point  $\bar{P}_2 = 0, \bar{Q}_2 = 0.1$ ). This separatrix was plotted for each case, to see how the region of stability has been affected by the coupling to  $J_3$ .

In all three cases we see that the stable region has been enlarged. This may be understood from the form of Hamiltonian (6.16). In the second nonlinear term, we see that the coupling to the  $\bar{\psi}_2 - \bar{I}_2$  motion (i.e, the coupling to mode  $J_3$ ) has resulted in a factor of  $\sqrt{\bar{I}_3}$  being replaced by  $\sqrt{\bar{I}_3 - 2\bar{I}_2}$ . This effectively decreases the nonlinearity associated with the negative energy resonance, and we therefore expect a stabilizing influence. While the new stable region does not change drastically in size with  $L$ , we find that for  $L = 2500$  the separatrix

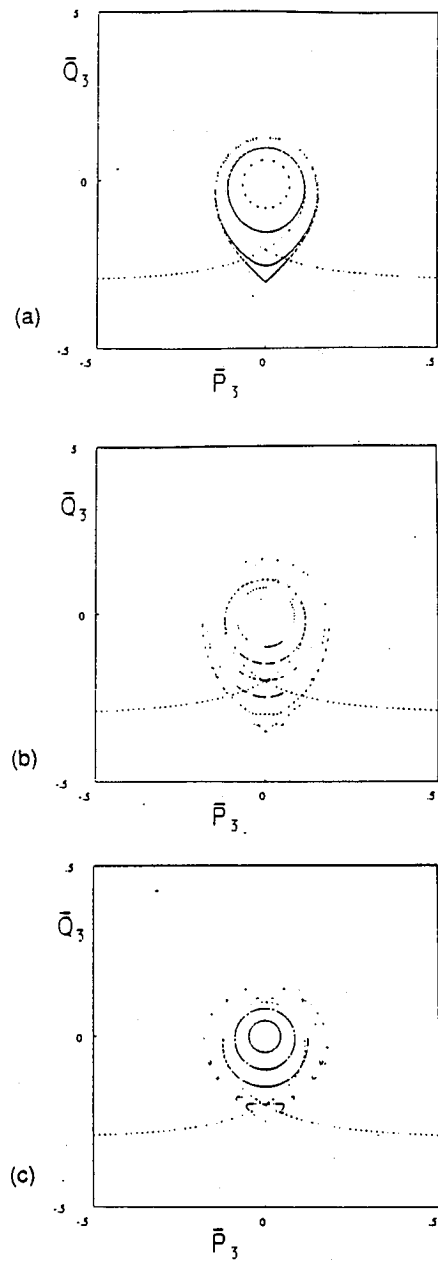


Figure 6.7: Surface-of-section plots for Hamiltonian (6.16), for (a)  $L = 2500$ , (b)  $L = 5000$  and (c)  $L = 9000$ .

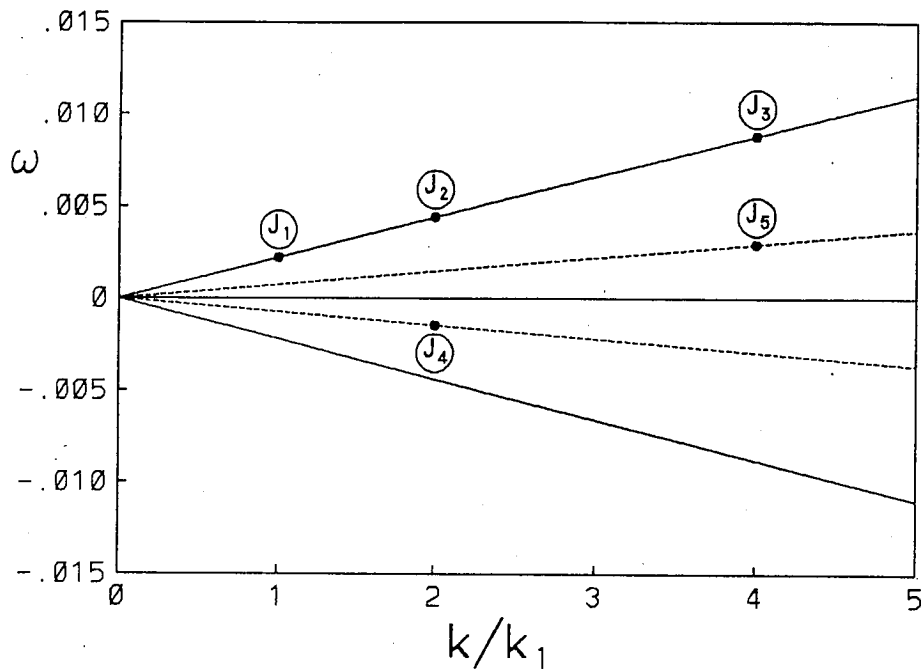


Figure 6.8: Five modes comprising a negative energy resonance and two positive energy near-resonances.

appears quite regular, while for larger  $L$  chaotic orbits and large island chains appear around the stable region.

### 6.3 Chaotic Transport in Three Degrees of Freedom

We now consider a system consisting of all five modes considered above, as shown in Figure 6.8. Modes  $J_2$ ,  $J_4$  and  $J_5$  form a negative energy triplet, while mode  $J_2$  forms two near-resonances with modes  $J_1$  and  $J_3$ . Recalling our earlier results: We saw above that the two near-resonances involving modes  $J_1$ ,  $J_2$  and  $J_3$  can generate strongly chaotic motion, depending on the value of  $k_1$ . The negative energy resonance will drive explosive instability when

the resonance condition  $\bar{\Omega}_3 = 0$  is satisfied. We then expect that any initial conditions will lead to immediate explosive growth. By changing  $v$  we detune this resonance, opening an islet of “stable” motion around  $\bar{I}_3 = 0$ . If the system is strongly chaotic then fast diffusion can occur in phase space, so that any orbits may quickly achieve large enough amplitude for explosive instability to occur. If the system is less chaotic and there are many invariant surfaces near the equilibrium point, then such fast diffusion cannot occur. However, unlike the two-degree-of-freedom case just considered, where two-dimensional surfaces partition the three-dimensional energy surface and provide absolute barriers to transport, these three-dimensional surfaces cannot partition the five-dimensional energy surface, and thus an orbit lying in a stochastic region very near the origin is not prevented from finding its way to large amplitude and subsequent explosive growth.

This system is of course much simpler than is likely to occur in reality. We would typically expect many more modes to be present and interacting via two-wave near-resonances. However, this system is of interest as the simplest highly chaotic system of more than two degrees of freedom that we can obtain from our counterstreaming ion model.

The Hamiltonian for the five-wave set is given by

$$\begin{aligned}
 H = & \omega_1 J_1 + \omega_2 J_2 + \omega_3 J_3 - \omega_4 J_4 - \omega_5 J_5 \\
 & + \alpha J_1 \sqrt{J_2} \sin(2\theta_1 - \theta_2) \\
 & + \beta J_2 \sqrt{J_3} \sin(2\theta_2 - \theta_3) \\
 & + \gamma \sqrt{J_2 J_4 J_5} \sin(\theta_2 + \theta_4 + \theta_5). \tag{6.17}
 \end{aligned}$$

The transformation to resonance variables is obtained from the generating function

$$\begin{aligned}
F = & \bar{I}_1(2\theta_1 - \theta_2) + \bar{I}_2(\theta_3 - 2\theta_2) + \bar{I}_3(\theta_2 + \theta_4 + \theta_5) \\
& + \bar{I}_4\theta_4 + \bar{I}_5\theta_5
\end{aligned} \tag{6.18}$$

which gives us

$$\begin{aligned}
J_1 = \frac{\partial F}{\partial \theta_1} = 2\bar{I}_1, & \quad \bar{\psi}_1 = \frac{\partial F}{\partial \bar{I}_1} = 2\theta_1 - \theta_2, \\
J_2 = \frac{\partial F}{\partial \theta_2} = \bar{I}_3 - 2\bar{I}_2 - \bar{I}_1, & \quad \bar{\psi}_2 = \frac{\partial F}{\partial \bar{I}_2} = \theta_3 - 2\theta_2, \\
J_3 = \frac{\partial F}{\partial \theta_3} = \bar{I}_2, & \quad \bar{\psi}_3 = \frac{\partial F}{\partial \bar{I}_3} = \theta_2 + \theta_4 + \theta_5, \\
J_4 = \frac{\partial F}{\partial \theta_4} = \bar{I}_4 + \bar{I}_3, & \quad \bar{\psi}_4 = \frac{\partial F}{\partial \bar{I}_4} = \theta_4, \\
J_5 = \frac{\partial F}{\partial \theta_5} = \bar{I}_5 + \bar{I}_3, & \quad \bar{\psi}_5 = \frac{\partial F}{\partial \bar{I}_5} = \theta_5.
\end{aligned} \tag{6.19}$$

From this we obtain the three-degree-of-freedom Hamiltonian

$$\begin{aligned}
\bar{H} = & H + \omega_4\bar{I}_4 + \omega_5\bar{I}_5 \\
= & \bar{\Omega}_1\bar{I}_1 + \bar{\Omega}_2\bar{I}_2 + \bar{\Omega}_3\bar{I}_3 + \alpha 2\bar{I}_1\sqrt{\bar{I}_3 - 2\bar{I}_2 - \bar{I}_1} \sin \bar{\psi}_1 \\
& - \beta(\bar{I}_3 - 2\bar{I}_2 - \bar{I}_1)\sqrt{\bar{I}_2} \sin \bar{\psi}_2 \\
& + \gamma\sqrt{(\bar{I}_3 - 2\bar{I}_2 - \bar{I}_1)(\bar{I}_4 + \bar{I}_3)(\bar{I}_5 + \bar{I}_3)} \sin \bar{\psi}_3,
\end{aligned} \tag{6.20}$$

where

$$\bar{\Omega}_1 \equiv 2\omega_1 - \omega_2,$$

$$\bar{\Omega}_2 \equiv \omega_3 - 2\omega_2,$$

$$\bar{\Omega}_3 \equiv \omega_2 - \omega_4 - \omega_5,$$

and

$$\bar{I}_4 = J_4 - \left(\frac{1}{2}J_1 + J_2 + 2J_3\right) = \text{constant},$$

$$\bar{I}_5 = J_5 - \left(\frac{1}{2}J_1 + J_2 + 2J_3\right) = \text{constant}.$$

As before, the resonance variables  $(\bar{I}_i, \bar{\psi}_i)$  are not well-suited to computations. Rather than doing our numerics with the original five-degree-of-freedom Hamiltonian (6.17), however, we note that it is possible, for the special case  $\bar{I}_4 = \bar{I}_5 = 0$  (i.e.,  $J_2 = J_4 = J_5$ ), to find a set of coordinates that transforms this into a three-degree-of-freedom polynomial Hamiltonian. This transformation, and the subsequent derivation of a numerical algorithm via Lie transformations, is carried out in Appendix D. Here we will summarize the numerical results.

We consider initial states where modes  $J_2$ ,  $J_4$  and  $J_5$  (those involved in the explosive instability) are of significant (and equal) amplitude, while modes  $J_1$  and  $J_3$  begin with very small amplitudes. In the transformed variables, this means that  $\bar{I}_3$  starts with significant amplitude, while  $\bar{I}_1$  and  $\bar{I}_2$  are very small. As in the last section, therefore, we will essentially see a perturbation of the constant-energy curves of Figure 4.6 due to the coupling to modes  $J_1$  and  $J_3$  ( $\bar{I}_1$  and  $\bar{I}_2$ ). As we have seen, for long enough wavelengths the nonlinear coupling between modes  $J_1$ ,  $J_2$  and  $J_3$  will lead to growth of  $J_1$  ( $\bar{I}_1$ ) via decay instability. The chaotic motion that originates along the associated separatrix (but which may be very widespread) will then drive diffusion in the value of  $\bar{I}_3$ .

Fixing the value  $\Lambda = 100$ , we scan various system sizes  $L$ . As in the last section, for each  $L$ ,  $\nu$  was chosen to yield an “unperturbed” separatrix of

the same size. The system is initialized with various values of  $\bar{P}_3(0)$ ,  $\bar{Q}_3(0)$  while always using  $\bar{P}_1(0) = \bar{P}_2(0) = 0$ ,  $\bar{Q}_1(0) = \bar{Q}_2(0) = 10^{-6}$ . (Again, the timestep was  $dt = 0.1$ .) Starting  $\bar{I}_3$  large enough should always lead to immediate explosive growth. If  $\bar{I}_3$  starts well within the “stable” islet, then it will exhibit fairly stable motion initially, but may undergo stochastic diffusion in amplitude until reaching large enough size for explosive growth to occur. An arbitrarily chosen amplitude of 100 marks “escape” if any of the computational variables  $\hat{P}_i$  or  $\hat{Q}_i$  gets larger than this. Mode amplitudes are not monitored once explosive growth sets in; we are interested only in how the modes achieve sufficient amplitude for this growth to begin.

Figures 6.9-6.13 show surface-of-section plots for various initial conditions, for the cases  $L = 5000$  and  $L = 10000$ , respectively. The unperturbed separatrix passes through the point  $\bar{P}_3 = 0$ ,  $\bar{Q}_3 = -0.2$ ; all initial conditions included  $\bar{P}_3(0) = 0$ , and  $-0.2 < \bar{Q}_3(0) < 0$  (within the separatrix). We examined the plane  $\bar{P}_2 = 0$ , plotting  $\bar{Q}_1$  vs.  $\bar{P}_1$  and  $\bar{Q}_3$  vs.  $\bar{P}_3$ . Superimposed on the  $\bar{P}_3$ - $\bar{Q}_3$  plot is the separatrix that would exist in the absence of modes  $J_1$  and  $J_3$ . Plots are shown for various time intervals. It should be noted that what is seen here is one possible projection of the five-dimensional energy surface. A surface-of-section for a two-degree-of-freedom Hamiltonian maps invariant surfaces into two-dimensional lines, so that all the essential qualitative behavior of the system is captured graphically. In a surface-of-section for a three-degree-of-freedom Hamiltonian, however, there is no unique way to plot the four independent variables. It is found, however, that the chosen projections still provide enlightening information on the phase space structure.

The  $\bar{P}_1$ - $\bar{Q}_1$  and  $\bar{P}_3$ - $\bar{Q}_3$  motions now strongly affect one another. When



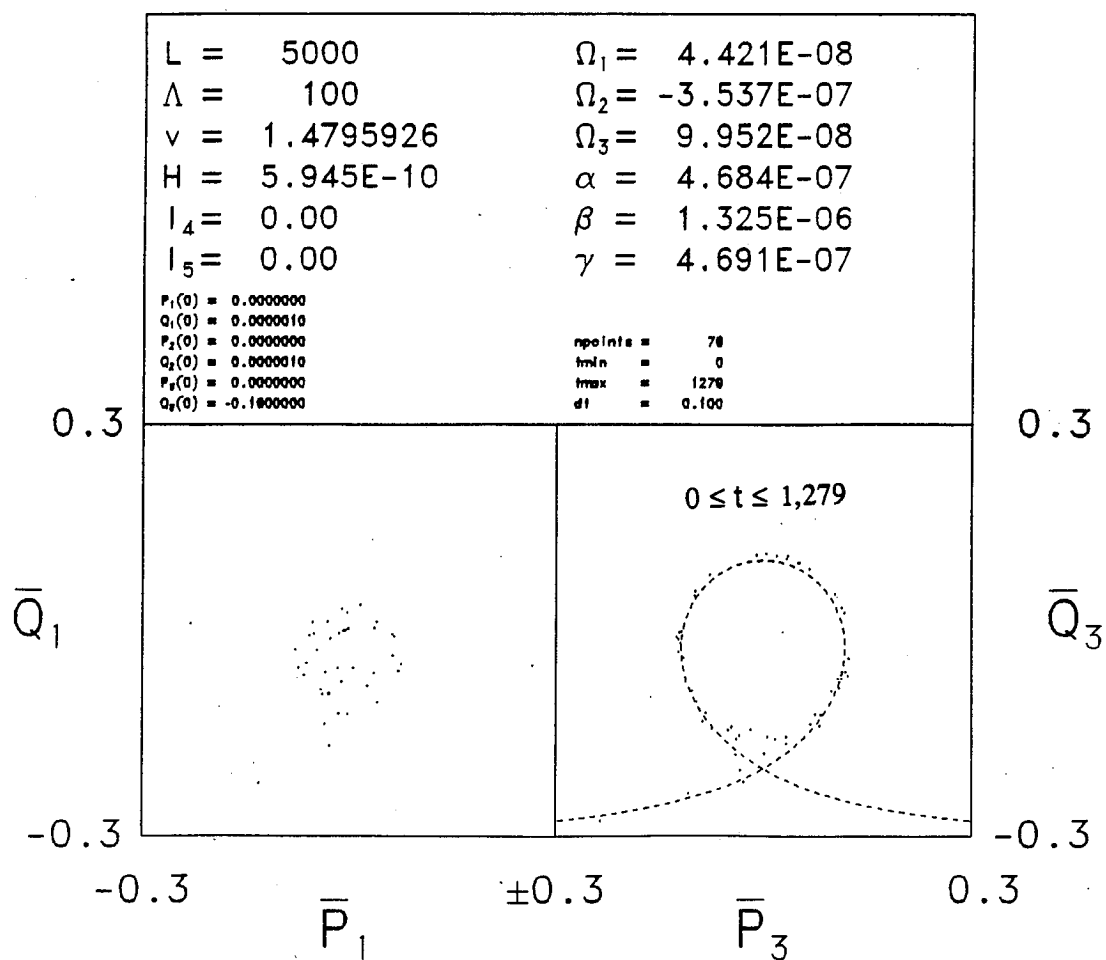


Figure 6.9: Phase space diffusion in three degrees of freedom, with  $L = 5000$  and  $\bar{Q}_3(0) = -0.16$ . Escape occurs at  $t = 1279$ .

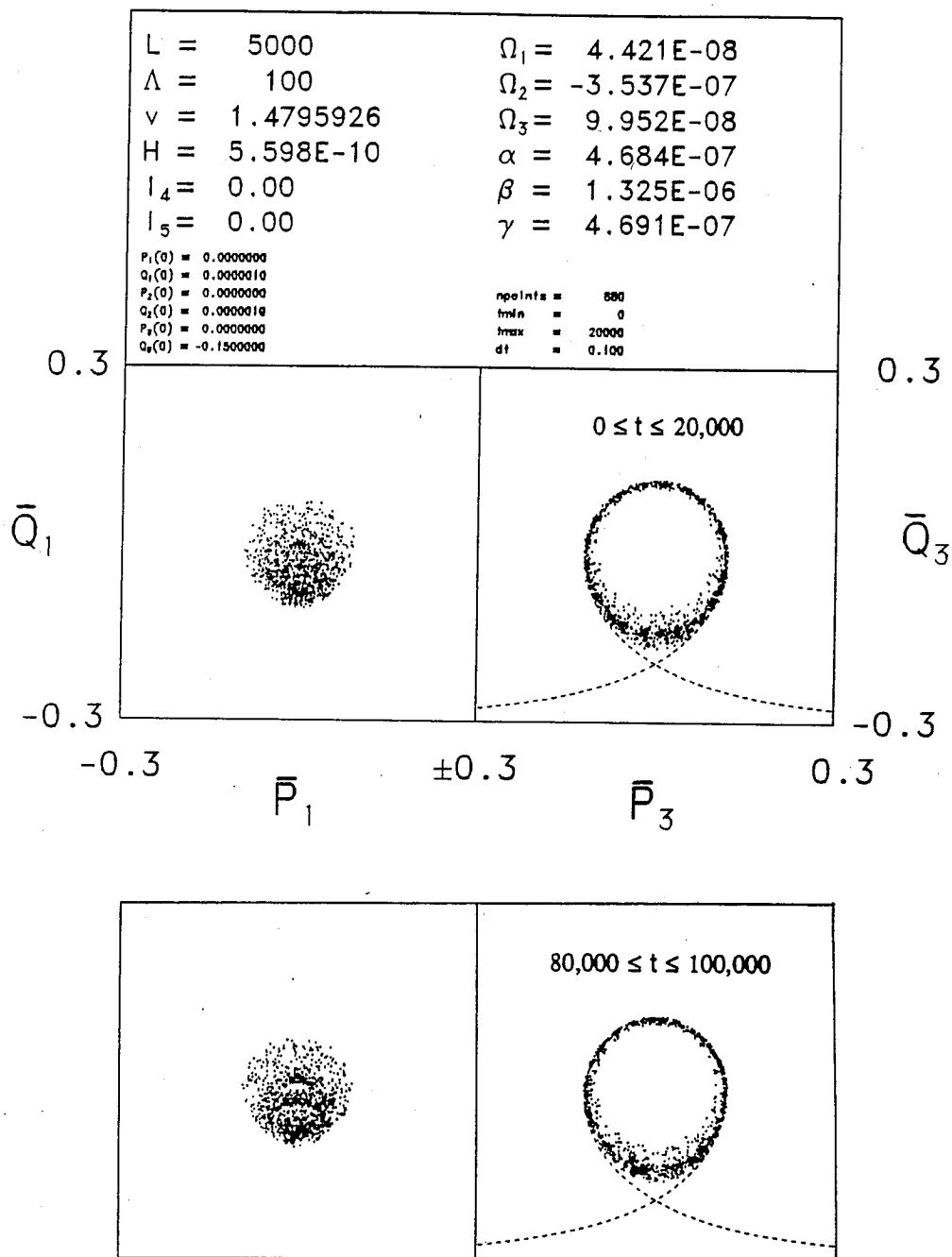


Figure 6.10: Phase space diffusion with  $L = 5000$  and  $\bar{Q}_3(0) = -0.14$ . Escape had not yet occurred at  $t = 100,000$ .

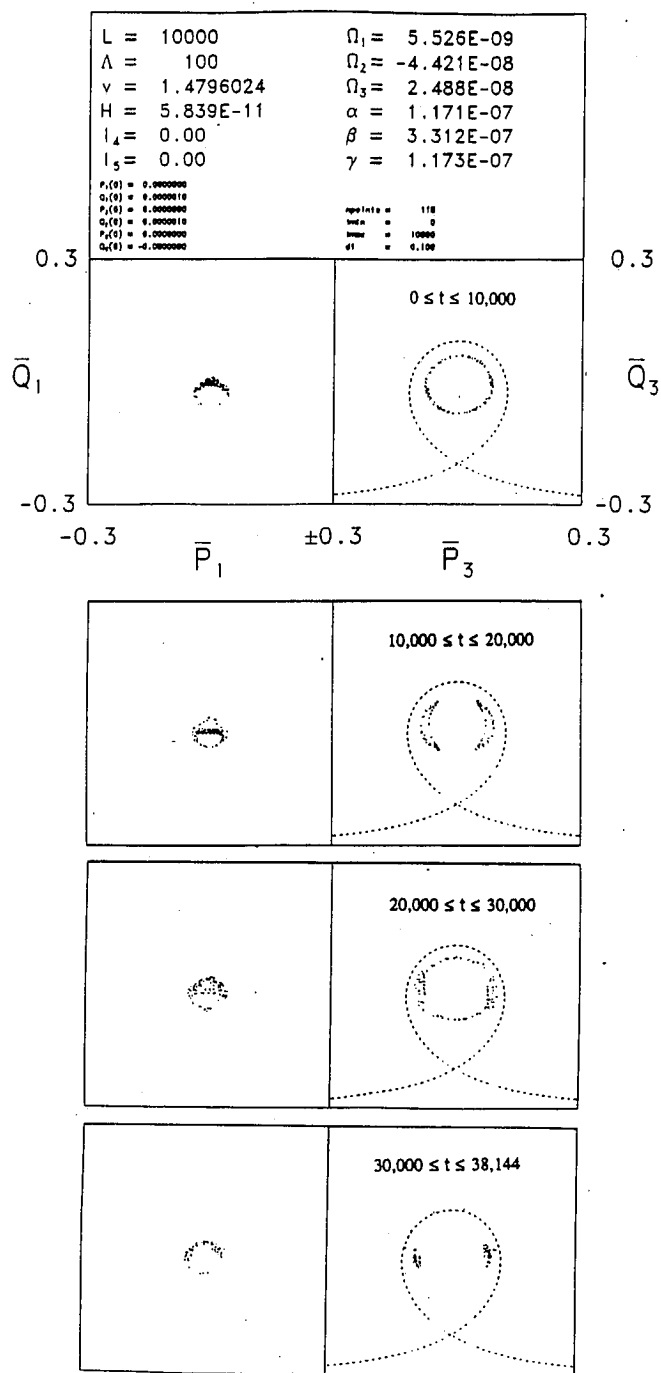


Figure 6.11: Phase space diffusion with  $L = 10000$  and  $\bar{Q}_3(0) = -0.08$ . Escape occurs at  $t = 38,144$ .

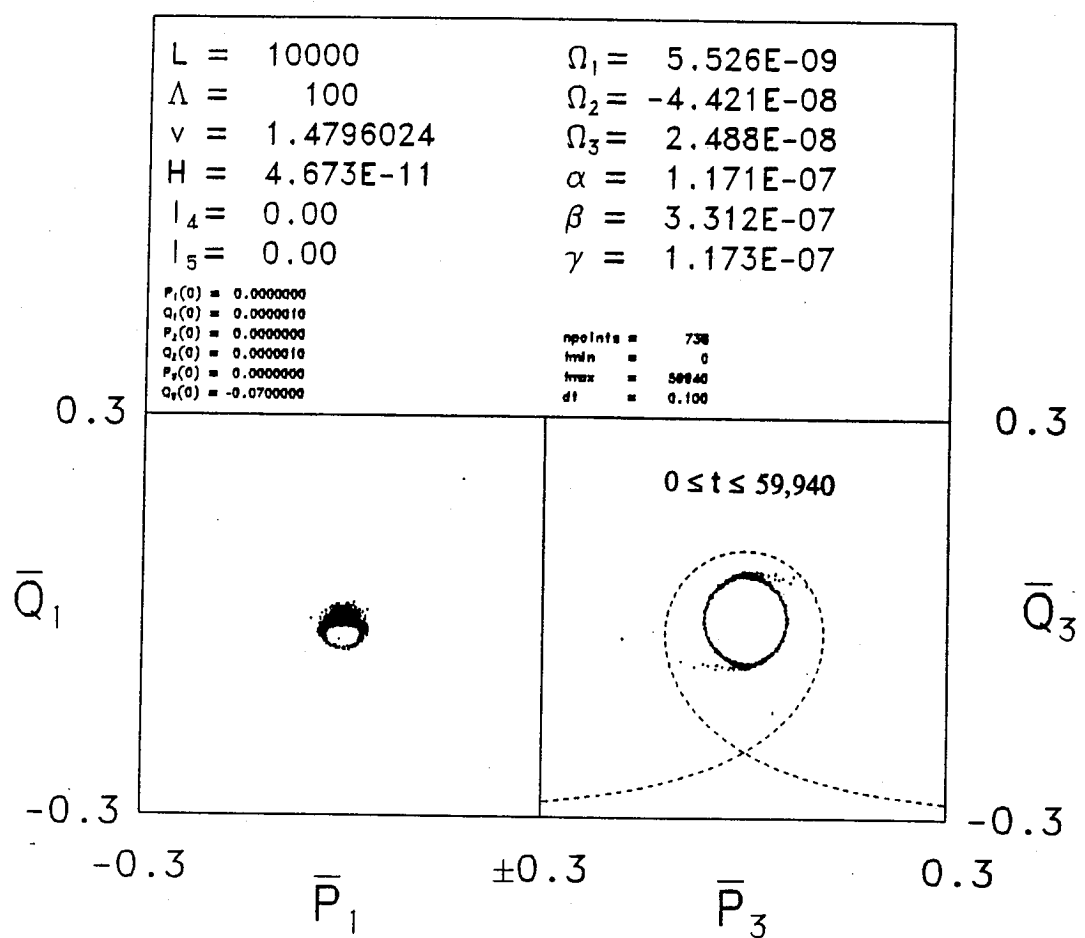


Figure 6.12: Phase space diffusion with  $L = 10000$  and  $\bar{Q}_3(0) = -0.07$ . Escape occurs at  $t = 59,940$ .

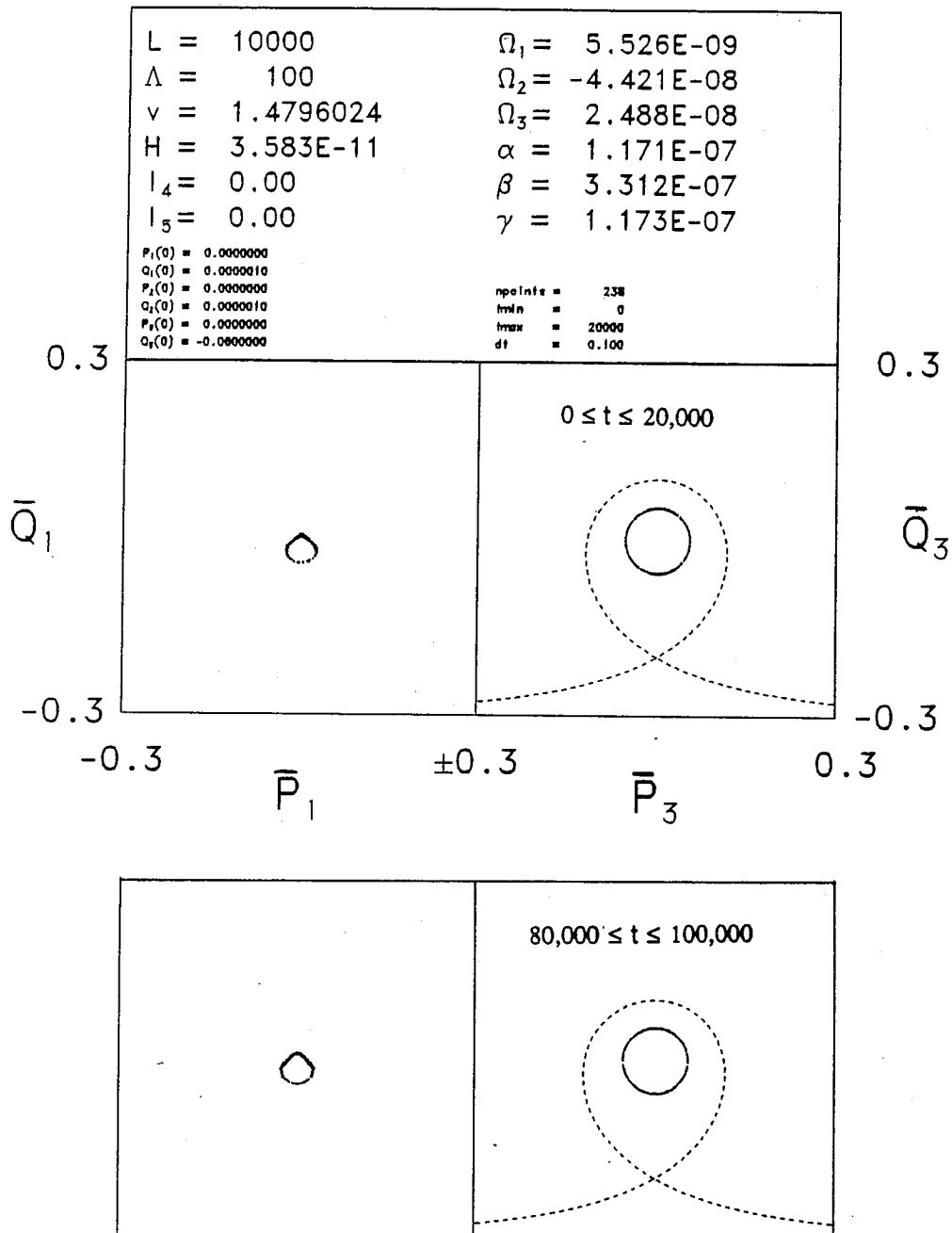


Figure 6.13: Phase space diffusion with  $L = 10000$  and  $\bar{Q}_3(0) = -0.06$ . Escape had not yet occurred at  $t = 100,000$ .

the initial value of  $\bar{Q}_3$  is very small, the  $\bar{P}_3$ - $\bar{Q}_3$  motion is just a small-amplitude, regular oscillation, and the behavior of  $\bar{P}_1$  and  $\bar{Q}_1$  is little changed from the two-degree-of-freedom case discussed earlier. For larger oscillations in  $\bar{P}_3$ - $\bar{Q}_3$ , we see an effective increase in the nonlinearity in the first two terms of Hamiltonian (6.20), which allows decay instability involving  $\bar{I}_1$  to occur for larger values of  $\bar{\Omega}_1$ , and leads to more chaos in the motion of  $\bar{P}_1$  and  $\bar{Q}_1$ . The amount of chaos evident in the motion of  $\bar{I}_3$  increases with the initial amplitude of this variable.

For all values of  $L$ , a large enough initial value of  $\bar{I}_3$  leads to immediate explosive instability. The coupling of the explosively unstable triplet to modes  $J_1$  and  $J_3$  allows this immediate growth to occur for smaller values of  $\bar{I}_3$  than was the case in the absence of these modes. For  $\bar{I}_3(0)$  somewhat deeper within the unperturbed separatrix, we see that the value of  $\bar{I}_3$  can fluctuate chaotically for some time, finally achieving large enough amplitude for explosive growth to occur (Figure 6.9 and Figures 6.11 and 6.12). For small enough  $\bar{I}_3(0)$ , the chaos in the system may be so limited that  $\bar{I}_3$  does not grow on any numerically observable time scale (Figure 6.13). (It is interesting to note that in Figure 6.10, despite what looks like very chaotic behavior near the unperturbed separatrix, explosive growth does not occur during the time interval examined.) In a number of such numerical runs, it was observed that the escape time typically rises very sharply as initial conditions are chosen deeper within the unperturbed separatrix. (This rise is not monotonic, of course, since nearby initial conditions in chaotic systems yield very different phase space trajectories.)

It will be recalled from Section 3.3 that the frequency of ion-electron collisions is roughly  $\nu \sim \sqrt{\frac{m_i}{m_e}} \frac{\omega_p}{\Lambda^3}$ . In ion-acoustic frequency units this is  $\frac{\nu}{k_1 \omega_p} \sim$

$\sqrt{\frac{m_i}{m_e}} \frac{1}{k_1 \Lambda^3}$ . Thus for  $\Lambda = 100$  and  $L = 5000$ , the typical time, in numerical units, for a collision to occur is  $\Delta t \sim 30$ . As discussed in Section 4.2, this collision frequency can be decreased by increasing  $\Lambda$ , at the cost of considering longer diffusion time scales since we must simultaneously decrease  $k_1$  (i.e., consider lower-frequency modes) in order to keep the resonance properties the same. All of the above numerical results will still hold if we consider these less collisional parameter regimes; the main effect of decreasing  $k_1$ , with  $k_1 \Lambda$  constant, will be to change the time units. It should also be noted that one effect of collisions might be to enhance the diffusion rates [35] by scattering orbits off of invariant surfaces and into the chaotic layers that provide channels for escape. The contribution of such extrinsic noise on Hamiltonian systems has been considered by a number of authors [53, 54, 55]. It would be interesting to attempt to include such effects in our numerical calculations; at the time of this writing, this has not been carried out.

## Chapter 7

### Effect of Three-Wave Positive Energy Resonance

#### 7.1 Introduction

The situation considered in the last section is fairly generic; for long wavelengths, many such two-wave near-resonances will automatically occur. We now consider the case where one mode of a nearly resonant explosive triplet is coupled, not to two other modes to form two nearly resonant decay doublets, but to one other mode in a doublet and to two more modes in a triplet that may be exactly resonant. One such set of modes is shown in Figure 7.1. Here the modes  $J_1$  through  $J_6$  are shown with wavenumbers  $k_1, 2k_1, k_1, 2k_1, 4k_1$  and  $3k_1$ , respectively. (Note that the numbering of modes in this chapter is independent of the numbering used in previous chapters!) Here we have neglected the third mode on the uppermost branch of the dispersion diagram that was considered in Chapter 6. While such a mode could still interact strongly with mode  $J_2$ , for computational simplicity we consider the smallest system which will exhibit the diffusion and instability of interest.

Mode  $J_2$  is now involved in two nearly resonant triplets. For some values of  $k_1$  and  $\nu$ , the resonance between modes  $J_2, J_3$  and  $J_6$  may be exact, yielding the phase space topology shown in Figure 4.10. For some other values of  $k_1$  and  $\nu$ , we may have resonance between modes  $J_2, J_4$  and  $J_5$  as discussed in previous chapters. Each of these resonance conditions occur only in isolated regions of parameter space; in Figure 4.1 we saw the resonance curves



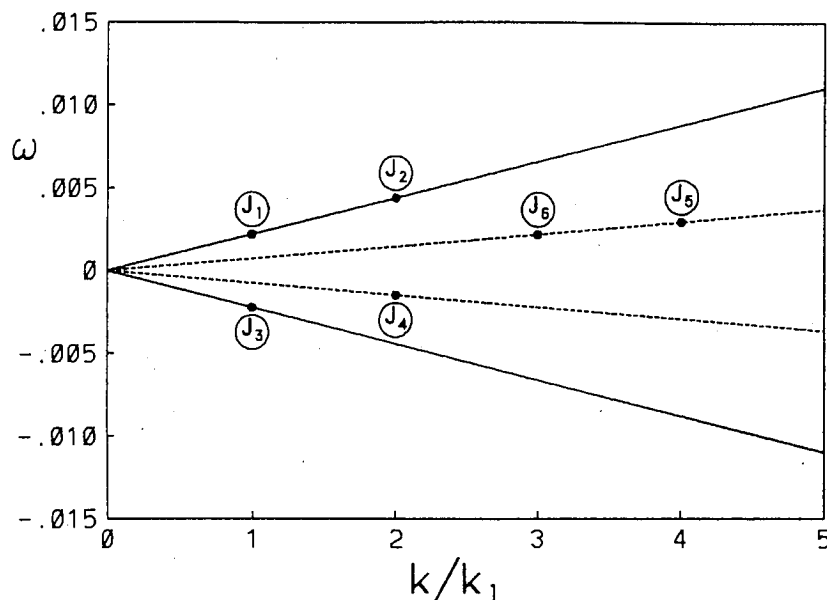


Figure 7.1: Six modes which can form one explosively unstable triplet, one resonant decay triplet and one nearly resonant doublet.

in  $(k_1, \nu)$ -space for both decay instability and explosive instability, involving mode numbers up to  $m = 10$ . We now seek regions of parameter space where both resonance conditions (with mode  $J_2$  in common) are nearly satisfied.

Figure 7.2.a shows resonance curves for interaction between  $J_2$ ,  $J_3$  and  $J_6$  (solid lines), and between  $J_2$ ,  $J_4$  and  $J_5$  (dashed lines) where we have  $m_2 = 2$  as above, but the other mode numbers are now arbitrary. The label on the solid curves is the value of  $m_6$ , and the label on the dashed curves is  $m_5$ . The uppermost two curves have  $m_6 = 3$  and  $m_5 = 4$ , which are exactly the modes shown in Figure 7.1. We see that the two resonance conditions are simultaneously satisfied (for some  $\nu$ ) in the limit  $k_1 \rightarrow 0$ , and are both nearly satisfied for some values of  $\nu$  over the entire range of  $k_1$  shown. This type of double resonance occurs for many modes in the system. Figure 7.2.b shows the resonance curves for  $m_2 = 3$ . Here we see that, for small  $k_1$ , near-resonance

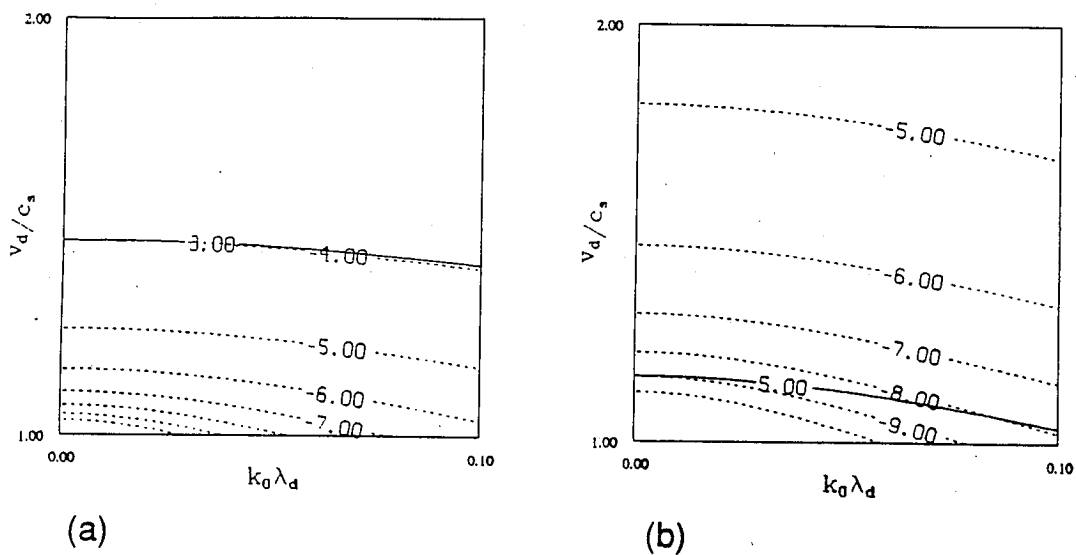


Figure 7.2: Locations in parameter space of three-wave resonances involving the modes of Figure 7.1, with various modenumbers including (a)  $m_2 = 2$  and (b)  $m_2 = 3$ . Solid lines indicate resonance between  $J_2$ ,  $J_3$  and  $J_6$  and are labelled with  $m_6$ ; dashed lines indicate resonance between  $J_2$ ,  $J_4$  and  $J_5$  and are labelled with  $m_5$ .

occurs simultaneously for the triplets having  $m_2 = 3, m_3 = 2, m_6 = 5$  and  $m_2 = 3, m_4 = 6, m_5 = 9$ . In addition, the resonance curves for  $m_2 = 3, m_3 = 2, m_6 = 5$  and  $m_2 = 3, m_4 = 5, m_5 = 8$  are seen to cross for a larger value of  $k_1$ . This type of crossing also occurs for many modes, but in these cases the resonance conditions are both nearly satisfied only in a very small region of parameter space.

The three-resonance situation depicted in Figure 7.1 is similar to that considered in Chapter 6, except that one of the two-wave near-resonances is now replaced by a three-wave resonance that may be exact. This resonance condition is nearly satisfied only for a small range of  $\nu$ , but when it is satisfied we expect that it will lead to very chaotic motion. Of course, as in Chapter 6, we have ignored a large number of two-wave near-resonances which also generate strongly chaotic motion. Thus the impact of chaotic diffusion that we observe in our numerical experiments may be considered a very conservative estimate.

## 7.2 Six-Wave Hamiltonian

The Hamiltonian for the set of waves indicated in Figure 7.1 is

$$\begin{aligned}
 H = & \omega_1 J_1 + \omega_2 J_2 + \omega_3 J_3 - \omega_4 J_4 - \omega_5 J_5 - \omega_6 J_6 \\
 & + \alpha J_1 \sqrt{J_2} \sin(2\theta_1 - \theta_2) \\
 & + \beta \sqrt{J_2 J_3 J_6} \sin(\theta_2 + \theta_6 - \theta_3) \\
 & + \gamma \sqrt{J_2 J_4 J_5} \sin(\theta_2 + \theta_4 + \theta_5), \tag{7.1}
 \end{aligned}$$

where the constants  $\alpha$  and  $\gamma$  are given in Eqs. 4.9 and 4.25, respectively, and  $\beta$  is equal to the constant  $\delta$  of Eq. 4.30. The Hamiltonian (7.1) cannot be transformed into a three-degree-of-freedom polynomial as was done for Hamiltonian (6.17); computations were therefore done in the full six degrees of freedom. (This Hamiltonian actually may, for some values of the constants of motion, be reduced to a five-degree-of-freedom polynomial for a slight gain in computational efficiency, but this was not done.) It will be useful for computations to eliminate the very large linear terms; this is done via the time-dependent transformation derived from the generating function

$$F = \hat{J}_1 \left( \theta_1 - \frac{1}{2} \omega_1 t \right) + \hat{J}_2 (\theta_2 - \omega_2 t) + \hat{J}_3 (\theta_3 - (\omega_2 - \omega_6) t) \\ + \hat{J}_4 (\theta_4 + \omega_4 t) + \hat{J}_5 (\theta_5 + (\omega_2 - \omega_4) t) + \hat{J}_6 (\theta_6 + \omega_6 t). \quad (7.2)$$

This gives us

$$\begin{aligned} J_1 &= \frac{\partial F}{\partial \theta_1} = \hat{J}_1, & \hat{\theta}_1 &= \frac{\partial F}{\partial \hat{J}_1} = \theta_1 - \frac{1}{2} \omega_1 t, \\ J_2 &= \frac{\partial F}{\partial \theta_2} = \hat{J}_2, & \hat{\theta}_2 &= \frac{\partial F}{\partial \hat{J}_2} = \theta_2 - \omega_2 t, \\ J_3 &= \frac{\partial F}{\partial \theta_3} = \hat{J}_3, & \hat{\theta}_3 &= \frac{\partial F}{\partial \hat{J}_3} = \theta_3 - (\omega_2 - \omega_6) t, \\ J_4 &= \frac{\partial F}{\partial \theta_4} = \hat{J}_4, & \hat{\theta}_4 &= \frac{\partial F}{\partial \hat{J}_4} = \theta_4 + \omega_4 t, \\ J_5 &= \frac{\partial F}{\partial \theta_5} = \hat{J}_5, & \hat{\theta}_5 &= \frac{\partial F}{\partial \hat{J}_5} = \theta_5 + (\omega_2 - \omega_4) t, \\ J_6 &= \frac{\partial F}{\partial \theta_6} = \hat{J}_6, & \hat{\theta}_6 &= \frac{\partial F}{\partial \hat{J}_6} = \theta_6 + \omega_6 t, \end{aligned} \quad (7.3)$$

yielding the Hamiltonian

$$\hat{H} = \hat{\Omega}_1 \hat{J}_1 + \hat{\Omega}_3 \hat{J}_3 + \hat{\Omega}_5 \hat{J}_5 \\ + \alpha \hat{J}_1 \sqrt{\hat{J}_2} \sin(2\hat{\theta}_1 - \hat{\theta}_2)$$

$$\begin{aligned}
& + \beta \sqrt{\hat{J}_2 \hat{J}_3 \hat{J}_6} \sin(\hat{\theta}_2 + \hat{\theta}_6 - \hat{\theta}_3) \\
& + \gamma \sqrt{\hat{J}_2 \hat{J}_4 \hat{J}_5} \sin(\hat{\theta}_2 + \hat{\theta}_4 + \hat{\theta}_5),
\end{aligned} \tag{7.4}$$

where

$$\begin{aligned}
\hat{\Omega}_1 &= \omega_1 - \frac{1}{2}\omega_2, \\
\hat{\Omega}_3 &= \omega_6 + \omega_3 - \omega_2, \\
\hat{\Omega}_5 &= \omega_2 - \omega_4 - \omega_5.
\end{aligned}$$

The transformation to resonance coordinates is now found from

$$\begin{aligned}
F &= \bar{I}_1(2\hat{\theta}_1 - \hat{\theta}_2) - \bar{I}_2(\hat{\theta}_2 + \hat{\theta}_6 - \hat{\theta}_3) + \bar{I}_3(\hat{\theta}_2 + \hat{\theta}_4 + \hat{\theta}_5) \\
& + \bar{I}_4\hat{\theta}_4 + \bar{I}_5\hat{\theta}_5 + \bar{I}_6\hat{\theta}_6,
\end{aligned} \tag{7.5}$$

giving us

$$\begin{aligned}
\hat{J}_1 &= \frac{\partial F}{\partial \hat{\theta}_1} = 2\bar{I}_1 & \bar{\psi}_1 &= \frac{\partial F}{\partial \bar{I}_1} = 2\hat{\theta}_1 - \hat{\theta}_2 \\
\hat{J}_2 &= \frac{\partial F}{\partial \hat{\theta}_2} = \bar{I}_3 - \bar{I}_2 - \bar{I}_1 & \bar{\psi}_2 &= \frac{\partial F}{\partial \bar{I}_2} = -\hat{\theta}_3 + \hat{\theta}_2 + \hat{\theta}_6 \\
\hat{J}_3 &= \frac{\partial F}{\partial \hat{\theta}_3} = \bar{I}_2 & \bar{\psi}_3 &= \frac{\partial F}{\partial \bar{I}_3} = \hat{\theta}_2 + \hat{\theta}_4 + \hat{\theta}_5 \\
\hat{J}_4 &= \frac{\partial F}{\partial \hat{\theta}_4} = \bar{I}_4 + \bar{I}_3 & \bar{\psi}_4 &= \frac{\partial F}{\partial \bar{I}_4} = \hat{\theta}_4 \\
\hat{J}_5 &= \frac{\partial F}{\partial \hat{\theta}_5} = \bar{I}_5 + \bar{I}_3 & \bar{\psi}_5 &= \frac{\partial F}{\partial \bar{I}_5} = \hat{\theta}_5 \\
\hat{J}_6 &= \frac{\partial F}{\partial \hat{\theta}_6} = \bar{I}_6 - \bar{I}_2 & \bar{\psi}_6 &= \frac{\partial F}{\partial \bar{I}_6} = \hat{\theta}_6.
\end{aligned} \tag{7.6}$$

The Hamiltonian then becomes

$$\bar{H} = \hat{H} - \hat{\omega}_5 \bar{I}_5$$

$$\begin{aligned}
&= \bar{\Omega}_1 \bar{I}_1 + \bar{\Omega}_2 \bar{I}_2 + \bar{\Omega}_3 \bar{I}_3 + \alpha 2 \bar{I}_1 \sqrt{\bar{I}_3 - \bar{I}_2 - \bar{I}_1} \sin \bar{\psi}_1 \\
&\quad - \beta \sqrt{(\bar{I}_3 - \bar{I}_2 - \bar{I}_1) \bar{I}_2 (\bar{I}_6 - \bar{I}_2)} \sin \bar{\psi}_2 \\
&\quad + \gamma \sqrt{(\bar{I}_3 - \bar{I}_2 - \bar{I}_1) (\bar{I}_4 + \bar{I}_3) (\bar{I}_5 + \bar{I}_3)} \sin \bar{\psi}_3, \tag{7.7}
\end{aligned}$$

where

$$\begin{aligned}
\bar{\Omega}_1 &\equiv 2\omega_1 - \omega_2 = 2\hat{\Omega}_1 \\
\bar{\Omega}_2 &\equiv -(\omega_2 - \omega_3 - \omega_6) = \hat{\Omega}_3 \\
\bar{\Omega}_3 &\equiv \omega_2 - \omega_4 - \omega_5 = \hat{\Omega}_5
\end{aligned} \tag{7.8}$$

are the detunings. The quantities  $\bar{I}_4$ ,  $\bar{I}_5$  and  $\bar{I}_6$  are constants of the motion. Computations are done using the cartesian form of equation (7.4):

$$\begin{aligned}
H &= \frac{\Omega_1}{2} (\hat{P}_1^2 + \hat{Q}_1^2) + \frac{\Omega_3}{2} (\hat{P}_3^2 + \hat{Q}_3^2) + \frac{\Omega_5}{2} (\hat{P}_5^2 + \hat{Q}_5^2) \\
&\quad + \frac{\alpha}{\sqrt{2}^2} [2\hat{Q}_1 \hat{P}_1 \hat{P}_2 - \hat{Q}_2 (\hat{P}_1^2 - \hat{Q}_1^2)] \\
&\quad + \frac{\beta}{\sqrt{2}^2} [\hat{Q}_2 (\hat{Q}_6 \hat{Q}_3 + \hat{P}_6 \hat{P}_3) + \hat{P}_2 (\hat{Q}_6 \hat{P}_3 - \hat{P}_6 \hat{Q}_3)] \\
&\quad + \frac{\gamma}{\sqrt{2}^2} [\hat{Q}_2 (\hat{Q}_4 \hat{Q}_5 - \hat{P}_4 \hat{P}_5) + \hat{P}_2 (\hat{Q}_4 \hat{P}_5 + \hat{P}_4 \hat{Q}_5)]. \tag{7.9}
\end{aligned}$$

### 7.3 Two Degrees of Freedom

Before examining the behavior of the full three-degree-of-freedom, five-wave system, we first consider two subsystems with two degrees of freedom. As in Chapter 6, the two cases of interest are that of two positive energy resonances, and that of one positive energy and one negative energy resonance.

Numerical results were obtained using the method of Lie transformations as described in Chapter 6 and Appendix D.

### 7.3.1 Two Positive Energy Resonances

If only modes  $J_1, J_2, J_3$  and  $J_6$  are present in the Hamiltonian 7.1 (or  $\hat{J}_1, \hat{J}_2, \hat{J}_3$  and  $\hat{J}_6$  in Hamiltonian 7.4), then we have two positive energy resonances which will interact to give strongly chaotic motion. The situation is similar to that considered in Section 6.2.1, but now one resonance condition can be exactly satisfied. The Hamiltonian is given by

$$\begin{aligned} \hat{H} = & \hat{\Omega}_1 \hat{J}_1 + \hat{\Omega}_3 \hat{J}_3 + \alpha \hat{J}_1 \sqrt{\hat{J}_2} \sin(2\hat{\theta}_1 - \hat{\theta}_2) \\ & + \beta \sqrt{\hat{J}_2 \hat{J}_3 \hat{J}_6} \sin(\hat{\theta}_2 + \hat{\theta}_6 - \hat{\theta}_3). \end{aligned} \quad (7.10)$$

The transformation to resonance variables is now given by

$$\begin{aligned} \hat{J}_1 = 2\bar{I}_1, & \quad \bar{\psi}_1 = 2\hat{\theta}_1 - \hat{\theta}_2, \\ \hat{J}_2 = \bar{I}_3 - \bar{I}_2 - \bar{I}_1, & \quad \bar{\psi}_2 = -\hat{\theta}_3 + \hat{\theta}_2 + \hat{\theta}_6, \\ \hat{J}_3 = \bar{I}_2, & \quad \bar{\psi}_3 = \hat{\theta}_2, \\ \hat{J}_6 = \bar{I}_6 - \bar{I}_2, & \quad \bar{\psi}_6 = \hat{\theta}_6, \end{aligned} \quad (7.11)$$

so that the Hamiltonian becomes

$$\begin{aligned} \bar{H} = & \bar{\Omega}_1 \bar{I}_1 + \bar{\Omega}_2 \bar{I}_2 + \alpha 2\bar{I}_1 \sqrt{\bar{I}_3 - \bar{I}_2 - \bar{I}_1} \sin \bar{\psi}_1 \\ & - \beta \sqrt{(\bar{I}_3 - \bar{I}_2 - \bar{I}_1) \bar{I}_2 (\bar{I}_6 - \bar{I}_2)} \sin \bar{\psi}_2. \end{aligned} \quad (7.12)$$

The quantities  $\bar{I}_3$  and  $\bar{I}_6$  are now both constants of the motion. In our numerical work we set  $\bar{I}_3 = \bar{I}_6 = 0.01$ .

Throughout this chapter we will always choose  $\nu$  to yield exact resonance between modes  $J_2, J_3$  and  $J_6$  (i.e.,  $\bar{\Omega}_2 = 0$ ) for the value of  $L$  under consideration, since it is this exact resonance that distinguishes this system from that considered in Chapter 6. We will consider  $L$  ranging from 2500 to 10000; in all of these cases the value of  $\nu$  that yields  $\bar{\Omega}_2 = 0$  is in the neighborhood  $\nu \approx 1.4796$ .

Figure 7.3 shows  $\bar{P}_1 = 0$  surface-of-section plots for  $L = 2500$  and  $L = 5000$ . For all of the orbits shown, the initial value  $\bar{Q}_1(0) = 10^{-6}$  was used. For  $L = 2500$  most of the orbits exhibit regular motion, and the topology is like that of the integrable case of Figure 4.10. For  $L = 5000$  the interaction between modes  $J_1$  and  $J_2$  is stronger, and is evidently enough to destroy most of the invariant surfaces, as shown in Figure 7.3. Chaos here is much stronger than in the analogous case of Section 6.2.1.

### 7.3.2 One Positive Energy and One Negative Energy Resonance

We now consider a system comprising the five modes  $J_2, J_3, J_4, J_5$  and  $J_6$ . If we consider equilibrium parameters along the upper curves of Figure 7.2.a, then mode  $J_2$  is simultaneously involved in two near-resonances, one involving decay instability and one involving explosive instability. The situation is analogous to that of Section 6.2.2, but now the positive energy resonance may be exact. The Hamiltonian for this set of waves is

$$\begin{aligned} \hat{H} = & \hat{\Omega}_3 \hat{J}_3 + \hat{\Omega}_5 \hat{J}_5 + \beta \sqrt{\hat{J}_2 \hat{J}_3 \hat{J}_6} \sin(\hat{\theta}_2 + \hat{\theta}_6 - \hat{\theta}_3) \\ & + \gamma \sqrt{\hat{J}_2 \hat{J}_4 \hat{J}_5} \sin(\hat{\theta}_2 + \hat{\theta}_4 + \hat{\theta}_5). \end{aligned} \quad (7.13)$$



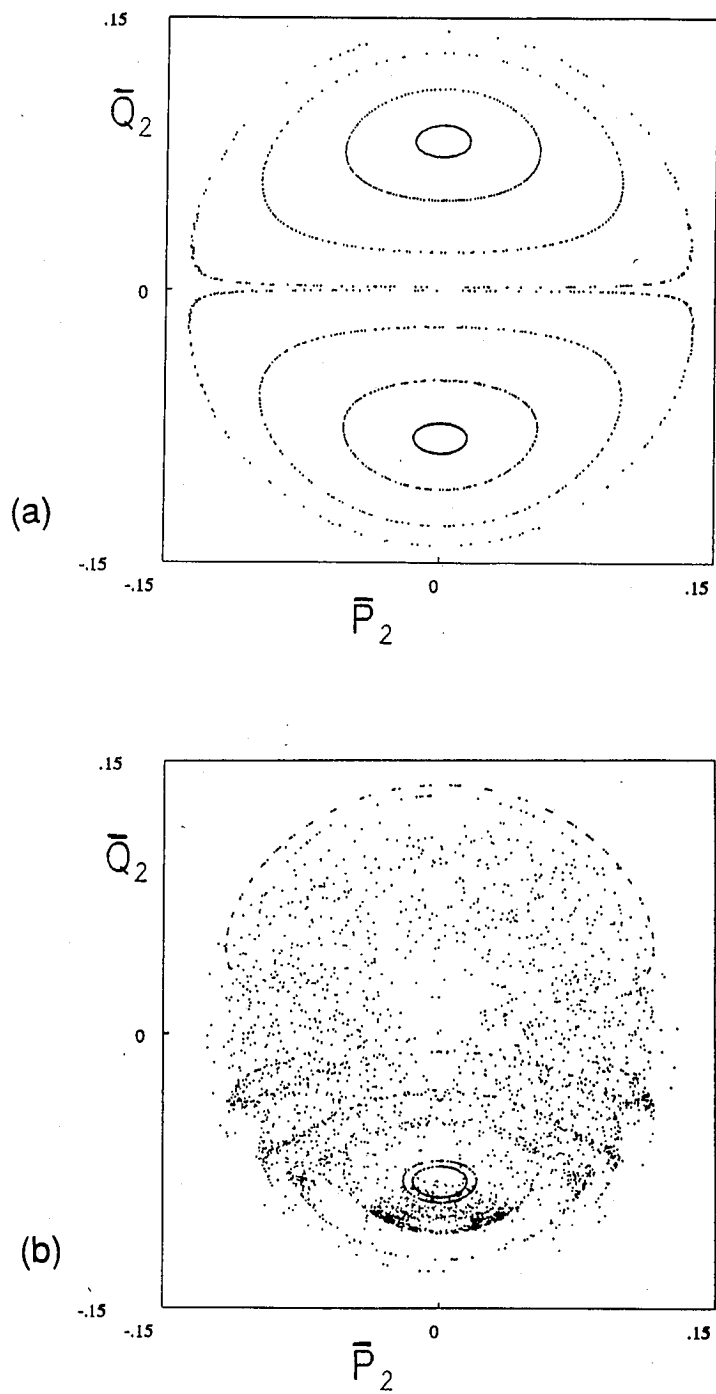


Figure 7.3:  $\bar{P}_1 = 0$  surface-of-section plots for Hamiltonian (7.12) with  $\bar{Q}_2 = 0$ .  
(a)  $L = 2500$ ; (b)  $L = 5000$ .

The transformation to resonance coordinates is now

$$\begin{aligned}
 \hat{J}_2 &= \bar{I}_3 - \bar{I}_2, & \bar{\psi}_2 &= -\hat{\theta}_3 + \hat{\theta}_2 + \hat{\theta}_6, \\
 \hat{J}_3 &= \bar{I}_2, & \bar{\psi}_3 &= \hat{\theta}_2 + \hat{\theta}_4 + \hat{\theta}_5, \\
 \hat{J}_4 &= \bar{I}_4 + \bar{I}_3, & \bar{\psi}_4 &= \hat{\theta}_4, \\
 \hat{J}_5 &= \bar{I}_5 + \bar{I}_3, & \bar{\psi}_5 &= \hat{\theta}_5, \\
 \hat{J}_6 &= \bar{I}_6 - \bar{I}_2, & \bar{\psi}_6 &= \hat{\theta}_6,
 \end{aligned} \tag{7.14}$$

yielding

$$\begin{aligned}
 \bar{H} &= \bar{\Omega}_2 \bar{I}_2 + \bar{\Omega}_3 \bar{I}_3 - \beta \sqrt{(\bar{I}_3 - \bar{I}_2 - \bar{I}_1) \bar{I}_2 (\bar{I}_6 - \bar{I}_2)} \sin \bar{\psi}_2 \\
 &\quad + \gamma \sqrt{(\bar{I}_3 - \bar{I}_2 - \bar{I}_1) (\bar{I}_4 + \bar{I}_3) (\bar{I}_5 + \bar{I}_3)} \sin \bar{\psi}_3.
 \end{aligned} \tag{7.15}$$

The quantities  $\bar{I}_4$ ,  $\bar{I}_5$  and  $\bar{I}_6$  are constants of the motion; we consider  $\bar{I}_4 = \bar{I}_5 = 0$  and  $\bar{I}_6 = 0.01$ . Surface-of-section plots are shown in Figure 7.4 for three values of  $L$ . The surface considered is again  $\bar{P}_1 = 0$ , and the initial value of  $\bar{Q}_1$  is again  $10^{-6}$  for all orbits. As described in the last section, for each value of  $L$  we choose  $v$  to yield exact resonance between modes  $J_2$ ,  $J_3$  and  $J_6$ . As the parameters are varied, we then move along the solid line of Figure 7.2.a, and the detuning  $\bar{\Omega}_3$  (measured by the distance to the nearby dashed line in the diagram) varies, increasing with  $k_1$ .

In all three cases the size of the stable region is decreased from what it would be in the absence of the positive energy resonance, which is indicated by the dashed separatrix. As  $L$  is increased and the detuning  $\bar{\Omega}_3$  decreases, the unperturbed islet decreases in size. For  $L = 5000$  the decrease in the size of the stable region from the unperturbed value appears more pronounced than for  $L = 2500$ . For  $L = 9000$  the system does not appear much more chaotic

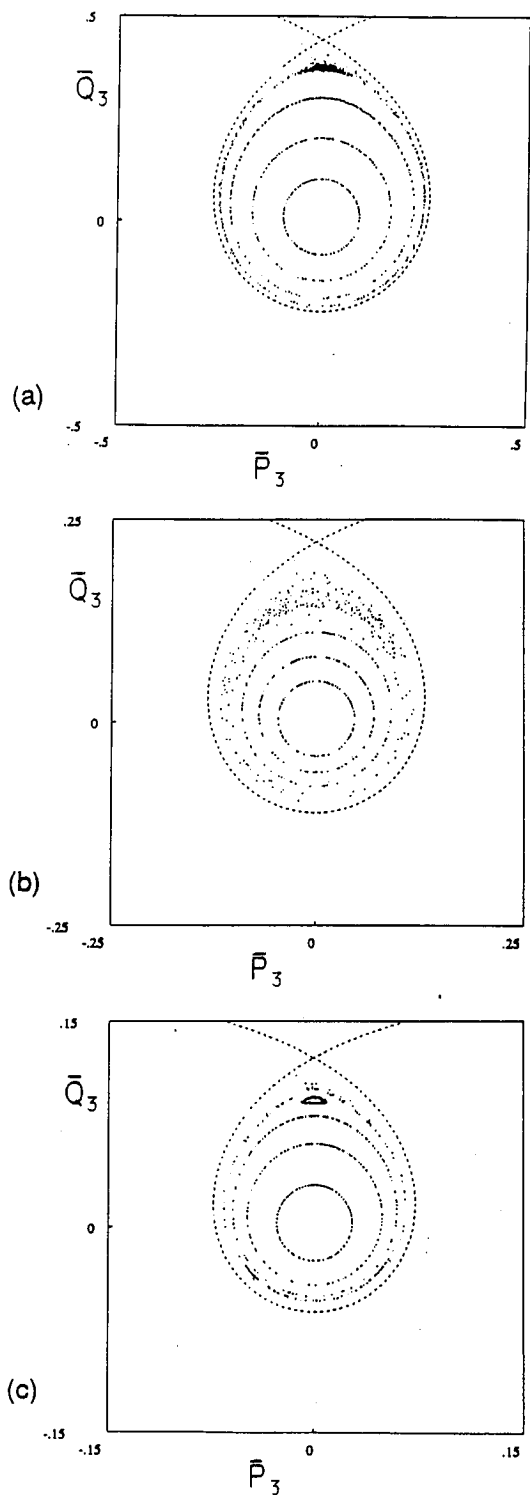


Figure 7.4:  $\bar{P}_1 = 0$  surface-of-section plots for Hamiltonian (7.15) with  $\bar{\Omega}_2 = 0$ .  
 (a)  $L = 2500$ ; (b)  $L = 5000$ ; (c)  $L = 9000$ .

than for  $L = 5000$ . We note that one of the initial conditions for the latter case landed on an island chain within the chaotic layer around the islet. The island chain is reminiscent of that observed in Figure 6.7.c. A notable difference from the results of Figure 6.7, however, is that the stabilization observed there is not evident here.

## 7.4 Three Degrees of Freedom

We now consider the three-degree-of-freedom Hamiltonian (7.7):

$$\begin{aligned} \bar{H} = & \bar{\Omega}_1 \bar{I}_1 + \bar{\Omega}_2 \bar{I}_2 + \bar{\Omega}_3 \bar{I}_3 + \alpha 2 \bar{I}_1 \sqrt{\bar{I}_3 - \bar{I}_2 - \bar{I}_1} \sin \bar{\psi}_1 \\ & - \beta \sqrt{(\bar{I}_3 - \bar{I}_2 - \bar{I}_1) \bar{I}_2 (\bar{I}_6 - \bar{I}_2)} \sin \bar{\psi}_2 \\ & + \gamma \sqrt{(\bar{I}_3 - \bar{I}_2 - \bar{I}_1) (\bar{I}_4 + \bar{I}_3) (\bar{I}_5 + \bar{I}_3)} \sin \bar{\psi}_3. \end{aligned}$$

Figures 7.5-7.14 show  $\bar{P}_1 = 0$  surface-of-section plots for  $L = 2500$ ,  $L = 5000$  and  $L = 9000$ . Again  $v$  was chosen to yield  $\bar{\Omega}_2 = 0$  for each  $L$ , with  $\bar{\Omega}_3$  increasing as we move to the right along the solid curve of Figure 7.2.a. The initial conditions for all cases included  $\bar{P}_1(0) = \bar{P}_2(0) = 0$ ,  $\bar{Q}_1(0) = \bar{Q}_2(0) = 10^{-6}$  and  $\bar{P}_3(0) = 0$ , with a range of positive initial values for  $\bar{Q}_3$ . The constants of the motion were set to  $\bar{I}_6 = .01$ ,  $\bar{I}_4 = \bar{I}_5 = 0$ .

Figures 7.5-7.8 show results for four values of  $\bar{Q}_3(0)$ , chosen progressively deeper within the unperturbed separatrix (which would be a stable region in the absence of the two positive energy resonances) for  $L = 2500$ . As with the five-wave system of the last chapter, explosive growth eventually occurs for initial conditions chosen within this region, although for small enough perturbations the motion was stable over the time interval considered (Figure 7.8).

This projection of the phase space yielded a rather unusual figure for the  $\bar{P}_3 - \bar{Q}_3$  motion. Points were very sparse in the region  $\bar{Q}_3 > 0$ , and where they were plotted they mapped out an interesting structure, looking like the projection of a curved tube. Similar results are shown for  $L = 5000$  in Figures 7.9-7.11, and for  $L = 9000$  in Figures 7.12-7.14.

The results here are similar to those in Section 6.3. Initial conditions within the unperturbed islet lead to chaotic motion followed by eventual explosive growth. Again, orbits deep enough within the islet do not exhibit detectable growth in amplitude.

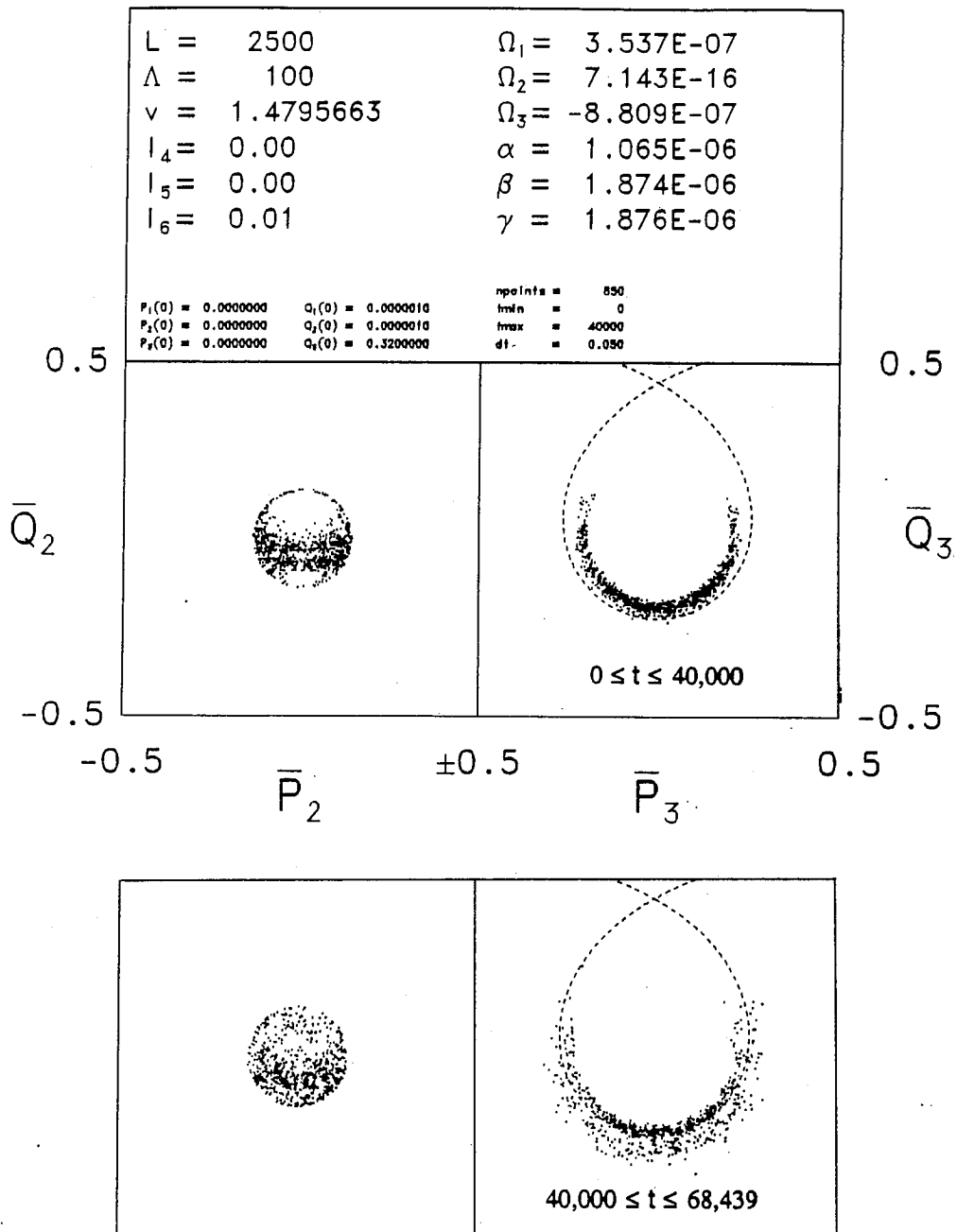


Figure 7.5: Phase space diffusion with  $L = 2500$  and  $\bar{Q}_3(0) = 0.32$ . Escape occurs at  $t = 68,439$ .

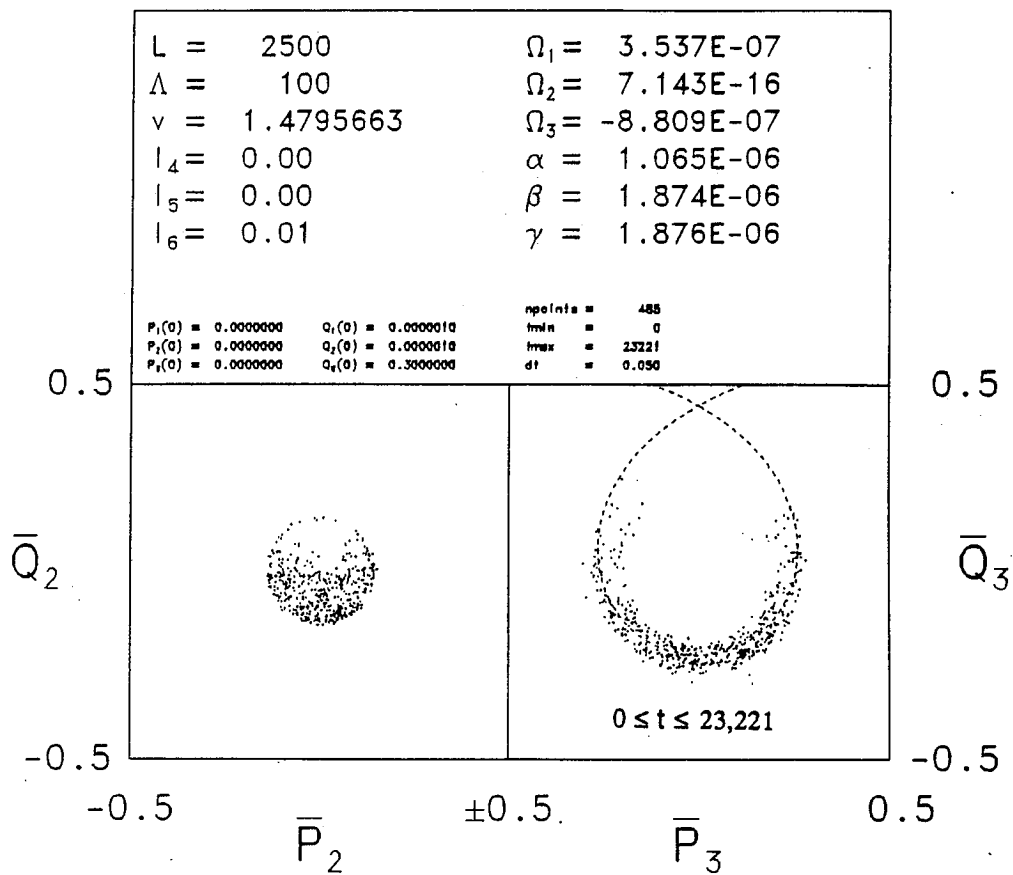


Figure 7.6: Phase space diffusion with  $L = 2500$  and  $\bar{Q}_3(0) = 0.30$ . Escape occurs at  $t = 23,221$ .

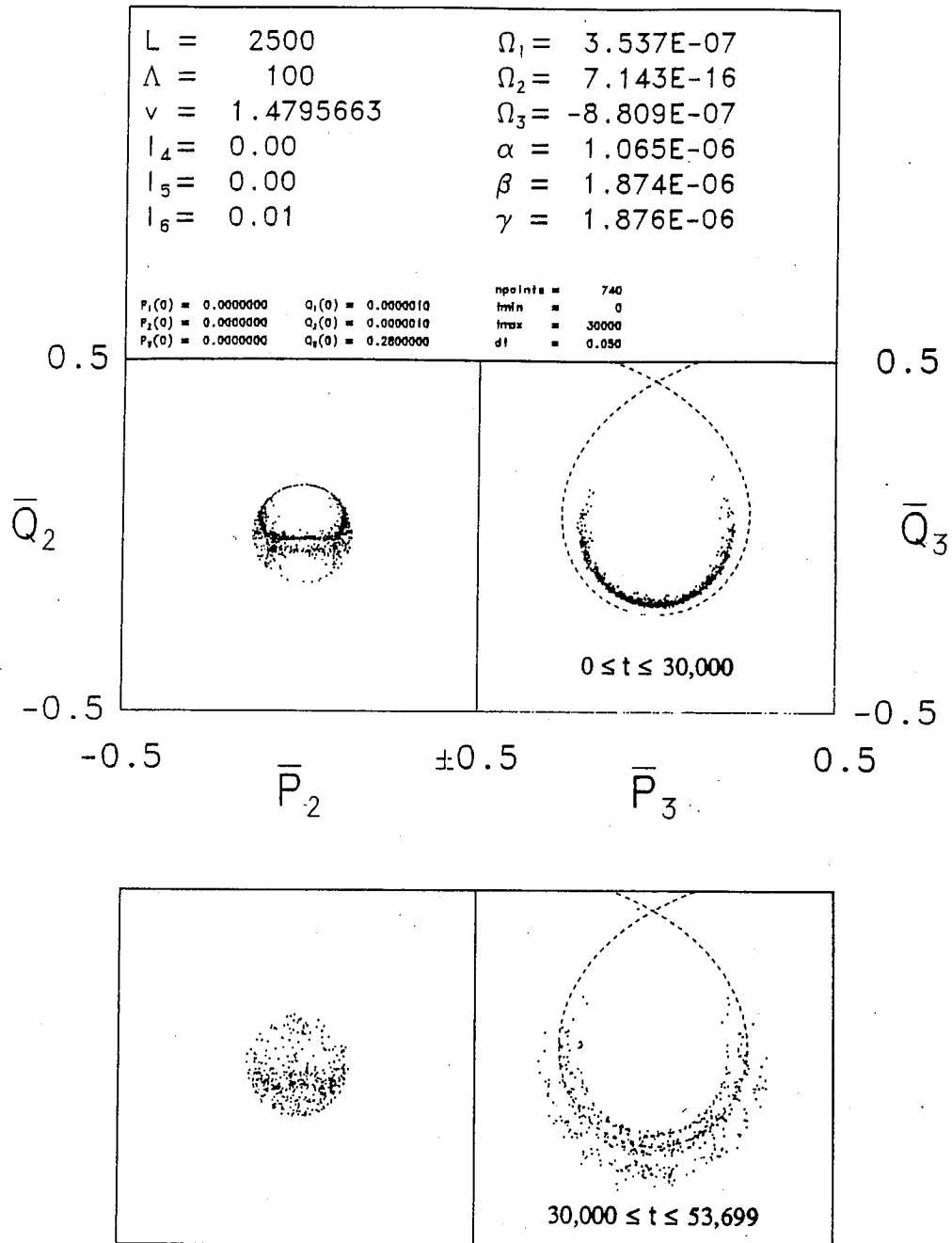


Figure 7.7: Phase space diffusion with  $L = 2500$  and  $\bar{Q}_3(0) = 0.28$ . Escape occurs at  $t = 53,699$ .



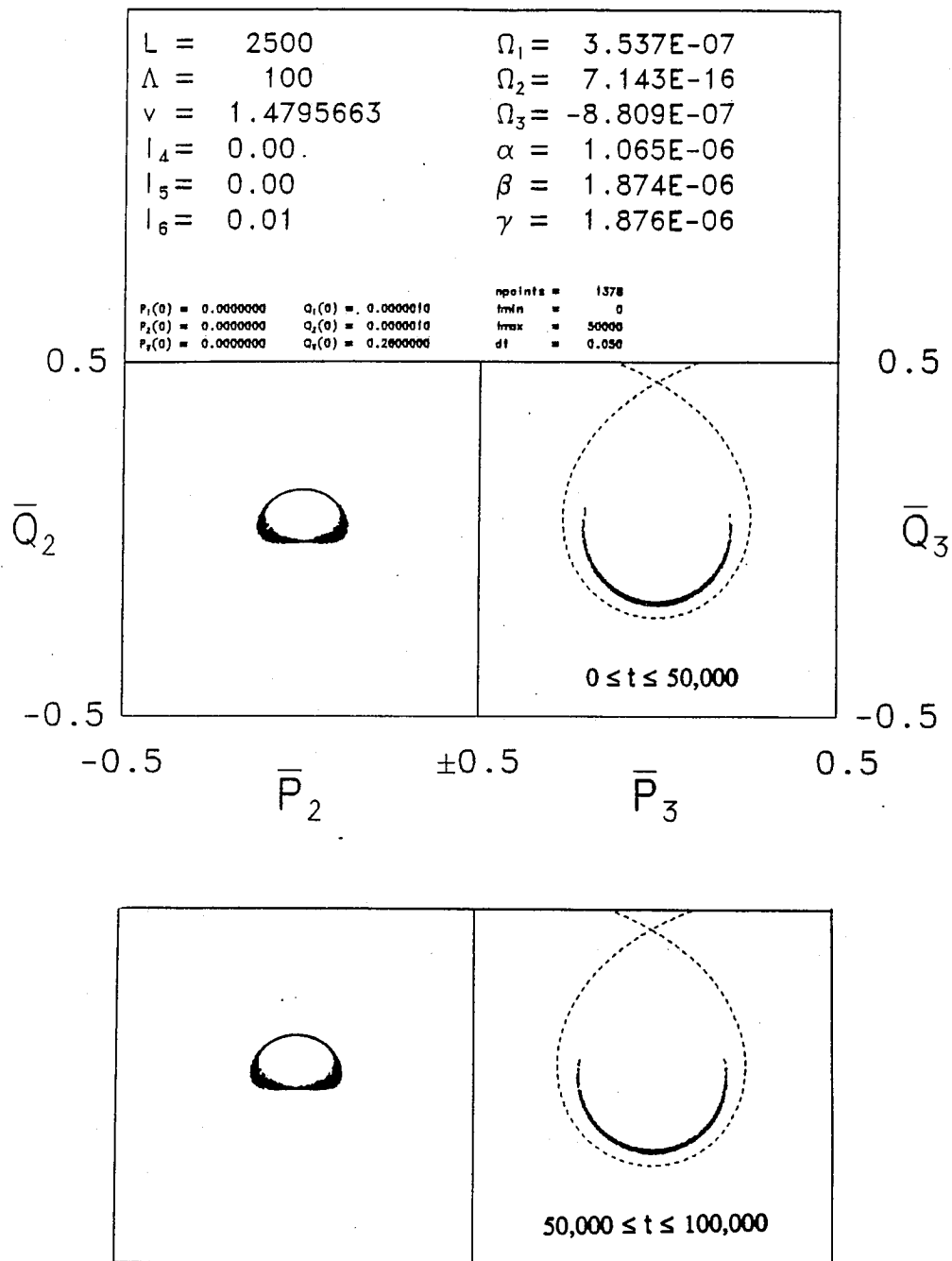


Figure 7.8: Phase space diffusion with  $L = 2500$  and  $\bar{Q}_3(0) = 0.26$ . No overall growth in  $\bar{I}_3$  was visible at  $t = 100,000$ .

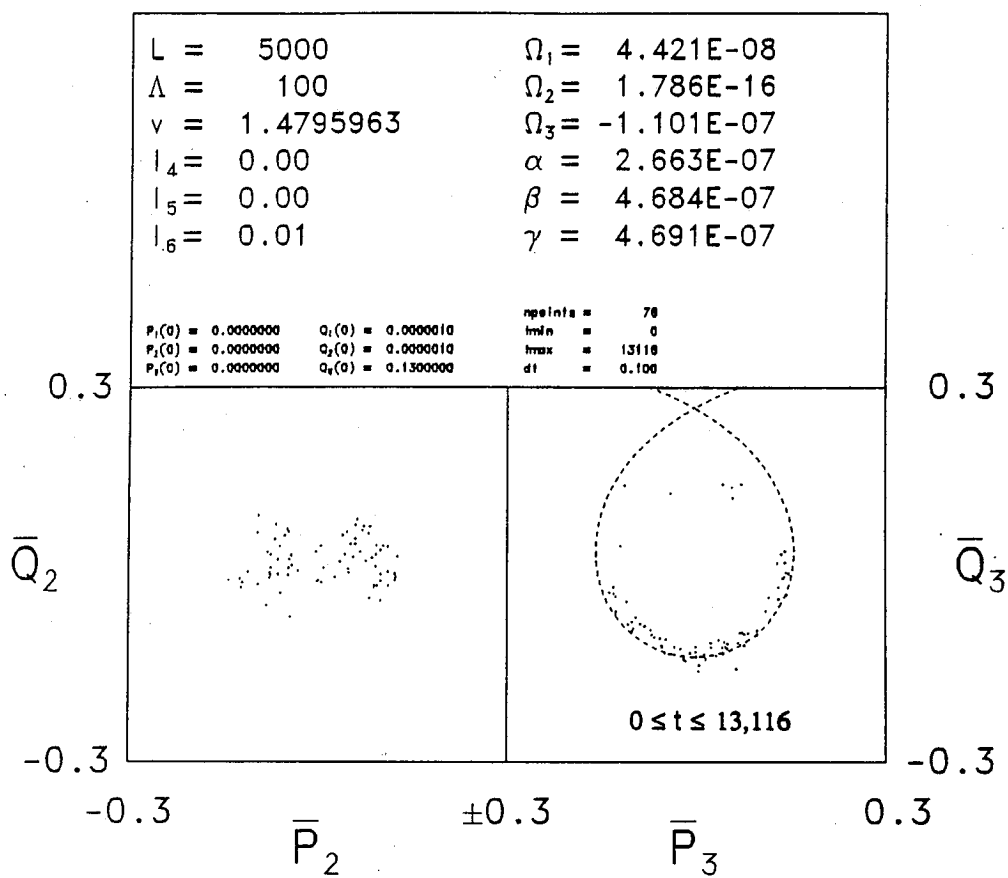


Figure 7.9: Phase space diffusion with  $L = 5000$  and  $\bar{Q}_3(0) = 0.13$ . Escape occurs at  $t = 13,116$ .

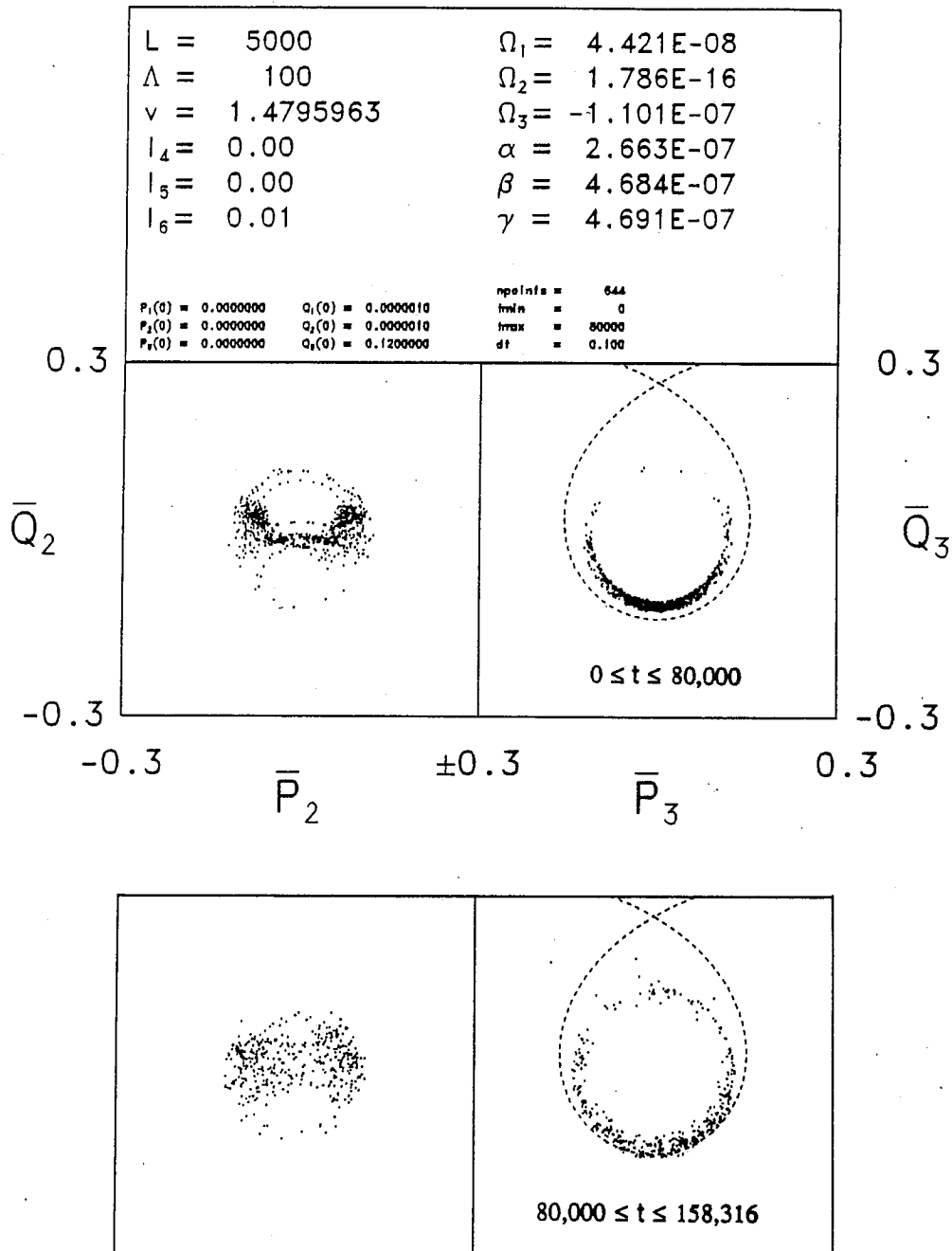


Figure 7.10: Phase space diffusion with  $L = 5000$  and  $\bar{Q}_3(0) = 0.12$ . Escape occurs at  $t = 158,316$ .

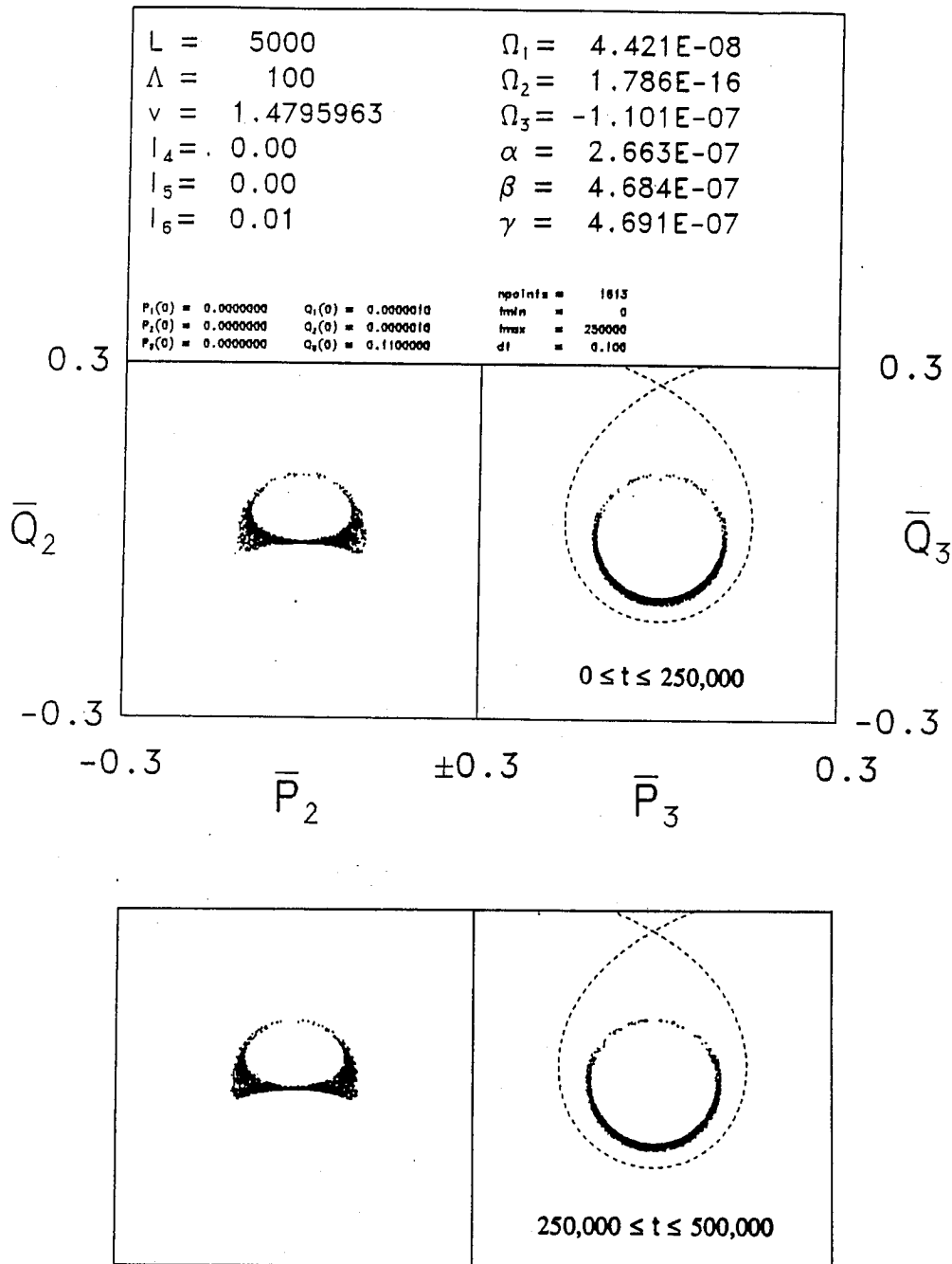


Figure 7.11: Phase space diffusion with  $L = 5000$  and  $\bar{Q}_3(0) = 0.11$ . No overall growth in  $\bar{I}_3$  was visible at  $t = 500,000$ .

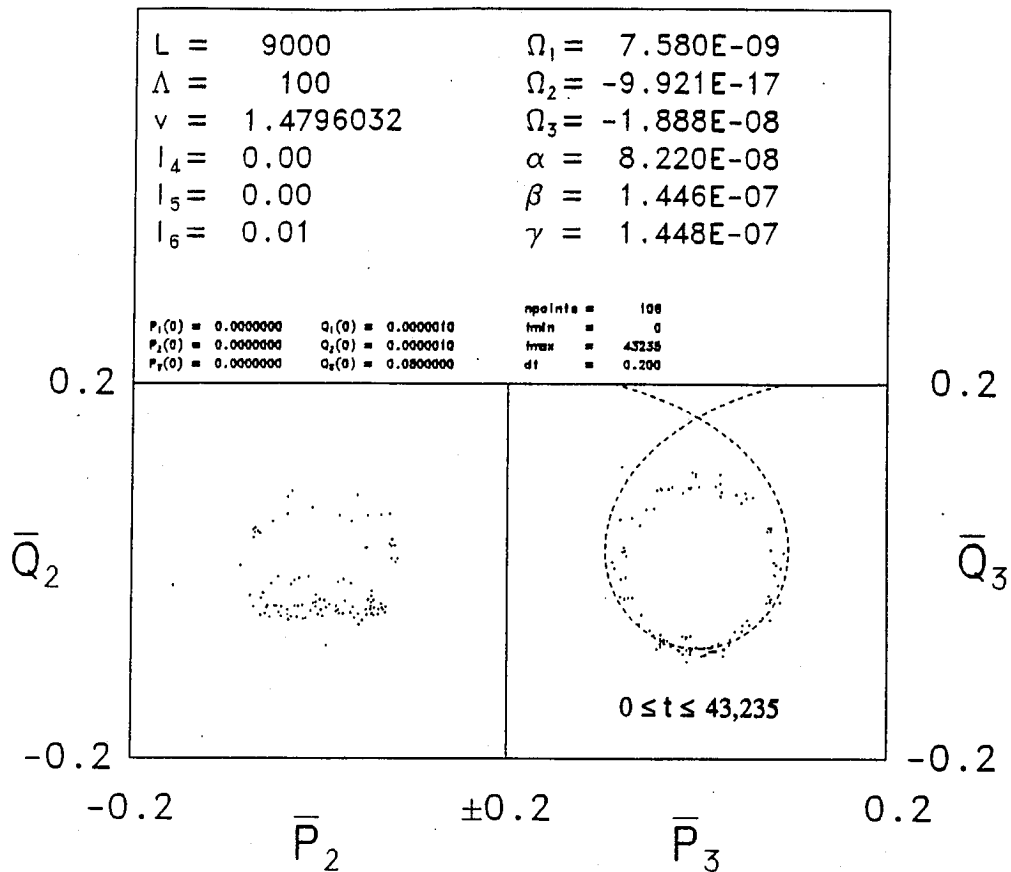


Figure 7.12: Phase space diffusion with  $L = 9000$  and  $\bar{Q}_3(0) = 0.08$ . Escape occurs at  $t = 43,235$ .

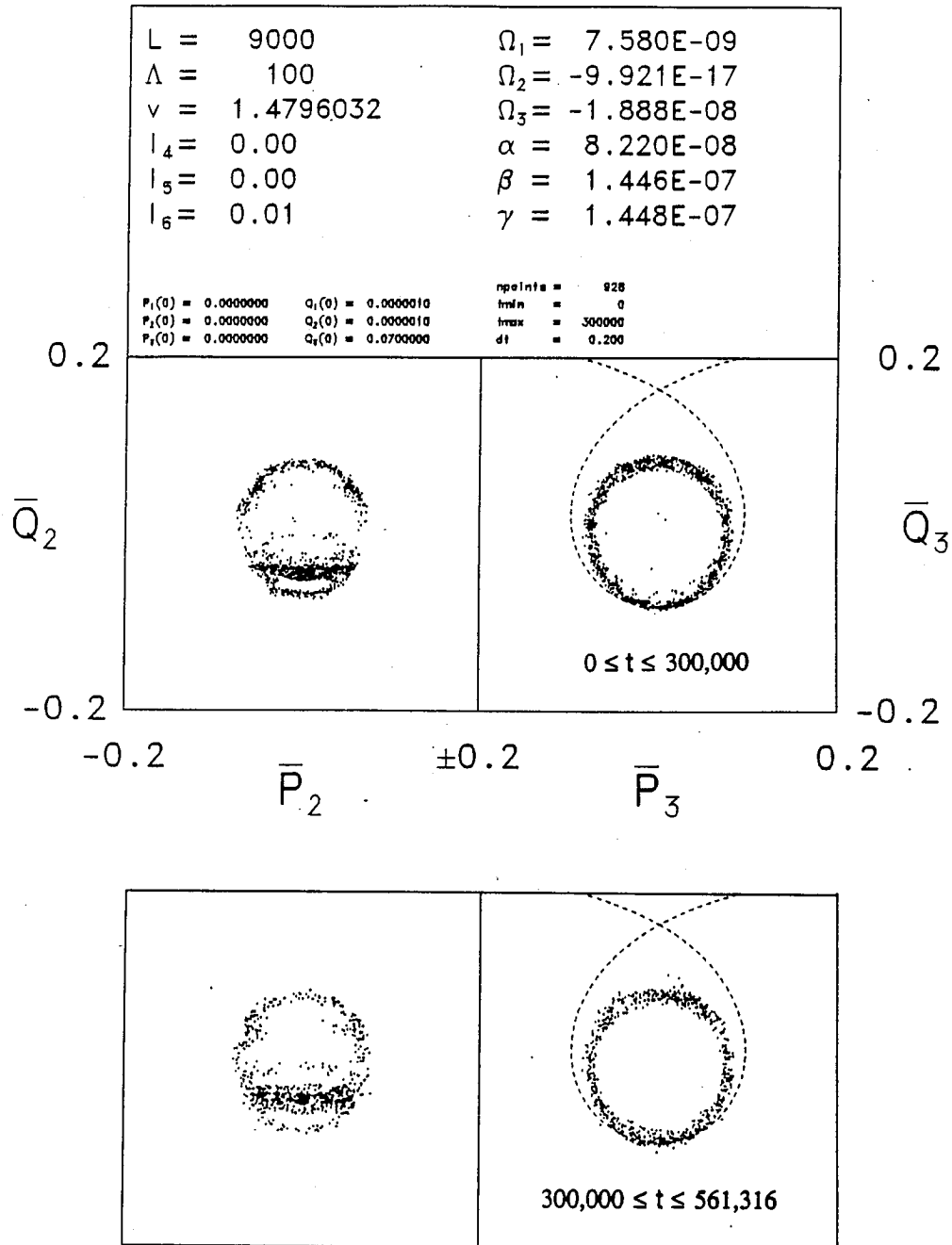


Figure 7.13: Phase space diffusion with  $L = 9000$  and  $\bar{Q}_3(0) = 0.07$ . Escape occurs at  $t = 561,316$ .

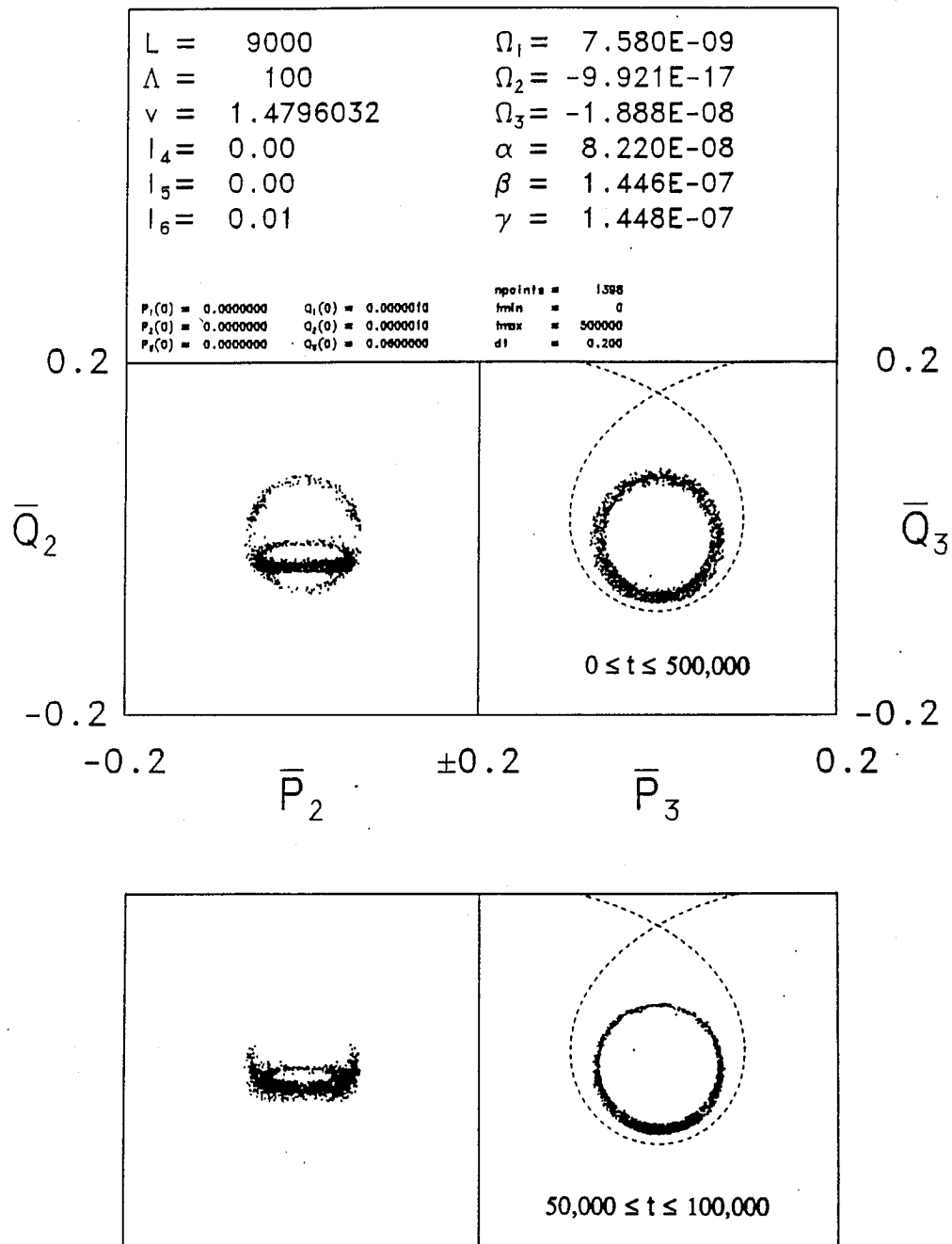


Figure 7.14: Phase space diffusion with  $L = 9000$  and  $\bar{Q}_3(0) = 0.06$ . No overall growth in  $\bar{I}_3$  was visible at  $t = 600,000$ .

## Chapter 8

### Conclusions

We have considered the role of intrinsic chaotic motion on the stability of plasma equilibria with free energy. Free energy permits the existence of negative energy waves. A system with negative energy waves, even if linearly stable, may become nonlinearly unstable due to the resonant interaction of positive and negative energy modes. Previous work, which assumed integrable behavior in order to describe the nonlinear explosive instability, was complemented here by consideration of the chaotic motion that is ubiquitous in nonlinear dynamical systems.

Describing a simple example via a Hamiltonian formulation allowed us to exploit the wealth of techniques available for understanding the behavior of such systems. Strict constraints on the phase space structure led to conclusions on what to expect in the nonintegrable case. The same constraints also led us to explore techniques for symplectic integration of the equations of motion. The application of Lie algebraic methods, including recently developed methods for obtaining explicit expressions, led to a fast explicit numerical algorithm which was used to study a number of simple subsystems of interacting waves. Regions of parameter space near explosive three-wave resonances were examined. Strong two-wave interactions that turned out to be very common in this system led to highly chaotic motion. This was a destabilizing influence, causing chaotic fluctuations in wave amplitudes and subsequent explosive growth for



initial amplitudes below the critical value calculated for the integrable case of an isolated three-wave resonance.

This paper considered only a very small portion of the possible parameter space. Many other initial conditions could be considered, and might lead to very different kinds of behavior. The small glimpses obtained here of the phase space structure and diffusion invite further study, as has been done for other many-dimensional Hamiltonian systems [56]. For further numerical studies of diffusion, it would be desirable to obtain an actual surface-of-section mapping, as has been done for other systems [14, 32]. Such a mapping would greatly extend the range of parameters and initial conditions that could be studied.

While the two- and three-degree-of-freedom systems considered here represent an improvement over the integrable approximation for three-wave interactions, they still include drastic simplifications. One major approximation is the neglect of a large number of other possible wave-wave interactions, particularly the two-wave interactions which lead to very chaotic motion even when only three waves are involved. At long wavelengths many such interactions can occur simultaneously. The explosive resonances (a very few of which are shown in Figure 4.1.b) are isolated in parameter space, but the highly chaotic nature of the system broadens the region over which they are important. It would be interesting to carry out further numerical modelling of this system, considering more than three resonances, and perhaps to develop a reasonably accurate treatment of a very large number. One would guess that a more realistic number of near-resonant interactions would lead to stronger chaos and faster diffusion than was seen in this paper.

Another effect that might lead to faster diffusion rates is scattering in phase space due to collisions. While the fluid model developed in this paper does not include collisions, their effect might be crudely incorporated by including small random perturbations in the numerical algorithm. As mentioned at the end of Chapter 6, this kind of extrinsic noise can sometimes enhance the intrinsic diffusion rate.

One might also consider further whether some flattening of the distribution function can actually eliminate the Landau damping discussed in Chapter 3. This damping is fatal to ion-acoustic waves, so that our waves might well not survive long enough to diffuse anywhere. It is nevertheless of interest to study one phenomenon, such as chaotic diffusion, in isolation, in order to gain some basic understanding.

Other physical systems can also be studied using the methods and concepts described here. The plasma equilibrium considered was chosen partly because it allowed analytical reduction to the simple action-angle form (3.44); this is not possible for all systems. Nevertheless, the  $\delta^2 F$  arguments addressing nonlinear stability are widely applicable, and the physical processes considered are quite common, so it is hoped that the results obtained will spur further investigations in these areas.

## Appendix A

### Transformation of the Bracket

The type of transformation described here was carried out by Gardner [57] in describing the Hamiltonian structure for the Korteweg-de Vries Equation.

We begin with Eq. (3.9):

$$\{\mathcal{F}, \mathcal{G}\} = \Lambda^{-1} \sum_{\alpha=\pm} \int_0^L dx \left[ \frac{\delta \mathcal{G}}{\delta v_\alpha} \frac{\partial}{\partial x} \frac{\delta \mathcal{F}}{\delta n_\alpha} - \frac{\delta \mathcal{F}}{\delta v_\alpha} \frac{\partial}{\partial x} \frac{\delta \mathcal{G}}{\delta n_\alpha} \right].$$

In terms of the perturbed quantities  $\delta n_\alpha$  and  $\delta v_\alpha$ , this becomes

$$\{\mathcal{F}, \mathcal{G}\} = \Lambda^{-1} \sum_{\alpha=\pm} \int_0^L dx \left[ \frac{\delta \mathcal{G}}{\delta(\delta v_\alpha)} \frac{\partial}{\partial x} \frac{\delta \mathcal{F}}{\delta(\delta n_\alpha)} - \frac{\delta \mathcal{F}}{\delta(\delta v_\alpha)} \frac{\partial}{\partial x} \frac{\delta \mathcal{G}}{\delta(\delta n_\alpha)} \right]. \quad (\text{A.1})$$

Now if  $u = \sum_{m=-\infty}^{\infty} u_m e^{ik_m x}$  is one of our variables  $\delta n_\alpha$  or  $\delta v_\alpha$ , then

$$\frac{\partial f}{\partial u_m} = \int_0^L \frac{\delta \mathcal{F}}{\delta u} \frac{\partial u}{\partial u_m} dx = \int_0^L \frac{\delta \mathcal{F}}{\delta u} e^{ik_m x} dx. \quad (\text{A.2})$$

We then have for the Fourier expansion of a functional derivative

$$\frac{\delta \mathcal{F}}{\delta u} = \frac{1}{L} \sum_{m=-\infty}^{\infty} \frac{\partial \mathcal{F}}{\partial u_{-m}} e^{ik_m x}. \quad (\text{A.3})$$

Using this in expression (A.1), we have

$$\begin{aligned} \{\mathcal{F}, \mathcal{G}\} = \sum_{\alpha=\pm} \frac{1}{\Lambda L^2} \int_0^L dx & \left[ \left( \sum_{m=-\infty}^{\infty} \frac{\partial \mathcal{G}}{\partial v_{-m}^\alpha} e^{ik_m x} \right) \frac{\partial}{\partial x} \left( \sum_{m=-\infty}^{\infty} \frac{\partial \mathcal{F}}{\partial n_{-m}^\alpha} e^{ik_m x} \right) \right. \\ & \left. - \left( \sum_{m=-\infty}^{\infty} \frac{\partial \mathcal{F}}{\partial v_{-m}^\alpha} e^{ik_m x} \right) \frac{\partial}{\partial x} \left( \sum_{m=-\infty}^{\infty} \frac{\partial \mathcal{G}}{\partial n_{-m}^\alpha} e^{ik_m x} \right) \right] \end{aligned}$$

$$\begin{aligned}
&= \sum_{\alpha=\pm} \sum_{m=-\infty}^{\infty} \left( -\frac{ik_m}{\Lambda L} \right) \left[ \frac{\partial \mathcal{G}}{\partial v_{-m}^{\alpha}} \frac{\partial \mathcal{F}}{\partial v_m^{\alpha}} - \frac{\partial \mathcal{F}}{\partial v_{-m}^{\alpha}} \frac{\partial \mathcal{G}}{\partial v_m^{\alpha}} \right] \\
&= \sum_{\alpha=\pm} \sum_{m=1}^{\infty} \left( \frac{ik_m}{\Lambda L} \right) \left[ \left( -\frac{\partial \mathcal{G}}{\partial v_{-m}^{\alpha}} \frac{\partial \mathcal{F}}{\partial v_m^{\alpha}} + \frac{\partial \mathcal{F}}{\partial v_{-m}^{\alpha}} \frac{\partial \mathcal{G}}{\partial v_m^{\alpha}} \right) \right. \\
&\quad \left. + \left( \frac{\partial \mathcal{G}}{\partial v_{-m}^{\alpha}} \frac{\partial \mathcal{F}}{\partial v_m^{\alpha}} - \frac{\partial \mathcal{F}}{\partial v_{-m}^{\alpha}} \frac{\partial \mathcal{G}}{\partial v_m^{\alpha}} \right) \right]. \tag{A.4}
\end{aligned}$$

## Appendix B

### Diagonalization of $\delta^2 F$

We have seen that the quadratic part of the perturbed energy and momentum may be written as

$$\delta^2 F = \frac{1}{2} \sum_{m=1}^{\infty} (\tilde{q} \mathbf{A} \mathbf{q} + \tilde{p} \mathbf{B} \mathbf{p}) \quad (\text{B.1})$$

$$\delta^2 P = \frac{1}{2} \sum_{m=1}^{\infty} (\tilde{q} \mathbf{C} \mathbf{q} + \tilde{p} \mathbf{C} \mathbf{p}) \quad (\text{B.2})$$

where

$$\mathbf{A} = k_m \begin{bmatrix} \frac{k_m k_0 v}{1+k_m^2} & v & \frac{k_m k_0 v}{1+k_m^2} & 0 \\ v & \frac{1}{2k_m k_0 v} & 0 & 0 \\ \frac{k_m k_0 v}{1+k_m^2} & 0 & \frac{k_m k_0 v}{1+k_m^2} & -v \\ 0 & 0 & -v & \frac{1}{2k_m k_0 v} \end{bmatrix} = \hat{k}_m \begin{bmatrix} \hat{k}_m \hat{k}_0 \hat{v} & \hat{v} & \hat{k}_m \hat{k}_0 \hat{v} & 0 \\ \hat{v} & \frac{1}{2\hat{k}_m \hat{k}_0 \hat{v}} & 0 & 0 \\ \hat{k}_m \hat{k}_0 \hat{v} & 0 & \hat{k}_m \hat{k}_0 \hat{v} & -\hat{v} \\ 0 & 0 & -\hat{v} & \frac{1}{2\hat{k}_m \hat{k}_0 \hat{v}} \end{bmatrix}$$

$$\mathbf{B} = k_m \begin{bmatrix} \frac{1}{2k_m k_0 v} & v & 0 & 0 \\ v & \frac{k_m k_0 v}{1+k_m^2} & 0 & \frac{k_m k_0 v}{1+k_m^2} \\ 0 & 0 & \frac{1}{2k_m k_0 v} & -v \\ 0 & \frac{k_m k_0 v}{1+k_m^2} & -v & \frac{k_m k_0 v}{1+k_m^2} \end{bmatrix} = \hat{k}_m \begin{bmatrix} \frac{1}{2\hat{k}_m \hat{k}_0 \hat{v}} & \hat{v} & 0 & 0 \\ \hat{v} & \hat{k}_m \hat{k}_0 \hat{v} & 0 & \hat{k}_m \hat{k}_0 \hat{v} \\ 0 & 0 & \frac{1}{2\hat{k}_m \hat{k}_0 \hat{v}} & -\hat{v} \\ 0 & \hat{k}_m \hat{k}_0 \hat{v} & -\hat{v} & \hat{k}_m \hat{k}_0 \hat{v} \end{bmatrix}$$

$$\mathbf{C} = k_m \begin{bmatrix} 0 & 1 & 0 & 0 \\ 1 & 0 & 0 & 0 \\ 0 & 0 & 0 & 1 \\ 0 & 0 & 1 & 0 \end{bmatrix}$$

where we have defined

$$\hat{k}_m \equiv \frac{k_m}{\sqrt{1+k_m^2}} \quad (\text{B.3})$$

$$\hat{k}_0 \equiv \frac{k_0}{\sqrt{1 + k_m^2}} \quad (\text{B.4})$$

$$\hat{v} \equiv v\sqrt{1 + k_m^2}. \quad (\text{B.5})$$

(Note that  $\hat{k}_0$  and  $\hat{v}$  both depend on the mode number  $m$  whereas  $k_0$  and  $v$  do not; since the former are occurring only inside matrices that depend upon a single  $m$ , this will not lead to confusion.)

The equations of motion are then

$$\frac{dz}{dt} = \mathbf{J}_c \nabla H = \mathbf{M}z \quad (\text{B.6})$$

where

$$\mathbf{z} = (q_1, q_2, q_3, q_4, p_1, p_2, p_3, p_4) \quad (\text{B.7})$$

and

$$\mathbf{M} = \begin{bmatrix} \mathbf{0} & \mathbf{B} \\ -\mathbf{A} & \mathbf{0} \end{bmatrix}. \quad (\text{B.8})$$

The eigenvalues of  $\mathbf{M}$  are given by

$$\lambda^2 = -\omega^2 \quad (\text{B.9})$$

where

$$\begin{aligned} \omega^2 &= k_m^2 \left[ \frac{1}{2(1 + k_m^2)} + v^2 \pm \sqrt{\frac{1}{4(1 + k_m^2)^2} + \frac{2v^2}{1 + k_m^2}} \right] \\ &= \hat{k}_m^2 \left[ \frac{1}{2} + \hat{v}^2 \pm \sqrt{\frac{1}{4} + 2\hat{v}^2} \right]. \end{aligned} \quad (\text{B.10})$$

By taking appropriate linear combinations of the complex eigenvectors of  $\mathbf{M}$

we obtain the following eight real eigenvectors:

$$\begin{bmatrix} 0 \\ 0 \\ 0 \\ 0 \\ (\hat{a}_1\hat{v} + \hat{b}_1)/R\sqrt{\hat{k}_m\hat{k}_0\hat{v}} \\ \hat{a}_1\sqrt{\hat{k}_m\hat{k}_0\hat{v}} \\ \hat{b}_1/\sqrt{\hat{k}_m\hat{k}_0\hat{v}} \\ (\hat{a}_1 - \hat{b}_14\hat{v})\sqrt{\hat{k}_m\hat{k}_0\hat{v}}/R \end{bmatrix} \begin{bmatrix} -\frac{1}{\hat{\omega}_+} \left[ \hat{a}_1\hat{v} \left( 1 + \frac{1}{R} \right) + \hat{b}_1 \left( 1 + \frac{1}{2R} \right) \right] \sqrt{\hat{k}_m\hat{k}_0\hat{v}} \\ -\frac{1}{\hat{\omega}_+} \left[ \frac{\hat{a}_1}{2} \left( 1 + \frac{2\hat{v}^2}{R} \right) + \frac{\hat{b}_1\hat{v}}{2R} \right] / \sqrt{\hat{k}_m\hat{k}_0\hat{v}} \\ -\frac{1}{\hat{\omega}_+} \left[ \frac{\hat{a}_1\hat{v}}{2R} + \hat{b}_1 \left( 1 + \frac{1+4\hat{v}^2}{2R} \right) \right] \sqrt{\hat{k}_m\hat{k}_0\hat{v}} \\ -\frac{1}{\hat{\omega}_+} \left[ \frac{\hat{a}_1}{4R} + \hat{b}_1\hat{v} \left( -1 - \frac{1}{R} \right) \right] / \sqrt{\hat{k}_m\hat{k}_0\hat{v}} \\ 0 \\ 0 \\ 0 \\ 0 \end{bmatrix}$$

$$\begin{bmatrix} 0 \\ 0 \\ 0 \\ 0 \\ -(\hat{a}_2\hat{v} + \hat{b}_2)/R\sqrt{\hat{k}_m\hat{k}_0\hat{v}} \\ \hat{a}_2\sqrt{\hat{k}_m\hat{k}_0\hat{v}} \\ \hat{b}_2/\sqrt{\hat{k}_m\hat{k}_0\hat{v}} \\ -(\hat{a}_2 - \hat{b}_24\hat{v})\sqrt{\hat{k}_m\hat{k}_0\hat{v}}/R \end{bmatrix} \begin{bmatrix} -\frac{1}{\hat{\omega}_-} \left[ \hat{a}_2\hat{v} \left( 1 - \frac{1}{R} \right) + \hat{b}_2 \left( 1 - \frac{1}{2R} \right) \right] \sqrt{\hat{k}_m\hat{k}_0\hat{v}} \\ -\frac{1}{\hat{\omega}_-} \left[ \frac{\hat{a}_2}{2} \left( 1 - \frac{2\hat{v}^2}{R} \right) - \frac{\hat{b}_2\hat{v}}{2R} \right] / \sqrt{\hat{k}_m\hat{k}_0\hat{v}} \\ -\frac{1}{\hat{\omega}_-} \left[ -\frac{\hat{a}_2\hat{v}}{2R} + \hat{b}_2 \left( 1 - \frac{1+4\hat{v}^2}{2R} \right) \right] \sqrt{\hat{k}_m\hat{k}_0\hat{v}} \\ -\frac{1}{\hat{\omega}_-} \left[ -\frac{\hat{a}_2}{4R} + \hat{b}_2\hat{v} \left( -1 + \frac{1}{R} \right) \right] / \sqrt{\hat{k}_m\hat{k}_0\hat{v}} \\ 0 \\ 0 \\ 0 \\ 0 \end{bmatrix}$$

$$\begin{bmatrix} 0 \\ 0 \\ 0 \\ 0 \\ (\hat{a}_3\hat{v} + \hat{b}_3)/R\sqrt{\hat{k}_m\hat{k}_0\hat{v}} \\ \hat{a}_3\sqrt{\hat{k}_m\hat{k}_0\hat{v}} \\ \hat{b}_3/\sqrt{\hat{k}_m\hat{k}_0\hat{v}} \\ (\hat{a}_3 - \hat{b}_34\hat{v})\sqrt{\hat{k}_m\hat{k}_0\hat{v}}/R \end{bmatrix} \begin{bmatrix} -\frac{1}{\hat{\omega}_+} \left[ \hat{a}_3\hat{v} \left( 1 + \frac{1}{R} \right) + \hat{b}_3 \left( 1 + \frac{1}{2R} \right) \right] \sqrt{\hat{k}_m\hat{k}_0\hat{v}} \\ -\frac{1}{\hat{\omega}_+} \left[ \frac{\hat{a}_3}{2} \left( 1 + \frac{2\hat{v}^2}{R} \right) + \frac{\hat{b}_3\hat{v}}{2R} \right] / \sqrt{\hat{k}_m\hat{k}_0\hat{v}} \\ -\frac{1}{\hat{\omega}_+} \left[ \frac{\hat{a}_3\hat{v}}{2R} + \hat{b}_3 \left( 1 + \frac{1+4\hat{v}^2}{2R} \right) \right] \sqrt{\hat{k}_m\hat{k}_0\hat{v}} \\ -\frac{1}{\hat{\omega}_+} \left[ \frac{\hat{a}_3}{4R} + \hat{b}_3\hat{v} \left( -1 - \frac{1}{R} \right) \right] / \sqrt{\hat{k}_m\hat{k}_0\hat{v}} \\ 0 \\ 0 \\ 0 \\ 0 \end{bmatrix}$$

$$\begin{bmatrix} 0 \\ 0 \\ 0 \\ 0 \\ -(\hat{a}_4\hat{v} + \hat{b}_4)/R\sqrt{\hat{k}_m\hat{k}_0\hat{v}} \\ \hat{a}_4\sqrt{\hat{k}_m\hat{k}_0\hat{v}} \\ \hat{b}_4/\sqrt{\hat{k}_m\hat{k}_0\hat{v}} \\ -(\hat{a}_4 - \hat{b}_4\hat{v})\sqrt{\hat{k}_m\hat{k}_0\hat{v}}/R \end{bmatrix} \begin{bmatrix} -\frac{1}{\hat{\omega}_-} \left[ \hat{a}_4\hat{v} \left(1 - \frac{1}{R}\right) + \hat{b}_4 \left(1 - \frac{1}{2R}\right) \right] \sqrt{\hat{k}_m\hat{k}_0\hat{v}} \\ -\frac{1}{\hat{\omega}_-} \left[ \frac{\hat{a}_4}{2} \left(1 - \frac{2\hat{v}^2}{R}\right) - \frac{\hat{b}_4\hat{v}}{2R} \right] / \sqrt{\hat{k}_m\hat{k}_0\hat{v}} \\ -\frac{1}{\hat{\omega}_-} \left[ -\frac{\hat{a}_4\hat{v}}{2R} + \hat{b}_4 \left(1 - \frac{1+4\hat{v}^2}{2R}\right) \right] \sqrt{\hat{k}_m\hat{k}_0\hat{v}} \\ -\frac{1}{\hat{\omega}_-} \left[ -\frac{\hat{a}_4}{4R} + \hat{b}_4\hat{v} \left(-1 + \frac{1}{R}\right) \right] / \sqrt{\hat{k}_m\hat{k}_0\hat{v}} \\ 0 \\ 0 \\ 0 \\ 0 \end{bmatrix}$$

where

$$R \equiv \sqrt{\frac{1}{4} + 2\hat{v}^2}, \quad (\text{B.11})$$

$$\hat{\omega}_{\pm} \equiv \omega_{\pm}/\hat{k}_m \quad (\text{B.12})$$

and the  $\hat{a}_i$  and  $\hat{b}_i$  are constants to be determined. These eigenvectors provide the basis for a diagonalizing transformation for the  $\mathbf{z}$ . We see that the transformation decouples into separate transformations for the  $\mathbf{p}$  and  $\mathbf{q}$ , given by

$$\mathbf{q} = \mathbf{S}\mathbf{Q} \quad (\text{B.13})$$

$$\mathbf{p} = \mathbf{T}\mathbf{P} \quad (\text{B.14})$$

where  $\mathbf{S}$  and  $\mathbf{T}$  are the  $4 \times 4$  matrices comprising the non-zero elements of the eigenvectors. (Since the transformation is symplectic, we will have  $\tilde{\mathbf{S}}\mathbf{T} = \mathbf{I}$ .)

We want to obtain for the perturbed energy and momentum

$$\delta^2 F = \sum_{m=1}^{\infty} \left[ \omega_+ \frac{P_1^2 + Q_1^2}{2} - \omega_- \frac{P_2^2 + Q_2^2}{2} + \omega_+ \frac{P_3^2 + Q_3^2}{2} - \omega_- \frac{P_4^2 + Q_4^2}{2} \right] \quad (\text{B.15})$$

and

$$\delta^2 P = \sum_{m=1}^{\infty} k_m \left[ \frac{P_1^2 + Q_1^2}{2} - \frac{P_2^2 + Q_2^2}{2} - \frac{P_3^2 + Q_3^2}{2} + \frac{P_4^2 + Q_4^2}{2} \right]. \quad (\text{B.16})$$



The resulting equations are then

$$\tilde{\mathbf{S}}\mathbf{A}\mathbf{S} = \tilde{\mathbf{T}}\mathbf{B}\mathbf{T} = \begin{bmatrix} \omega_+ & 0 & 0 & 0 \\ 0 & -\omega_- & 0 & 0 \\ 0 & 0 & \omega_+ & 0 \\ 0 & 0 & 0 & -\omega_- \end{bmatrix} \quad (\text{B.17})$$

$$\tilde{\mathbf{S}}\mathbf{C}\mathbf{T} = \tilde{\mathbf{T}}\mathbf{C}\mathbf{T} = \frac{1}{2} \begin{bmatrix} 1 & 0 & 0 & 0 \\ 0 & -1 & 0 & 0 \\ 0 & 0 & -1 & 0 \\ 0 & 0 & 0 & 1 \end{bmatrix}. \quad (\text{B.18})$$

Solving for the normalization coefficients we find

$$\mathbf{S} = \begin{bmatrix} -b_3 & -b_4 & -b_1 & -b_2 \\ a_1 & a_2 & a_3 & a_4 \\ b_1 & b_2 & b_3 & b_4 \\ a_3 & a_4 & a_1 & a_2 \end{bmatrix} \quad \mathbf{T} = \begin{bmatrix} a_1 & -a_2 & -a_3 & a_4 \\ -b_3 & b_4 & b_1 & -b_2 \\ a_3 & -a_4 & -a_1 & a_2 \\ b_1 & -b_2 & -b_3 & b_4 \end{bmatrix} \quad (\text{B.19})$$

where

$$a_i \equiv \hat{a}_i \sqrt{\hat{k}_m \hat{k}_0 \hat{v}}, \quad (\text{B.20})$$

$$b_i \equiv \hat{b}_i / \sqrt{\hat{k}_m \hat{k}_0 \hat{v}} \quad (\text{B.21})$$

and

$$\begin{aligned} \hat{a}_1 &\equiv \frac{\hat{\omega}_+ + \hat{v}}{\sqrt{4R\hat{\omega}_+}}, & \hat{b}_1 &\equiv \sqrt{\frac{(\hat{\omega}_+ - \hat{v})^2 - \frac{1}{2}}{8R\hat{\omega}_+}} \\ \hat{a}_2 &\equiv \frac{\hat{\omega}_- + \hat{v}}{\sqrt{4R\hat{\omega}_-}}, & \hat{b}_2 &\equiv -\sqrt{\frac{(\hat{\omega}_- - \hat{v})^2 - \frac{1}{2}}{8R\hat{\omega}_-}} \\ \hat{a}_3 &\equiv \frac{\hat{\omega}_+ - \hat{v}}{\sqrt{4R\hat{\omega}_+}}, & \hat{b}_3 &\equiv -\sqrt{\frac{(\hat{\omega}_+ + \hat{v})^2 - \frac{1}{2}}{8R\hat{\omega}_+}} \\ \hat{a}_4 &\equiv \frac{\hat{\omega}_- - \hat{v}}{\sqrt{4R\hat{\omega}_-}}, & \hat{b}_4 &\equiv \sqrt{\frac{(\hat{\omega}_- + \hat{v})^2 - \frac{1}{2}}{8R\hat{\omega}_-}} \end{aligned} \quad (\text{B.22})$$

Here the diagonalization transformation is expressed simply in terms of the  $a_i$  and  $b_i$ ; the utility of originally introducing the  $\hat{a}_i$  and  $\hat{b}_i$  in the eigenvectors was that the latter variables are of order unity and depend relatively weakly on  $k_0$  and  $v$ .

## Appendix C

### Nonlinear Stability for Three-Wave Interactions

It is easy to determine a necessary and sufficient condition for nonlinear stability of three-wave interactions. Consider a Hamiltonian given to lowest order by

$$H = \sigma_1 \omega_1 J_1 + \sigma_2 \omega_2 J_2 + \sigma_3 \omega_3 J_3, \quad (\text{C.1})$$

where here the  $\omega_i$  are signed frequencies and  $\sigma_i = \text{sgn} \left( \frac{\partial \varepsilon}{\partial \omega_i} \right) = \pm 1$ , so that the energy signature of each wave is given by  $\sigma_i \omega_i$ . The lowest-order momentum is given by

$$P = \sigma_1 k_1 J_1 + \sigma_2 k_2 J_2 + \sigma_3 k_3 J_3. \quad (\text{C.2})$$

(Here we will let the subscripts on the  $k_m$  simply be labels, *not* meaning  $\frac{m2\pi}{L}$  as elsewhere in this paper.) Now assume that nonlinear coupling leads to resonant interaction between the waves. If the  $\sigma_i \omega_i$  are not all of the same sign (i.e., a mixture of positive and negative energy waves) then it would appear from (C.1) that exchange of energy between the waves could result in unbounded growth in the amplitudes  $J_i$  (nonlinear instability) while the total energy  $H$  is conserved. Conversely, if all  $\sigma_i \omega_i$  are of the same sign, then it is clear by the constancy of  $H$  that only limited growth of any  $J_i$  is possible. However, this argument must hold in any reference frame, since wave energy is frame-dependent.

In a reference frame moving with speed  $u$ , the wave energy is given

by

$$\begin{aligned} H' &= H - uP \\ &= \sigma_1(\omega_1 - k_1u)J_1 + \sigma_2(\omega_2 - k_2u)J_2 + \sigma_3(\omega_3 - k_3u)J_3. \end{aligned} \quad (\text{C.3})$$

(The frequency-matching condition is not affected by the frame shift.) Therefore nonlinear stability requires that all of the  $\sigma_i(\omega_i - k_iu)$  be of the same sign for any  $u$ . It turns out that this is true if and only if the wave with the largest  $|\omega_i|$  has energy signature  $\sigma_i\omega_i$  opposite in sign to that of the other two waves [11]. This may be simply proved as follows.

Consider a system of one negative energy wave and two positive energy waves, so that the linear part of the Hamiltonian has the form

$$H = -\omega_1J_1 + \omega_2J_2 + \omega_3J_3, \quad (\text{C.4})$$

where here the frequencies are taken to be positive; i.e.,  $\omega_i = |\omega_i|$ . Consider first a resonance condition of the form

$$\omega_2 = \omega_1 + \omega_3, \quad (\text{C.5})$$

$$k_2 = k_1 + k_3, \quad (\text{C.6})$$

so that the largest frequency corresponds to one of the positive energy waves. In the moving reference frame, the Hamiltonian becomes

$$H' = -(\omega_1 - k_1u)J_1 + (\omega_2 - k_2u)J_2 + (\omega_3 - k_3u)J_3. \quad (\text{C.7})$$

The system will be nonlinearly stable if there is some  $u$  such that the mode  $J_1$  is a positive energy mode (i.e.,  $\omega_1 - k_1u < 0$ ) while the other two modes do not

change energy signature (i.e.,  $\omega_2 - k_2 u > 0$  and  $\omega_3 - k_3 u > 0$ ). The mode  $J_1$  has positive energy when  $u > \omega_1/k_1$ . At the critical speed  $u_c = \omega_1/k_1$  when its energy signature changes, the energy signatures of the other two waves are given by the signs of

$$\begin{aligned}
 \omega_2 - k_2 u &= \omega_2 - k_2 \frac{\omega_1}{k_1} \\
 &= \frac{\omega_2 k_1 - \omega_1 k_2}{k_1} \\
 &= \frac{\omega_2(k_2 - k_3) - (\omega_2 - \omega_3)k_2}{k_1} \\
 &= \frac{-\omega_2 k_3 + \omega_3 k_2}{k_1}
 \end{aligned} \tag{C.8}$$

and

$$\begin{aligned}
 \omega_3 - k_3 u &= \omega_3 - k_3 \frac{\omega_1}{k_1} \\
 &= \frac{\omega_3 k_1 - \omega_1 k_3}{k_1} \\
 &= \frac{\omega_3(k_2 - k_3) - (\omega_2 - \omega_3)k_3}{k_1} \\
 &= \frac{\omega_3 k_2 - \omega_2 k_3}{k_1},
 \end{aligned} \tag{C.9}$$

which are equal. Now if  $\omega_2 - k_2 u_c = \omega_3 - k_3 u_c > 0$ , then all three modes have positive energy for  $u \gtrsim u_c$ , and the system is therefore nonlinearly stable. If  $\omega_2 - k_2 u_c = \omega_3 - k_3 u_c < 0$ , then all three modes have negative energy for  $u \lesssim u_c$ , and the system is again stable.

Now suppose that instead of (C.6), the resonance conditions are of the form

$$\omega_1 = \omega_2 + \omega_3, \tag{C.10}$$

$$k_1 = k_2 + k_3, \quad (\text{C.11})$$

so that the largest frequency corresponds to the negative energy mode, while the two lower frequencies correspond to positive energy modes. (This case is of general interest, but cannot actually occur for the plasma system of Chapter 3.) Then at the speed  $u_c = \omega_1/k_1$  where mode  $J_1$  becomes a positive energy mode, the energy signatures of the other two waves are determined by

$$\begin{aligned} \omega_2 - k_2 u &= \omega_2 - k_2 \frac{\omega_1}{k_1} \\ &= \frac{\omega_2 k_1 - \omega_1 k_2}{k_1} \\ &= \frac{\omega_2(k_2 + k_3) - (\omega_2 + \omega_3)k_2}{k_1} \\ &= \frac{\omega_2 k_3 - \omega_3 k_2}{k_1} \end{aligned} \quad (\text{C.12})$$

and

$$\begin{aligned} \omega_3 - k_3 u &= \omega_3 - k_3 \frac{\omega_1}{k_1} \\ &= \frac{\omega_3 k_1 - \omega_1 k_3}{k_1} \\ &= \frac{\omega_3(k_2 + k_3) - (\omega_2 + \omega_3)k_3}{k_1} \\ &= \frac{\omega_3 k_2 - \omega_2 k_3}{k_1}, \end{aligned} \quad (\text{C.13})$$

which are opposite in sign. Thus there is no frame in which all three waves have the same energy signature, and the system is therefore nonlinearly unstable.

For a Hamiltonian describing one positive energy wave and two negative energy waves,

$$H = \omega_1 J_1 - \omega_2 J_2 - \omega_3 J_3, \quad (\text{C.14})$$

exactly the same type of argument may be used, and it is again found that nonlinear instability occurs if and only if the mode with the highest frequency has energy signature opposite in sign to that of the other two waves (i.e., it must be the positive energy mode). For this wave triplet in the counterstreaming ion system of Chapter 3, the type of resonance that occurs is one where the positive energy wave has the highest frequency, so that this system is unstable.

## Appendix D

### Numerical Algorithm for the Five-Wave and Six-Wave Hamiltonians

Here we reduce the five degree-of-freedom Hamiltonian 6.20 to a three degree-of-freedom polynomial Hamiltonian, and then employ the Lie transformation methods of Section 5.3.2 to obtain a computational algorithm.

#### D.1 Transformation to Computational Variables

Recall the Hamiltonian:

$$\begin{aligned}
 H = & \omega_1 J_1 + \omega_2 J_2 + \omega_3 J_3 - \omega_4 J_4 - \omega_5 J_5 \\
 & + \alpha J_1 \sqrt{J_2} \sin(2\theta_1 - \theta_2) \\
 & + \beta J_2 \sqrt{J_3} \sin(2\theta_2 - \theta_3) \\
 & + \gamma \sqrt{J_2 J_4 J_5} \sin(\theta_2 + \theta_4 + \theta_5). \tag{D.1}
 \end{aligned}$$

In Section 6.3 we employed a transformation to resonance coordinates to re-express this as a three degree-of-freedom system:

$$\begin{aligned}
 \bar{H} = & \bar{\Omega}_1 \bar{I}_1 + \bar{\Omega}_2 \bar{I}_2 + \bar{\Omega}_3 \bar{I}_3 + \alpha 2 \bar{I}_1 \sqrt{\bar{I}_3 - 2\bar{I}_2 - \bar{I}_1} \sin \bar{\psi}_1 \\
 & - \beta (\bar{I}_3 - 2\bar{I}_2 - \bar{I}_1) \sqrt{\bar{I}_2} \sin \bar{\psi}_2 \\
 & + \gamma \sqrt{(\bar{I}_3 - 2\bar{I}_2 - \bar{I}_1)(\bar{I}_4 + \bar{I}_3)(\bar{I}_5 + \bar{I}_3)} \sin \bar{\psi}_3. \tag{D.2}
 \end{aligned}$$

The resonance coordinates  $(\bar{I}_i, \bar{\psi}_i)$  (or their cartesian counterparts  $(\bar{P}_i, \bar{Q}_i)$ ) are convenient ones in which to view the phase space topology, but they are not good for numerical computations, due to the difficulty of evaluating  $\sqrt{\bar{I}_3 - 2\bar{I}_2 - \bar{I}_1}$  when the argument is near zero. We therefore define another set of coordinates for computational work, derived from the generating function

$$F^{(2)} = I_1\theta_1 + I_3\theta_2 + I_2\theta_3 + \left(I_4 + I_3 + 2I_2 + \frac{1}{2}I_1\right)\theta_4 + \left(I_4 + I_3 + 2I_2 + \frac{1}{2}I_1\right)\theta_5. \quad (\text{D.3})$$

This yields

$$\begin{aligned} J_1 &= \frac{\partial F^{(2)}}{\partial \theta_1} = I_1, & \psi_1 &= \frac{\partial F^{(2)}}{\partial I_1} = \theta_1 + \frac{1}{2}(\theta_4 + \theta_5), \\ J_2 &= \frac{\partial F^{(2)}}{\partial \theta_2} = I_3, & \psi_2 &= \frac{\partial F^{(2)}}{\partial I_2} = \theta_3 + 2(\theta_4 + \theta_5), \\ J_3 &= \frac{\partial F^{(2)}}{\partial \theta_3} = I_2, & \psi_3 &= \frac{\partial F^{(2)}}{\partial I_3} = \theta_2 + \theta_4 + \theta_5, \\ J_4 &= \frac{\partial F^{(2)}}{\partial \theta_4} = I_4 + I_3 + 2I_2 + \frac{1}{2}I_1, & \psi_4 &= \frac{\partial F^{(2)}}{\partial I_4} = \theta_4, \\ J_5 &= \frac{\partial F^{(2)}}{\partial \theta_5} = I_5 + I_3 + 2I_2 + \frac{1}{2}I_1, & \psi_5 &= \frac{\partial F^{(2)}}{\partial I_5} = \theta_5. \end{aligned} \quad (\text{D.4})$$

From this we obtain for the new Hamiltonian

$$\begin{aligned} \bar{H} &= H + \omega_4 I_4 + \omega_5 I_5 \\ &= \Omega_1 I_1 + \Omega_2 I_2 + \Omega_3 I_3 + \alpha I_1 \sqrt{I_3} \sin(2\psi_1 - \psi_3) \\ &\quad + \beta I_3 \sqrt{I_2} \sin(2\psi_3 - \psi_2) \\ &\quad + \gamma \sqrt{I_3 \left(I_4 + I_3 + 2I_2 + \frac{1}{2}I_1\right) \left(I_5 + I_3 + 2I_2 + \frac{1}{2}I_1\right)} \sin \psi_3, \end{aligned} \quad (\text{D.5})$$

where

$$\Omega_1 = \omega_1 - \frac{1}{2}\omega_4 - \frac{1}{2}\omega_5 = \frac{1}{2}(\bar{\Omega}_1 + \bar{\Omega}_3),$$



$$\Omega_2 = \omega_3 - 2\omega_4 - 2\omega_5 = 2\bar{\Omega}_3 + \bar{\Omega}_2,$$

$$\Omega_3 = \omega_2 - \omega_4 - \omega_5 = \bar{\Omega}_3.$$

For the special case  $I_4 = I_5$ , this Hamiltonian may be written in cartesian coordinates  $\hat{P}_i = \sqrt{2I_i} \cos \psi_i$  and  $\hat{Q}_i = \sqrt{2I_i} \sin \psi_i$ :

$$\begin{aligned} \hat{H} = & \frac{\Omega_1}{2} (\hat{P}_1^2 + \hat{Q}_1^2) + \frac{\Omega_2}{2} (\hat{P}_2^2 + \hat{Q}_2^2) + \frac{\Omega_3}{2} (\hat{P}_3^2 + \hat{Q}_3^2) \\ & + \frac{\alpha}{2\sqrt{2}} [2\hat{Q}_1\hat{P}_1\hat{P}_3 - \hat{Q}_3(\hat{P}_1^2 - \hat{Q}_1^2)] \\ & + \frac{\beta}{2\sqrt{2}} [2\hat{Q}_3\hat{P}_3\hat{P}_2 - \hat{Q}_2(\hat{P}_3^2 - \hat{Q}_3^2)] \\ & + \frac{\gamma}{\sqrt{2}}\hat{Q}_3 \left[ I_{4,5} + \frac{1}{4} (\hat{P}_1^2 + \hat{Q}_1^2) + (\hat{P}_2^2 + \hat{Q}_2^2) + \frac{1}{2} (\hat{P}_3^2 + \hat{Q}_3^2) \right]. \end{aligned} \quad (\text{D.6})$$

This three-degree-of-freedom Hamiltonian is now in the form of a cubic polynomial. We can now employ Lie transformations to obtain an algorithm for time-advancing the system.

## D.2 Derivation of the Algorithm

We now apply the method of Lie transformations (see Section 5.3) to derive a small-timestep integrator for the Hamiltonian (D.6), correct to third order in  $\Delta t$  and in the dynamical variables  $\hat{z}_i \equiv (\hat{Q}_i, \hat{P}_i)$ .

Let us express our Hamiltonian as

$$\begin{aligned} H &= H_2 + H_3 \\ &= H_2 + H_3^{(\alpha)} + H_3^{(\beta)} + H_3^{(\gamma)} \end{aligned} \quad (\text{D.7})$$

where  $H_2$  comprises the three terms of (D.6) quadratic in the  $\hat{P}_i, \hat{Q}_i$  (linear in the  $I_i$ ), and the  $H^{(\alpha, \beta, \gamma)}$  are the three cubic (nonlinear in the  $I_i$ ) terms. As discussed in Section 5.3.2, the linear transformation is given by

$$\begin{bmatrix} Q'_i \\ P'_i \end{bmatrix} = \begin{bmatrix} \cos(\Omega_i \Delta t) & \sin(\Omega_i \Delta t) \\ -\sin(\Omega_i \Delta t) & \cos(\Omega_i \Delta t) \end{bmatrix} \begin{bmatrix} Q_i \\ P_i \end{bmatrix}. \quad (\text{D.8})$$

(Also as discussed before, in practice we split the linear transformation into two half-steps, making the algorithm accurate to third order in  $\Delta t$ .)

The polynomial  $f_3$  is given by

$$f_3 \equiv - \int_0^{\Delta t} dt H_3(\hat{z}'_i) \quad (\text{D.9})$$

which may be written as

$$\begin{aligned} f_3 &= f_3^{(\alpha)} + f_3^{(\beta)} + f_3^{(\gamma)} \\ &= - \int_0^{\Delta t} dt H_3^{(\alpha)}(\hat{z}'_i) - \int_0^{\Delta t} dt H_3^{(\beta)}(\hat{z}'_i) - \int_0^{\Delta t} dt H_3^{(\gamma)}(\hat{z}'_i). \end{aligned} \quad (\text{D.10})$$

Carrying out the operations, we obtain

$$\begin{aligned} f_3^{(\alpha)} &= -\frac{\alpha}{\sqrt{8\bar{\Omega}_1}} \left\{ \sin(\bar{\Omega}_1 \Delta t) \left[ \hat{Q}_3(\hat{Q}_1^2 - \hat{P}_1^2) + 2\hat{Q}_1\hat{P}_1\hat{P}_3 \right] \right. \\ &\quad \left. + 2\sin^2(\bar{\Omega}_1 \Delta t/2) \left[ \hat{P}_3(\hat{Q}_1^2 - \hat{P}_1^2) - 2\hat{Q}_1\hat{P}_1\hat{Q}_3 \right] \right\} \\ f_3^{(\beta)} &= -\frac{\beta}{\sqrt{8\bar{\Omega}_2}} \left\{ \sin(\bar{\Omega}_2 \Delta t) \left[ \hat{Q}_2(\hat{Q}_3^2 - \hat{P}_3^2) + 2\hat{Q}_3\hat{P}_3\hat{P}_2 \right] \right. \\ &\quad \left. + 2\sin^2(\bar{\Omega}_2 \Delta t/2) \left[ \hat{P}_2(\hat{Q}_3^2 - \hat{P}_3^2) - 2\hat{Q}_3\hat{P}_3\hat{Q}_2 \right] \right\} \\ f_3^{(\gamma)} &= -\frac{\gamma}{\sqrt{2\bar{\Omega}_3}} \left( \hat{Q}_3 \sin(\bar{\Omega}_3 \Delta t) + \hat{P}_3 2\sin^2(\bar{\Omega}_2 \Delta t/2) \right) \\ &\quad \times \left[ \frac{1}{4} (\hat{P}_1^2 + \hat{Q}_1^2) + (\hat{P}_2^2 + \hat{Q}_2^2) + \frac{1}{2} (\hat{P}_3^2 + \hat{Q}_3^2) \right] \end{aligned} \quad (\text{D.11})$$

The operators  $e^{[f_3^{(\alpha,\beta,\gamma)}, \cdot]}$  are now replaced with new operators  $e^{[g_3^{(\alpha,\beta)}, \cdot]}$ , where

$$g_3^{(\alpha,\beta)} = \sum_{i=1}^6 \rho_i^{(\alpha,\beta)} (\hat{Q}_m \cos \phi_x^{(i)} + \hat{P}_m \sin \phi_y^{(i)})^2 (\hat{Q}_n \cos \phi_x^{(i)} + \hat{P}_n \sin \phi_y^{(i)}) \quad (\text{D.12})$$

and we have  $(m = 1, n = 3)$  for  $g^{(\alpha)}$  and  $(m = 3, n = 2)$  for  $g^{(\beta)}$ . The new operators yield series expansions that terminate at second order.

The angles comprising the linearly independent pairs  $(\phi_x, \phi_y)$  are again chosen to be evenly spaced in the interval  $(0, 2\pi)$ , and the coefficients  $\rho_i$  are found by solving the systems of equations  $f_3^{(\alpha)} = g_3^{(\alpha)}$  and  $f_3^{(\beta)} = g_3^{(\beta)}$ , each of which comprises six linear equations in the six unknowns  $\rho_i^{(\alpha)}$  or  $\rho_i^{(\beta)}$ .

The operator  $e^{[f_3^{(\gamma)}, \cdot]}$  may be split into two factors

$$e^{[-\frac{\gamma}{\sqrt{2}\bar{\Omega}_3} [\hat{Q}_3 \sin(\bar{\Omega}_3 \Delta t) + \hat{P}_3 \cos(\bar{\Omega}_3 \Delta t)] [\frac{1}{4}(\hat{P}_1^2 + \hat{Q}_1^2) + (\hat{P}_2^2 + \hat{Q}_2^2)], \cdot]} \quad (\text{D.13})$$

and

$$e^{[-\frac{\gamma}{\sqrt{2}\bar{\Omega}_3} [\hat{Q}_3 \sin(\bar{\Omega}_3 \Delta t) + \hat{P}_3 \cos(\bar{\Omega}_3 \Delta t)] [\frac{1}{2}(\hat{P}_3^2 + \hat{Q}_3^2)], \cdot]} \quad (\text{D.14})$$

The first of these couples two degrees of freedom and is treated in the same manner as  $e^{[f_3^{(\alpha,\beta)}, \cdot]}$ . The second operator (which drives the explosive instability) involves only one degree of freedom. It is replaced by the operator

$$e^{[\sum_{i=1}^4 \rho_i^{(\gamma)} (\hat{Q}_3 \cos \chi^{(i)} + \hat{P}_3 \sin \chi^{(i)})^3, \cdot]} \quad (\text{D.15})$$

Again the  $\rho_i^{(\gamma)}$  are found by equating the polynomials of the old and new operators, yielding in this case four equations in four unknowns. If we choose the  $\chi^{(i)}$  to be evenly distributed around  $(0, 2\pi)$  then we obtain a singular system of equations for the  $\rho_i^{(\gamma)}$ ; therefore we instead choose them from the interval  $(0, \pi)$ .

The angles  $\phi_{(x,y)}^{(i)}$  and  $\chi^{(i)}$  were chosen as follows:

$$\left. \begin{array}{ll} \phi_x^{(1)} = 0 & \phi_y^{(1)} = \pi/3 \\ \phi_x^{(2)} = 0 & \phi_y^{(2)} = 2\pi/3 \\ \phi_x^{(3)} = \pi/3 & \phi_y^{(3)} = 0 \\ \phi_x^{(4)} = \pi/3 & \phi_y^{(4)} = 2\pi/3 \\ \phi_x^{(5)} = 2\pi/3 & \phi_y^{(5)} = 0 \\ \phi_x^{(6)} = 2\pi/3 & \phi_y^{(6)} = \pi/3 \end{array} \right\} \quad (\text{D.16})$$

$$\left. \begin{array}{l} \chi^{(1)} = 0 \\ \chi^{(2)} = \pi/4 \\ \chi^{(3)} = \pi/2 \\ \chi^{(4)} = 3\pi/4 \end{array} \right\} \quad (\text{D.17})$$

An exactly analogous algorithm was derived for the six degree-of-freedom Hamiltonian (7.1). Unlike the case just treated, this Hamiltonian includes one nonlinear term that couples three degrees of freedom. The kick-factorization method was extended to this situation via a set of three-dimensional rotation angles  $\phi_{(x,y,z)}^{(i)}$ ,  $i = 1, \dots, 6$ , again evenly distributed around  $(0, 2\pi)$ . The other two nonlinear terms each couple two degrees of freedom and are treated exactly as described above. It will be recalled that a time-dependent transformation was used to eliminate the large linear terms of Hamiltonian (7.1), resulting in Hamiltonian (7.4). It turns out that this affects only the linear part of our algorithm; the nonlinear operators  $e^{[f_3^{(\alpha,\beta,\gamma)}, \cdot]}$  are the same in either coordinate system.

## BIBLIOGRAPHY

- [1] P.A. Sturrock, *J. Appl. Phys.* **31**, 2052 (1960).
- [2] P.J. Morrison and D. Pfirsch, *Phys. Rev. A* **40**, 3898 (1989).
- [3] P.J. Morrison and D. Pfirsch, *Phys. Fluids B* **2**, 1105 (1990).
- [4] V.M. Dikasov, L.I. Rudakov, and D.D. Ryutov, *Sov. Phys. JETP* **21**, 608 (1965).
- [5] B. Coppi, M.N. Rosenbluth, and R.N. Sudan, *Ann. Phys.* **55**, 207 (1969).
- [6] R.Z. Sagdeev and A.A. Galeev, in *Nonlinear Plasma Theory*, edited by T.M. O'Neil and D.L. Book (W.A. Benjamin, New York, 1969).
- [7] R.E. Aamodt and M.L. Sloan, *Phys. Rev. Lett.* **19**, 1227 (1967).
- [8] C.T. Dum and E. Ott, *Plasma Phys.* **13**, 177 (1971).
- [9] J.A. Byers, M.E. Rensink, J.L. Smith, and G.M. Walters, *Phys. Fluids* **14**, 826 (1971).
- [10] R.C. Davidson, *Methods in Nonlinear Plasma Theory* (Academic Press, New York, 1972).
- [11] J. Weiland and H. Wilhelmsson, *Coherent Nonlinear Interaction of Waves in Plasmas* (Pergamon Press, New York, 1977).
- [12] R.C. Davidson and A.N. Kaufman, *J. Plasma Phys.* **3**, 97 (1969).
- [13] M.V. Berry, in *Topics in Nonlinear Dynamics*, edited by S. Jorna (American Institute of Physics, New York, 1978).

- [14] A.J. Lichtenberg and M.A. Lieberman, *Regular and Stochastic Motion* (Springer-Verlag, New York, 1983).
- [15] M. Tabor, *Chaos and Integrability in Nonlinear Dynamics* (John Wiley and Sons, New York, 1989).
- [16] B.V. Chirikov, *Phys. Rep.* **52**, 265 (1979).
- [17] M.A. Lieberman and J.L. Tennyson, in *Long-Time Prediction in Dynamics*, edited by C.W. Horton, Jr., L.E. Reichl, and V.G. Szebehely (John Wiley and Sons, New York, 1983).
- [18] P.J. Morrison and S. Eliezer, *Phys. Rev. A* **33**, 4205 (1986).
- [19] P.J. Morrison and M. Kotschenreuther, In *Nonlinear World: IV International Workshop on Nonlinear and Turbulent Processes in Physics*, edited by V.G. Bar'yakhtar et al. (World Scientific, Singapore, 1990).
- [20] T.M. Cherry, *Trans. Cambridge Philos. Soc.* **23**, 199 (1925).
- [21] E.T. Whittaker, *Analytical Dynamics* (Cambridge University Press, 1937).
- [22] D.R. Nicholson, *Introduction to Plasma Theory* (John Wiley and Sons, New York, 1983).
- [23] P.J. Channel and C. Scovel, *Nonlinearity* **3**, 231 (1990).
- [24] J.R. Cary, *Bull. Amer. Phys. Soc.* **34**, 1927 (1989).
- [25] A.J. Dragt and J. Finn, *J. Math. Phys.* **17**, 2215 (1976).
- [26] A.J. Dragt and E. Forest, *J. Math. Phys.* **24**, 2734 (1983).
- [27] J. Irwin, Technical Report SSC-28, SSC Central Design Group (1989).

- [28] G. Rangarajan, A.J. Dragt, and F. Neri, *Particle Accelerators* **28**, 119 (1990).
- [29] I. Gjaja, *Exact Evaluation of Arbitrary Symplectic Maps*, to be published.
- [30] H. Goldstein, *Classical Mechanics*, second edition (Addison-Wesley, Reading, 1980).
- [31] L.D. Landau and E.M. Lifshitz, *Electrodynamics of Continuous Media* (Pergamon Press, New York, 1960).
- [32] C.S. Kueny and P.J. Morrison, *Bull. Amer. Phys. Soc.* **33**, 1875 (1988).
- [33] V.I. Arnold, *Russian Math. Surveys* **18**, 85 (1964).
- [34] B.V. Chirikov, *Research Concerning the Theory of Nonlinear Resonance and Stochasticity*, Technical Report CERN Trans. 71-40, Geneva (1971).
- [35] B.V. Chirikov, *Sov. J. Plasma Phys.* **4**, 289 (1978).
- [36] A.J. Lichtenberg, *Phys. Fluids B* **4**, 3132 (1992).
- [37] V.D. Il'in and A.N. Il'ina, *Sov. J. of Plasma Phys.* **8**, 83 (1982).
- [38] G. Contopoulos, L. Galgani, and A. Giorgilli, *Phys. Rev. A* **18**, 1183 (1978).
- [39] P.J. Morrison, in *Mathematical Methods in Hydrodynamics and Integrability in Dynamical Systems*, edited by M. Tabor and Y.M. Treve (American Institute of Physics, New York, 1982).
- [40] P.J. Morrison, *Z. Naturforsch.* **42a**, 1115 (1987).
- [41] N.A. Krall and A.W. Trivelpiece, *Principles of Plasma Physics* (McGraw-Hill, New York, 1973).
- [42] W.E. Drummond and D. Pines, *Suppl. Nucl. Fusion Part 3*, 1049 (1962).

- [43] G. Contopoulos, *Celestial Mechanics* **17**, 167 (1978).
- [44] J. Ford and G.H. Lunsford, *Phys. Rev. A* **1**, 59 (1970).
- [45] M. Kummer, *J. Math. Anal. Appl.* **52**, 64 (1975).
- [46] N.N. Nekhoroshev, *Russ. Math. Surv.* **32**, 1 (1977).
- [47] G. Benettin and G. Gallavotti, *J. Stat. Phys.* **44**, 293 (1986).
- [48] V.I. Arnold, *Mathematical Methods of Classical Mechanics* (Springer-Verlag, New York, 1978).
- [49] E.T. Whittaker, *A Treatise on the Analytical Dynamics of Particles and Rigid Bodies* (Cambridge University Press, 1964).
- [50] J.M. Sanz-Serna, *Physica D* **60**, 293 (1992).
- [51] W.H. Press, S.A. Teukolsky, W.T. Vetterling, and B.P. Flannery, *Numerical Recipes in FORTRAN*, second edition (Cambridge University Press, 1992).
- [52] H. Ye, Private communication.
- [53] B.V. Chirikov, *Sov. J. Plasma Phys.* **5**, 492 (1979).
- [54] R.H. Cohen and G. Rowlands, *Phys. Fluids* **24**, 2295 (1981).
- [55] J.L. Tennyson, *Physica D* **5**, 123 (1982).
- [56] H. Kook, *Chaotic Transport in Hamiltonian Dynamical Systems with Several Degrees of Freedom*, PhD thesis, University of Texas at Austin (1989).
- [57] C.S. Gardner, *J. Math. Phys.* **12**, 1548 (1971).



## VITA

Christopher Shane Kueny was born in Vinton, Iowa on December 11, 1959, the son of Francis and Bess Kueny. Upon graduating from Washington High School in 1978, he entered Cornell College in Mt. Vernon, Iowa. After two years of school and one year of full-time employment, he entered the University of Iowa in September 1981. He received the Bachelor of Science degree in physics in December 1984. After one semester as a graduate student at Iowa, and one summer of full-time employment at the Institute for Fusion Studies at the University of Texas at Austin, he entered the graduate school of the University of Texas in September 1985. He was supported for two years by a Texas Atomic Energy Research Foundation Fellowship, and has been employed since that time as a Graduate Research Assistant. Since August 1989, he has also been employed part-time at Austin Research Associates.

Permanent address: 1508 Washington Drive  
Vinton, Iowa 52349

This dissertation was typeset with  $\text{\LaTeX}$  by the author.